Exciton-Induced Morphological Changes in Carbazole Based PhOLEDs and the Influence of the Device Fabrication Process

by

Hyeonghwa Yu

A thesis
presented to the University of Waterloo
in fulfillment of the
thesis requirement for the degree of
Doctor of Philosophy
in
Electrical and Computer Engineering

Waterloo, Ontario, Canada, 2020

Examining Committee Membership

The following served on the Examining Committee for this thesis.

External Examiner:	Jun Gao Professor, Dept. of Physics, Engineering Physics and Astronomy, Queen's University
Supervisor:	Hany Aziz Professor, Dept. of Electrical & Computer Engineering, University of Waterloo
Internal Member:	Dayan Ban Professor, Dept. of Electrical & Computer Engineering, University of Waterloo
Internal Member:	Siva Sivoththaman Professor, Dept. of Electrical & Computer Engineering, University of Waterloo
Internal-External Member:	Yuning Li Professor, Dept. of Chemical Engineering, University of Waterloo

AUTHOR'S DECLARATION

I hereby declare that I am the sole author of this thesis. This is a true copy of the thesis, including any required final revisions, as accepted by my examiners.

I understand that my thesis may be made electronically available to the public.

Abstract

Organic light-emitting devices (OLEDs) have increasingly attracted attention from both academia and industry alike in the last three decades because of their low cost, easy fabrication, light weight, and mechanical flexibility; a unique set of features that makes them particularly well-suited for utilization in flat panel displays and solid-state lighting. In general, display and lighting applications demand high efficiency and long lifetime OLEDs, characteristics that strongly depend on the photophysical properties of the materials involved. While those properties are predominantly governed by material chemistry and molecular structure, they are also influenced by intermolecular processes and thus by molecular packing and morphology in the solid state. A better understanding of the dependence and interplay between photophysical properties and morphology, especially with regards to the effects of exciton stress on morphology in the context of device performance, therefore, becomes critical. This is because while excitons are prerequisites for light emission in OLEDs, they are also one of the main degradation agents in these devices as the excitation energy that molecules have in this state can drive various chemical and physical aging processes.

This work studies the effects of exciton-stress in organic small molecule electroluminescent materials with the specific purpose of investigating two aspects: (i) the effect of exciton stress on material morphology and the subsequent effect of that on device performance; and (ii) the dependence of exciton-induced aging on device fabrication processes. Because of its prevalent use in phosphorescent OLEDs (PhOLEDs), the carbazole material system is used for these investigations.

This study leads to a number of new findings.

First, exciton-stress has been found to lead to increased surface roughness in thin films of organic electroluminescent material, representing the first direct evidence of exciton-induced ag-

gregation in these systems. Results show that exciton stress leads to the formation of molecular aggregates that can then act as nucleation sites for subsequent crystal growth.

Next, exciton-stress in both the hole transport layer (HTL) and electron transport layer (ETL) of PhOLEDs has been found to have a detrimental effect on device performance revealing that exciton-induced degradation in these devices may not be limited to the light emitting layer of the devices as was believed before, but rather extend to the charge transport layers. Interactions between the ETL materials and exciton-induced host molecular aggregates are found to produce complex species, a phenomenon that underlies the red shift often observed in the electroluminescent spectra of carbazole-based PhOLEDs over time. Similarly, exciton stress in HTL also affects device performance, in this case through the formation of quenchers that degrade efficiency and stability. Reducing exciton-induced degradation of the HTL is found to be crucial for improving device efficiency and stability.

Comparative investigations of solution-coated versus vacuum-deposited OLEDs shows that solution-coated materials have a greater susceptibility to exciton-induced degradation. They are also found to have a lower host-to-guest energy transfer efficiency, an effect that likely originates in differences in morphology.

Finally, exposure of PEDOT:PSS, the hole injection material most widely used in solution-coated OLEDs, to solvents during the HTL coating process has been found to degrade the hole injection efficiency of the contact. This phenomenon has been found to play a major role in the lower electroluminescence stability of solution-coated OLEDs.

Acknowledgements

I would like to thank all the little people who made this thesis possible.

To Professor Hany Aziz, I would like to express my deepest gratitude to you as my supervisor for the opportunity you gave me to pursue my graduate studies. Your tremendous guidance and encouragement helped me in all aspects of research. Your advice on both research as well as on my career has been invaluable.

I would also like to thank my committee members, Professor Dayan Ban, Professor Siva Sivoththaman and Professor Yuning Li, for their helpful advice for my research work. I would also like to extend my thanks to Professor Woo Young Kim for his support to pursue graduate studies in Canada.

I would like to acknowledge all the current and past group members: Tyler Davidson-Hall, Mozhgan Sadeghianlemraski, Viviane Nogueira Hamanaka, Elizabeth Salsberg,Dr. Mike Zhang, and Dr. Yong Joo Cho, for their insightful thoughts and productive critics. I would also like to acknowledge Mr. Richard Barber, the manager of G2N lab, for his valuable technical support throughout my study.

I wish to thank my family for their great love and unfailing support throughout my years of study. I always knew that you believed in me and encouraged me in all of my pursuits. Last but not the least, I must also thank my fiancé Hyunjae Lee for his continuous encouragement. It was a great comfort and relief to be with you when time times got rough. You all kept me going on, and this work would not have been possible without your unwavering love and encouragement given to me at all times.

Table of Contents

List of Figures

List of Tables

List of Abbreviations

AFM	Atomic Force Microscopy
BmPyPb	1,3-Bis(3,5-dipyrid-3- ylphenyl)benzene
Bphene	4,7-Diphenyl-1,10- phenanthroline
C545T	10-(2-Benzothiazolyl)-2,3,6,7-tetrahydro-1,1,7,7-tetramethyl-1H,5H,11H-(1)benzopyropyrano(6,7-8-I,j)quinolizin-11-one
CBP	4,4'-Bis(N-carbazolyl)-1,1'-biphenyl
CIE	International Commission on Illumination
EBL	Exciton Blocking Layer
EIL	Electron Injection Layer
EL	Electroluminescence
EML	Emitting Layer
ETL	Electron Transport Layer
EQE	External Quantum Efficiency
FTIR	Fourier Transform Infra-Red
HBL	Hole Blocking Layer
HIL	Hole Injection Layer
HTL	Hole Transport Layer
HOMO	Highest Occupied Molecular Orbital
$Ir(piq)_3$	Tris(1- phenylisoquinoline)iridium(III)
$Ir(ppy)_3$	Tris(2- phenylpyridine)iridium(III)
J-V	Current Density vs. Voltage Characteristic
J-V-L	Current Density vs. Volage vs. Luminance Characteristics
LiF	Lithium Fluoride
LUMO	Lowest Unoccupied Molecular Orbital
LT50	Luminescence Half Life

NPB	N,N'-Di(1-naphthyl)-N,N'- diphenyl-(1,1'-biphenyl)-4,4'- diamine
OLED	Organic Light-Emitting Device
PEDOT:PSS	Poly(3,4- ethylenedioxythiophene) polystyrene sulfonate
PhOLED	Phosphorescent Organic Light-Emitting Device
PL	Photoluminescence
POM	Polarized Optical Microscopy
Rms	Root Mean Square Roughness
Rpv	Peak to Vally Roughness
TAPC	1,1-Bis[(di-4- tolylamino)phenyl]cyclohexane
TBADN	2-tert-Butyl-9,10-di(naphth-2-yl)anthracene
TPBi	2,2',2"-(1,3,5-Benzinetriyl)- tris(1-phenyl-1-H- benzimidazole)
TRPL	Time Resolved Photoluminescence
UV	Ultraviolet
XPS	X-Ray Spectroscopy

Chapter 1

Introduction

Organic semiconductors have been used for optoelectronics devices, such as organic light-emitting devices (OLEDs), organic photovoltaics, organic transistors, and organic photodetectors. Among these applications, there has been a particular interest in OLEDs due to their inherent advantages of self-emission, planar architecture, thinner and lighter weight, potentially lower fabrication price, and better mechanical flexibility. In this chapter, Section 1.1 introduces the OLED operational mechanism. Section 1.2 explains the OLED architecture and functional layers. Section 1.3 explains the performance metrics of OLEDs, and Section 1.4 addresses the OLED fabrication processes.

1.1 Working Princiles of OLEDs

The basic mechanism of electroluminescence (EL) involves the generation of light as a result of the formation of electron-hole pairs (excitons), which radiatively relax to provide photons. The operational mechanism of OLEDs is based on four distinct steps: (1) charge carrier injection from electrodes; (2) charge carrier transport across the organic layers; (3) exciton formation; and (4) the radiative decay of excitons producing photons of light. Figure 1.1 presents the energy level diagram of a typical bilayer OLED under an electrical bias and illustrates the operational mechanism.

When a voltage is applied, the electric field facilitates the carrier injection. Electrons are injected from the cathode into the lowest unoccupied molecular orbital (LUMO) of the electron

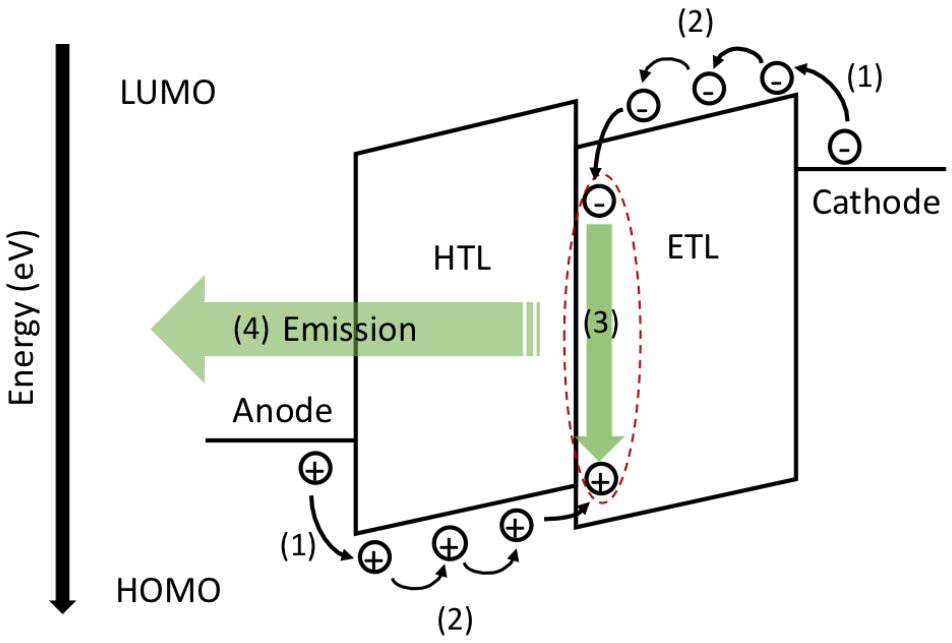

Figure 1.1: OLED operation mechanism: (1) charge carrier injection; (2) charge carrier transport; (3) exciton formation; and (4) radiative decay of exciton as photons.

transport layer (ETL) and are collected from the highest occupied molecular orbital (HOMO) of the hole transport layer (HTL) to the anode. The collection of electrons at the anode can be visualized as the injection of holes. In general, charge injection barriers at electrodes into organic layers lead to a high driving voltage, and hence high power consumption. In order to achieve an effective charge carrier injection, charge carrier injection layers are utilized.

After the holes and electrons are injected into the HTL and ETL, respectively, the charges are then transported through the charge transport layers. The HTL materials need high hole mobility to ensure adequate hole transport properties and proper orbital energy levels to ensure efficient hole injection into the EML. Similarly, the ETL materials require high electron mobility and proper orbital energy levels. The holes ad electrons recombine each other to form excitons

at an EML. The EML, where charges recombine and form the excitons, is the most important layer. Instead of a single material layer, the EML consists of two components- a host material as the matrix and a guest material in the host matrix as the emitter. Within the host:guest system, the guest material plays a role in achieving the desired emission color. The host material is responsible for charge transport and reducing concentration quenching and triplet-triplet annihilation. It is therefore important that guest material is widely dispersed in the host matrix at a low concentration to avoid quenching and annihilation. Generally, two processes can lead to guest emission: (1) excitons formed in the host can be transferred to the guest via Förster and Dexter energy transfer and then radiatively decay or (2) the holes and electrons can directly recombine on the guest by charge trapping, and the excitons then relax radiatively.

1.1.1 Exciton

Excitons are electron-hole (e-h) pairs bound by Coulomb forces. Depending on the degree of delocalization and the strength of the e-h binding energy, excitons can be generally classified into three types: Frenkel, Wannier-Mott, and charge transfer excitons, as illustrated in Figure 1.2. Due to a lower degree of charge delocalization and smaller dielectric constant in organic semiconductors, the excitons have a very large binding energy and small Bohr radius, and hence reside on a single molecule. In contrast, in case of inorganic semiconductors, Wannier-Mott excitons, which are characterized by having a much larger e-h separation and thus are more loosely bound, are formed. In addition to the Frenkel excitons which are essentially unimolecular, charge transfer excitons which have electrons and holes located on adjacent molecules, and are thus essentially bimolecular, are often also formed.

In the presence of strong intermolecular interactions, various bimolecular excited species can also be formed, such as; excimers, electromers, exciplexes, and electroplexes. Excimers and electromers are excited bimolecular species that comprise chemically identical molecules one of

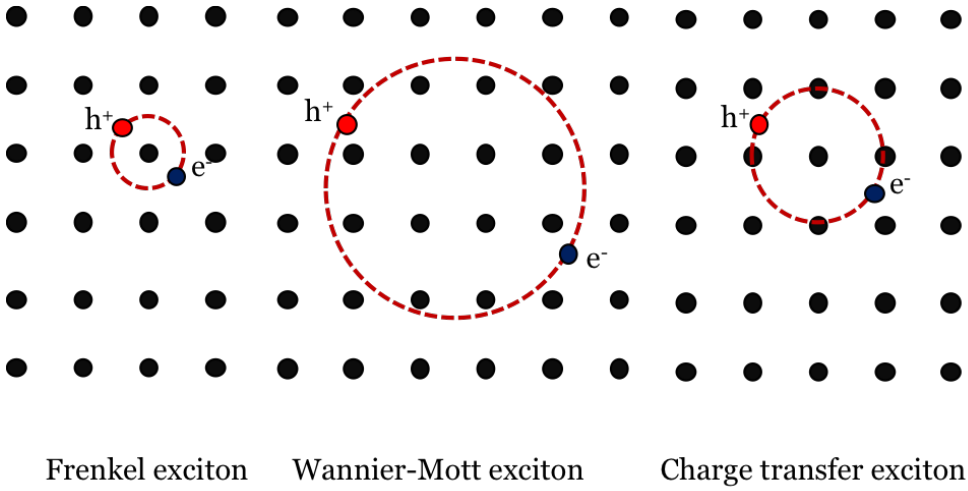

Figure 1.2: Schematic illustrations of the three main types of excitons: Frenkel exciton, Wannier-Mott exciton and intermediate charge-transfer exciton.

which is in an excited state and the other in the ground state. In contrast, in exciplexes and electroplexes the molecules are chemically different, and the electron and hole are usually not on the same molecule. Exciplexes and electroplexes can therefore be seen as charge transfer excitons. In general, excimers and exciplexes can be generated by either optical or electrical excitation, and can thus be observed in PL and EL. Electromers and electroplexes on the other hand involve charged species and can therefore be only generated via electrical excitation (and thus observed only in EL).

1.2 Charge Carrier Transport in OLEDs

The charge carrier injection at the interface occurs by tunneling or thermionic emission (as illustrated in Figure 1.3) [1]. According to the tunneling model, the charge injection efficiency is related to the width of the barrier at the interface[1]. With an increased external field or

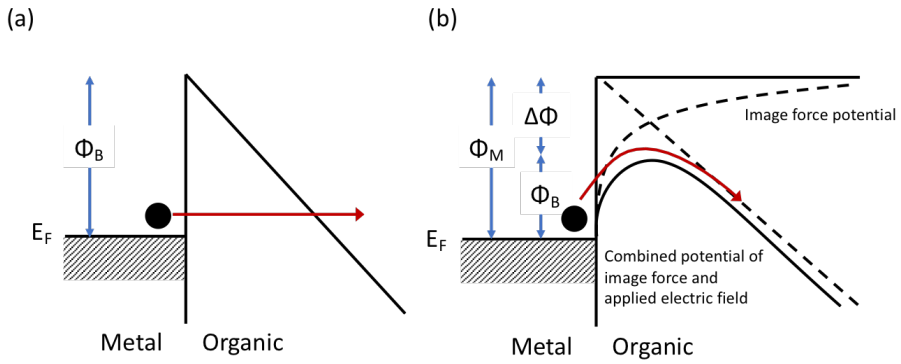

Figure 1.3: Charge carrier injection models: (a) tunneling model; and (b) thermionic model.

reduced energy barrier, the barrier width decreases, resulting in efficient electron injection. In the thermionic emission model, electrons need to have sufficient thermal energy to overcome the potential barrier, which depends on the image force potential, and the energy barrier is lowered by increasing the external field [1].

In most cases, organic semiconductors are molecular solids in which molecules are bonded by weak intermolecular interaction, called "Van der Waals forces". In these molecular solids, the charge density is localized within each molecule, and long-range structures containing conduction and valence bands are not formed.Instead, localized frontier orbital (HOMO and LUMO) are formed. Figure 1.4 illustrates the electronic structure of single organic molecules, organic semiconductors, and inorganic semiconductors. In organic semiconductors, the weak intermolecular interactions and the relatively long residence time of charges on a molecule allows for stronger intermolecular coupling between electrons and phonons. As a result, polarization or distortion of surrounding molecules induced by the motion of a charge is generally significant. The combination of a charge carrier (i.e., Electron or hole) and its accompanying molecular distortion leads to the formation of a polaron. The polaron acts like a charge carrier and becomes responsible for electrical conduction. The charge carrier transport process requires the polarons to hop from one molecule to another.

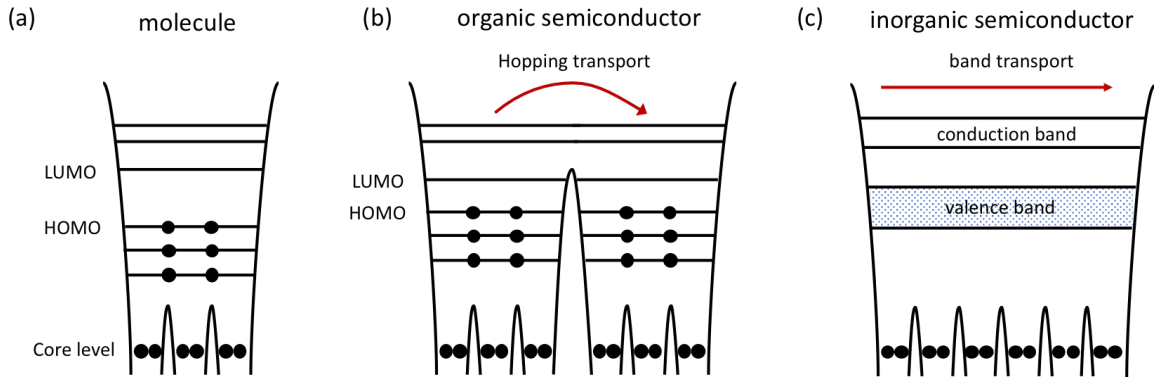

Figure 1.4: Electronic structure for (a) molecules; (b) organic semiconductors; and (c) inorganic semiconductors.

Because the charge carriers are strongly localized on molecules, charge transport in organic semiconductor materials occurs by carrier hopping between localized sites, which differs from the typical band type transport that occurs in the case of inorganic semiconductors. In hopping transport, because charge carriers need to overcome energy barriers caused by the intermolecular separation or self-induced polaronic effects, charge mobility in organic semiconductors is typically much lower than in inorganic semiconductors and depends on the electric field.

1.3 Photophysical Properties of OLEDs

The hole and electron carry a spin of $+\frac{1}{2}$ or $-\frac{1}{2}$. When a hole and an electron recombine to form an exciton in an excited state, four different spin combinations are possible, as illustrated in Figure 1.5. When the spin of the hole and electron pair is anti-parallel, the total spin S is 0 in singlet states. Other spin arrangements provide three non-zero spin vectors and thus create triplet states. According to the spin-statistics, about 25% of excitons (S=0) are in singlet states, and 75% of excitons (S=1) are in triplet states [2]. Since these excitons are in metastable states, they eventually lose their energy via several deactivation pathways.

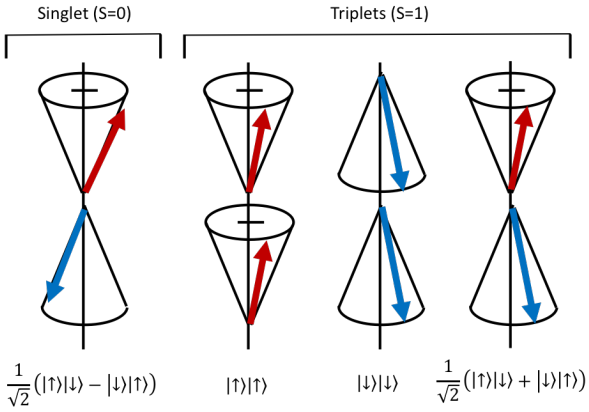

Figure 1.5: Spin statics for singlet and triplet excitons.

The Jablonski diagram in Figure 1.6 shows possible electronic transitions within a molecule in an excited state. Excitons can experience nonradiative processes through internal conversion or vibrational relaxation by which the exciton energy is dissipated via phonons. Excitons also can undergo radiative processes to produce photons via fluorescence or phosphorescence. In general, transitions between states with different spin vectors are forbidden, and therefore the decay from the triplet state is not allowed. Fluorescent materials emit from the singlet state, from which only singlet excitons decay radiatively and triplet excitons are lost to a nonradiative decay process. In the case of phosphorescent materials, however, spin-orbital coupling allows triplet-singlet transitions. Spin-orbital coupling also allows excitons in singlet states to transit to triplet states via intersystem crossing such that potentially all excitons formed in singlet and triplet states relax radiatively to ground states. The magnitude of the spin-orbital coupling is proportional to atomic number and is thus more effective for organometallic transition metal complexes that contain heavy metals, such as iridium and platinum. According to the spin-statistics, therefore, although only 25% of singlet excitons in fluorescent organic materials can produce photons, almost 100% of excitons (including 25% of singlets and 75% of triplets) can be converted into photons in phosphorescent organic materials.

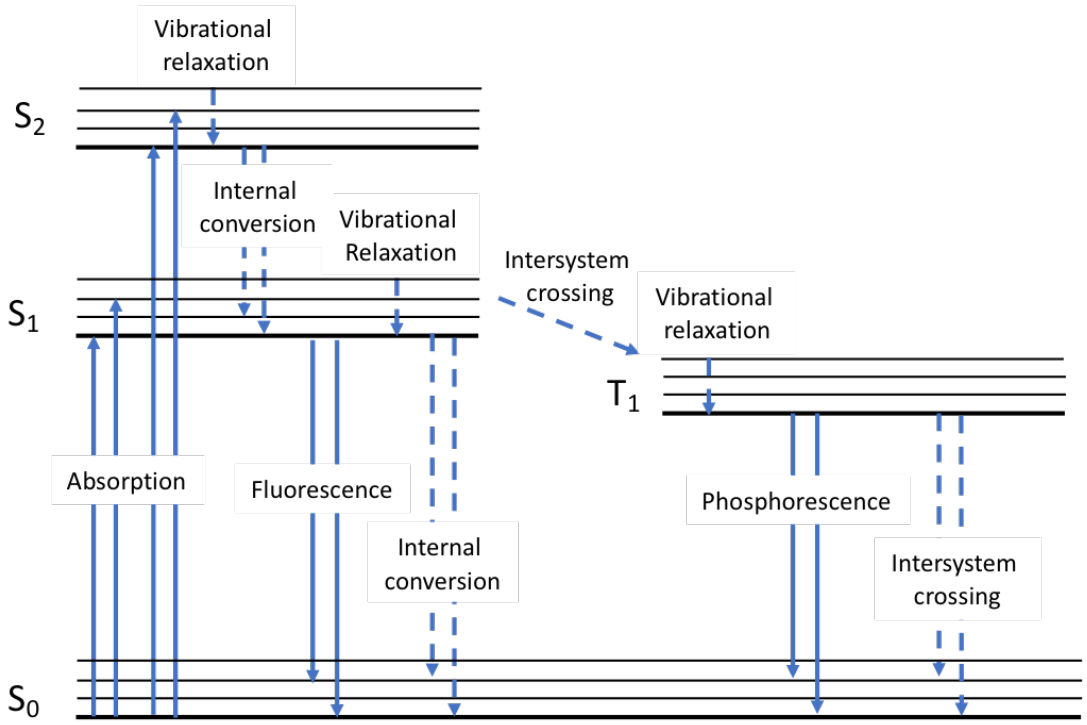

Figure 1.6: Jablonski diagram showing electronic states and possible transitions in an organic molecule.

1.4 OLED Performance Metrics

In general, the performance of OLEDs is quantified by a number of metrics, including the external quantum efficiency (EQE), power conversion efficiency (lm W^{-1}), and operational stability.

1.4.1 External Quantum Efficiency

The most important efficiency aspect is EQE, which is defined by the ratio of the total number of photons leaving the device to the total number of electrons injected. The EQE can be described

as the product of the internal quantum efficiency (IQE) and the outcoupling efficiency η_{out}:

$$EQE(\%) = IQE \cdot \eta_{out}$$

$$IQE(\%) = \eta_{rec} \cdot \eta_{spin} \cdot \eta_{PL}$$

IQE describes how well the injected carriers are converted into photons and is itself the product of three factors: the electron-hole recombination factor η_{rec}, the exciton spin state factor η_{spin}, and the photoluminescence (PL) quantum yield factor η_{PL}. η_{rec} describes the probability of injected charge carriers to combine with the opposite charge carriers to form excitons. Theoretically, it can approach 100% when the charges are balanced. Some injected charge carriers, however, can flow through the device to reach the counter electrode. This factor can be optimized by varying the material and thickness of each layer, using the bipolar hosts or mixed hosts in the EML, and using the exciton or charge blocking layers. η_{spin} describes the fraction of emissive excitons. From the spin-statistics, 25% of singlet and 75% of triplet electronic states will be presented. However, not all the excitons may emit light. Some excitons are spin-prohibited to decay radiatively, so fluorescent materials have less than a 25% η_{spin} because only the singlet excitons undergo radiative decay, while phosphorescent materials can reach a 100% η_{spin} because both singlets and triplets decay radiatively. η_{PL} depends on the radiative excitons that actually generate light because some radiative excitons can be lost to nonradiative processes through interaction with other excitons (i.e., triplet-triplet annihilation) or charges (i.e., triplet-polaron annihilation) and quenching into the adjacent layers, which have lower triplet or singlet energy [10].

Nonetheless, not all the generated photons able to leave the device. Some generated photons will suffer total internal reflection because photons travel from the high refractive index of the organic materials into air, a low index material. On this path, photons can face several waveguide modes: the glass/substrate mode, that is trapped in the substrate; the organic mode, that is trapped in the organic layers; and the surface plasmonic mode, that is coupled to the surface

plasmons at the organic/metal interface. Therefore, η_{out} is largely dependent on the optical structure of the organic layers (i.e., their thickness and refractive indices). η_{out} has been roughly calculated to be only about n^{-2}, where n is the refractive index of the organic materials [11]. Because n is generally between 1.7 and 1.8, it is generally accepted that only 20% of the generated photons actually reach the air and contribute to light emission. Hence, the theoretical maximum EQE values will be 5% and 20% for fluorescent OLEDs (FOLEDs) and phosphorescent OLEDs (PhOLEDs), respectively.

1.4.2 Operational Stability

During device operation, the luminance of OLEDs decreases gradually, a process governed by several distinct degradation phenomena. The following chapter discusses various degradation mechanisms. Device stability is usually quantified using a lifetime parameter LT X, which gives the time collapsed until device EL output decreases by a certain percentage (X%) of the initial EL at a constant current density. Often, the lifetime of OLEDs is defined as half-lifetime (LT 50). OLED degradation is a complex issue, and device stability generally depends on the choice of materials, device structure, fabrication process, and operation and storage conditions. Presently, green and red PhOLEDs have reached market demand by demonstrating good performance and lifetime upward of 10^6 hours, but blue PhOLEDs lag behind. While high efficiency blue PhOLEDs have been demonstrated, their major challenge is device stability, as their LT 50 is only thousands of hours at the brightness required for commercial application.

1.5 OLED Fabrication processes

In general, the organic layers of an OLED can be fabricated by one of two fabrication approaches: vacuum deposition or solution coating. The standard method for fabricating organic

films for most commercialized OLEDs based on small molecules is the vacuum deposition of materials. Meanwhile, the organic films can potentially be deposited by solution coating processes, since the materials can generally be dissolved in certain organic solvents. The two processes have their advantages and disadvantages, which are discussed below.

1.5.1 Vacuum Deposition

Since the early days of OLED development by Tang and VanSlyke [3], vacuum deposition has been the most common fabrication process for small molecule-based OLEDs. The vacuum deposition process involves heating organic materials inside a high vacuum chamber at a base pressure of 10^{-6} torr or lower, at which the materials evaporate by sublimation and condense onto a substrate placed above them, thus forming the films.

Most OLED thermal deposition systems have multiple sources to fabricate devices with several layers. Organic material is evaporated through resistive heating in ceramic or metal crucibles. Because many common organic materials reach their high vapor pressures at temperature below their melting points, they evaporate via sublimation. A quartz crystal monitor (QCM) sensor monitors flux from a single evaporated source to achieve a nominal thickness of the deposited material. QCM works by vibrating a small quartz crystal exposed to the deposition flux. As the deposited material on the QCM increases, the resonance frequency of the QCM decreases. By knowing the frequency decrease and physical properties of the deposited material (or the geometrical tooling factor for calibrating the distance between the QCM and the substrate), the deposition rate can be estimated. The deposition rates affect the film morphology and carrier mobility and thereby the performance of OLEDs [12, 13]. The substrate temperature during deposition also affects the density, molecular orientation, and thermal and kinetic properties of the film [14, 15, 16]. Therefore, the preparation conditions of the organic films during the deposition process can have profound effects on the organic films and thereby the devices.

One of the greatest advantages of vacuum deposition is that it enables the fabrication of multilayer devices in a single deposition procedure. Using fine metal masks as shadow masks, RGB OLEDs can be fabricated on the same substrate, which is necessary for full-color OLED displays. In addition, systematic device fabrication, in which various parameters such as thickness or layer composition may be varied, can be performed relatively easily. Although vacuum-deposited OLED have been commercialized successfully because of their outstanding performance, the most obvious challenges are their scalability and cost-effective manufacturing capabilities. For flexible OLEDs in particular, high temperature procedures are limited by the poor thermal stability of flexible plastic substrates.

1.5.2 Solution Coating

To overcome the limitations of vacuum deposition processes, solution coating processes have been considered. Solution coating, in principle, provides a low-cost approach to fabricate devices because it does not require high vacuum and thus costly equipment. It also allows more efficient utilization of materials, easier scalability to the mass production of large-area devices, and compatibility with R2R fabrication on flexible substrates.

In order to fabricate solution-coated OLEDs, organic material is first dissolved into the appropriate solvent and, organic films are deposited from the solution precursors onto a substrate by additive methods such as gravure printing, screen printing, inkjet printing, blade coating, and spin coating. Among the above processes, spin coating is the most widely used for research purposes. In this method, the solution dispensed onto the substrate is accelerated to a high velocity to spread the liquid by centrifugal force and simultaneously evaporate the solvent. The film thickness is controlled by the solution concentration and spin speed because the film thickness is determined by the viscous flow rate, which is equal to the evaporation rate in the vacuum thermal evaporation process. However, it may not be used for large-area applications or patterning RGB

structures for full-color displays. One the other hand, inkjet printing is considered an alternative process for large-area OLEDs. During printing, the ink can be locally deposited over a substrate and then solidified to be deposited onto a substrate. The film thickness is controlled by the flow rate of the ink and the scan speed of the printer. By applying different layers of inks with different functional materials, complex patterns can be printed.

Nonetheless, solution coating processes present significant difficulties. First, they significantly limit device design possibilities due to the need for orthogonal solvents. During solution coating of one organic layer on top of another, the solvent may dissolve or even remove the underlying layer because most of the small molecules have low molecular weights and do not adhere strongly to the underlying layer. In other words, each layer cannot use a solvent that dissolves the underlying layers. This fact significantly limits the total number of organic layers, so it is difficult to fabricate multilayer structures, which are usually required for good exciton confinement and therefore high efficiency. Another challenge in solution-coated OLEDs is choosing an appropriate organic material which have adequate solubility in organic solvents. For example, Tris(8-hydroxyquinoline)aluminum(III) (Alq_3), one of the two materials used by Tang and VanSlyke for their OLED [3], has a very limited solubility in organic solvents. Some materials therefore need to be modified to become more soluble and stable. However, increasing material solubility while maintaining its photophysical and charge transport properties is not straightforward.

Despite some difficulties, remarkable progress in the performance of solution-coated OLEDs has been made in the past several years. Table 1.1 summarizes the current device performance of vacuum-deposited and solution-coated OLEDs. As the table shows, the efficiency of solution-coated OLEDs no longer lags behind the efficiency of the vacuum-deposited OLEDs, but not in terms of lifetime. Obviously, the relatively low operational lifetime of solution-coated OLEDs is an issue for their commercialization in the display and general lighting markets.

Table 1.1: State-of-the-art device performances of vacuum-deposited and solution-coated phosphorescent OLEDs [17, 18].

Color	Process	Efficiency (cd/A)	CIE (x, y)	Lifetime (LT 50 at 1000 cd/m^2)
Red	Vacuum deposition	30	(0.64, 0.36)	900 000
	Solution coating	23	(0.65, 0.35)	200 000
Green	Vacuum deposition	85	(0.31, 0.63)	400 000
	Solution coating	83	(0.32, 0.63)	125 000
Blue	Vacuum deposition	7.6	(0.14, 0.17)	33 000
	Solution coating	5.7	(0.14, 0.13)	17 000

1.6 Thesis Outline

The thesis is organized into ten chapters. Chapter 1 provides an introduction to OLEDs and their fabrication processes. Chapter 2 gives a literature review of OLED degradation mechanisms. Chapter 3 proposes the objectives of this study and then presents the methodology regarding materials, device configuration, and characterization techniques used in this study. Chapter 4-9, as the main body of the thesis, discuss exciton stress on material morphology, exciton-induced degradation on charge transport layers and their subsequent effect on device performance, the comparative investigations of solution-coated versus vacuum-deposited materials in host:guest systems, and the effect of solvents on the hole injection layer. Chapter 10 summarizes the main findings of this work.

Chapter 2

Literature Review on Degradation Mechanisms

Toward developing more efficient and long-lived OLEDs, a large body of research has attempted to explain various observations related to OLED degradation behavior. In general, device degradation mechanisms can be divided into two categories - extrinsic and intrinsic. Extrinsic degradation is caused by environmental factors, such as oxygen and moisture from the ambient [19]. These extrinsic factors prompt the formation of dark spots and localized defects, leading to the growth of non-emissive areas over time and the occurrence of electrical shorts [20, 21]. Most of these extrinsic phenomena can be controlled through improving fabrication conditions or eliminating the or other reactive agents from the OLED environment by proper encapsulation. Therefore, they are no longer considered a significant obstacle to commercial applications. One the other hand, intrinsic degradation is linked to a gradual loss in luminance over time, which is measured under a constant current density and therefore signifies a decrease in IQE. It is also accompanied by an increase in the operating voltage required to maintain a constant current density. Intrinsic degradation mainly originates in physical and chemical changes that take place in the materials under electrical stress. These changes can be influenced by factors including device architecture and fabrication process. EL decay, voltage rise, and PL quenching during device operation are more likely associated with the generation of permanent defect sites; they can act as deep traps, luminescence quenchers, and nonradiative recombination centers; and a variety of pathways can cause the formation of these defects.

2.1 Charge Carrier-Induced Degradation

One of the first suggested explanations of OLED intrinsic degradation was that material aging is caused by the flow of charges in them. The instability of cationic or anionic state of conjugated molecules can lead to molecular decomposition and thus defect formation. It has been reported that the degradation of Alq_3-based devices is attributed to the instability of cationic species [22]. Alq_3 molecules undergo degradation upon exposure to hole currents. The degradation of unstable cationic Alq_3 produces luminescence quencher sites, which decrease the PL quantum yield of Alq_3 molecules and the device EL. This charge-induced degradation has been investigated in other OLED materials [23, 24]. For instance, because of the instability of 4,4'-Di(9H-carbazol-9-yl)-1,1'-biphenyl (mCBP) anions, the degradation of these materials could form defect sites that more likely act as nonradiative recombination centers due to their deep trapping natures [23]. Moreover, the mCBP anions become more unstable in their excited states through interaction with excitons in nearby molecules, causing molecular degradation via so-called polaron-exciton annihilation [23, 25].

In some OLED architectures, charge carriers can accumulate at the HTL/EML interface, which also can serve as the charge recombination zone where EL originates, due to significant energy level mismatch, leading to the formation of space charges. It has been found that luminance efficiency decreases with increases in the accumulation of immobile charges at or near interfaces, and the two quantities are linearly correlated [26, 27, 28]. Within this region, electrical aging generates deep trap sites, which can act as nonradiative recombination centers or exciton quenchers.

2.2 Exciton-Induced Chemical Degradation

Similar to charge carriers, excitons, which are inevitably formed during device operation and are a prerequisite for electroluminescence, are also believed to play a major role in material degradation. Various organic materials have been demonstrated to be susceptible to exciton-induced chemical decomposition via the direct dissociation of molecules in excited states or bimolecular annihilation [23, 25, 29, 30, 31].

During device operation, organic molecules when in an electronic excited state can undergo chemical decomposition due to bond cleavage. This process produces degradation products. One of the most commonly encountered chemical changes identified in OLED materials originates from the dissociation of homolytic bonds [30]. Because their relatively low dissociation energy is comparable to the singlet excited state energy of the respective organic molecules, this bond cleavage can occur during device operation. The corresponding reaction products then act as efficient charge traps, exciton quenchers, and nonradiative recombination centers.

Bimolecular annihilation reactions involve either two excitons (either singlet or triplet excitons) or one exciton (either a singlet or triplet exciton) and a polaron [23, 25]. The interaction of two excitons yields a higher-lying excited state through energy transfer from one exciton to another. Similarly, energy transfer from an exciton to a polaron leads to a higher-lying polaron excited state. As the higher-lying excited state has almost double the energy of the lower excited state, such excited states can easily induce chemical dissociation, similar to the aforementioned process. The by-products of the dissociation can quench excitons and trap charge carriers.

2.3 Exciton Polaron-Induced Morphological Degradation

Another proposed consequence of the co-existence of charge carriers and excitons is morphological changes in the material [32, 33, 34]. Similar to the bimolecular annihilation model, interactions between excitons and polarons transfer exciton energy to polarons, producing excited polarons with high energy. Unlike the chemical model, no detectable material chemistry changes are associated with this process. Since molecules with excited polarons have larger dipole moments, such molecules may re-orient in certain directions to interact with neighboring molecules, leading to the formation of irreversible molecular aggregation [34]. These exciton-polaron interactions can occur in both host molecules and guest molecules but affect host molecules more due to their higher concentration [33, 34]. Because aggregates have narrower band gaps than those of their monomers, they can act not only as charge trap sites that increase voltage over time but also as exciton quenching sites that can decay radiatively in the longer-wavelength region. Therefore, such molecular aggregation is expected to decrease the EL intensity corresponding to the molecule emission and simultaneously involve the presence of the shoulder band that is red-shifted from its original emission. This exciton polaron-induced degradation is more likely to occur in materials with wide band gaps due to their higher exciton energy [33, 34]. The rates of this aggregation have been found to influence device EL lifetime and correlate with the energy band gaps of the materials where materials with wider energy band gaps tend to aggregate by this mechanism faster [33, 34, 35]. In this regard, the relatively lower stability of blue OLEDs than red and green OLEDs can be ascribed to the wide band gaps of blue guest molecules and their required host molecules with wide band gaps because energetically higher excited polarons increase the rate of aggregate formation.

Quite interestingly, the aggregation rate of the host material depends not only on its band gap but also on the choice of the guest material and its concentration [36]. As host EL intensity increases with increasing rates of exciton polaron-induced host molecular aggregation, phase

segregation between the host and the guest materials can occur, resulting in decreased energy transfer from host to guest. This decrease in energy transfer is associated with a decrease in device efficiency and is also a significant factor affecting device stability.

2.4 Solution-Coated versus Vacuum-Deposited OLEDs

While OLEDs have long offered the promise of low-cost manufacturing via amenability to solution-coating techniques such as ink-jet printing and blade-coating, the vast majority of OLEDs used in commercial products continue to be fabricated by costly vacuum-deposition processes [37, 38]. This is due in part to the fact that OLEDs fabricated by solution-coating generally have a much lower EL stability, and despite the progress in developing solution-processible materials with high EL efficiencies [39, 40, 41, 42, 43, 44, 45]. Investigations of the root causes of this behavior to date have revealed that differences in morphology between solution-coated and vacuum-deposited films play a leading role in the lower stability of solution-coated OLEDs [43, 44, 46, 47, 48].

To date, a number of studies have compared organic films and devices fabricated by vacuum deposition and solution coating [46, 49, 50]. Kim et al. reported that solution-processed N,N'-Di(1-naphthyl)-N,N'-diphenyl-(1,1'-biphenyl)-4,4'-diamine (NPB) film has a much lower refractive index than that of the vacuum-deposited film [49]. A lower refractive index is generally related to the lower packing density attributed to the presence of free volume within the film, which in turn leads to higher driving voltage for a device. Xing et al. investigated the internal molecular arrangements in films prepared by vacuum deposition and solution coating [46]. From their X-ray diffraction results, tris(4-carbazoyl-9-ylphenyl)amine (TCTA) film fabricated from vacuum deposition showed a highly oriented arrangement with face to face pi-pi stacking, whereas the solution-coated film had a random arrangement. The vacuum deposition process, therefore, leads to higher hole mobility and device efficiency. These studies compared the morphologies of

films fabricated by vacuum deposition and solution coating along with device efficiency; however, no device stability conclusions have been reached regarding the morphology differences between films. As a consequence, the mechanism governing the low device stability of solution-coated OLEDs remains unclear.

There is limited literature available on the root causes of the lower stability of solution-coated OLEDs. As mentioned previously, the exciton polaron-induced molecular aggregation observed in materials with wide band gaps is one major degradation mechanism in vacuum-deposited OLEDs [33, 34, 35]. Recently, Cho et al. reported a systematic experimental study of various host materials prepared by vacuum deposition and solution coating, revealing that exciton polaron-induced molecular aggregation occurs much more severely in solution-coated OLEDs than in the vacuum-deposited ones [44]. Due to this increased rate of aggregation, device efficiency decreased, and driving voltage increased more rapidly in the solution-coated OLEDs than in the vacuum-deposited ones. The author also compared the behaviors and properties of host molecules in neat (undoped) and doped films prepared via vacuum deposition and solution coating [51]. The formation of aggregation results in a faster decrease in their luminescent quantum yield, and the decrease proceeds more quickly in solution-coated films than in their vacuum-deposited counterparts.

Interestingly, the extent of the molecular aggregation in solution-coated films also depends on the choice of solvent used [47, 51, 52], suggesting that the solvents utilized in making the coating solution may influence film morphology. In addition to their direct effect on the morphology of the film being coated, the presence of solvents can also affect other device layers, especially the underlying (i.e. pre-coated) ones, and change their surface properties such as work function, sheet resistance and roughness [53, 54, 55]. A recent work by Yun et al. has shown that exposure to solvents can alter the electrical and physical properties of PEDOT:PSS [55]. PEDOT:PSS is widely used in HIL because of its high conductivity, good film-forming property, and high thermal stability [56, 57]. Water-miscible solvents such as ethanol and acetone can diffuse into

the PEDOT:PSS film and change the conformation between PEDOT and PSS. This leads to a significant effect on the electrical properties of PEODT:PSS. Water-immiscible solvents (e.g. toluene and chloroform), on the other hand, get partially adsorbed on the PEDOT:PSS surface and therefore more strongly affect surface properties including work function rather than bulk properties.

2.5 Outstanding Issues

Although OLEDs are already being used in the commercial display market with outstanding performance, a number of limitations remain for further development.

Exciton stress has been found to lead to morphological changes in organic luminescent materials [33, 34, 36, 58, 59]. This phenomenon causes a decrease in the luminescence quantum yield of the materials as well as in host-to-guest energy transfer efficiency, leading to a deterioration in OLED EL efficiency [36]. The occurrence of such exciton-induced molecular aggregation, however, has been inferred from indirect experimental observations, such as from changes in the EL and PL spectral characteristics and time-resolved decay rates of the materials involved or from the effects of intermixing a second material on modulating these intermolecular interactions. It is therefore important to explore approaches for direct observation of exciton-induced molecular aggregation.

In general, confining excitons within the EML has been found to be crucial for realizing high efficiency and long device stability [60, 61]. In PhOLEDs, the exciton population is high at either the HTL/EML interface or the EML/ETL interface of the EML, depending on the relative mobilities of the electrons versus holes within the EML [62]. Therefore, aside from the EML where most excitons are generated, a small fraction of excitons might be presented in the adjacent charge transport layers [63, 64]. Controlling the exciton distribution by reducing

exciton density near the ETL/EML interface or exciton migration from the EML into the HTL have both been shown to enhance device stability [61, 62, 63]. The effect of the excitons on the charge transport layer and their influence on device performance, however, has not been studied. Because device performance generally depends on the choice of charge transport layer materials, the influence of charge transport layers in exciton-induced degradation should be considered.

The lower stability of solution-coated OLEDs still remains a long-standing problem. However, the underlying mechanisms are still not clearly understood. In addition, most of the studies so far have focused on neat material systems. In particular, an investigation of this behavior in small molecule host:guest material systems, the systems typically used in the EL layers of OLEDs, has not been adequately investigated. In the case of vacuum-deposited OLEDs, it has been shown that host aggregation by exciton-polaron interactions can occur in host:guest systems, and this phenomenon can lead to phase segregation between the host and guest materials, in turn leading to a change in energy transfer rate from the host to guest [36]. This study, however, focused on vacuum-deposited systems. Since solution-coated films are known to have a considerably different morphology, the question of whether solution-coated host:guest systems could be more susceptible to host aggregation and phase segregation arises.

The solvent system utilized in making a coating solution can have a significant influence on the morphology of the film being coated and the surface properties of other device layers, especially the underlying (i.e. pre-coated) one. Understanding the effects of solvents on other device layers is, therefore, critical for addressing the performance limitations of solution-coated OLEDs. It has been shown that exposure of PEDOT:PSS to solvents can alter the electrical and physical properties [55]. During the solution-coating process of HTLs, the underlying PEDOT:PSS HIL is inevitably exposed to solvents in the HTL solution. It is, therefore, reasonable to suspect that the exposure to these solvents may lead to changes in the PEDOT:PSS that can influence device performance.

Chapter 3

Research Objectives and Methodology

3.1 Research Objectives

The objective of this work is to study the effects of exciton-stress in organic small molecule electroluminescent materials with the specific purpose of investigating two aspects; (i) the effect of exciton stress on material morphology and the subsequent effect of that on device performance, and (ii) the dependence of exciton-induced aging on device fabrication processes. Because of its prevalent use in PhOLEDs, the carbazole material system is used for these investigations.

First, exciton-induced morphological changes in organic luminescent materials are investigated. Although the occurrence of such exciton-induced molecular aggregation has been deduced from earlier work, it was only inferred from indirect experimental observation from changes in the PL and EML spectral characteristics.

The effects of exciton-stress in both the HTL and the ETL on device performance are investigated. In general, the study of exciton-induced degradation in PhOLEDs has been extensively limited to the EML of the devices. Although the electron-hole recombination zone and exciton formation occur in the vicinity of the HTL/EML or the EML/ETL interfaces in PhOLEDs during operation, the role of the charge transport layers in exciton-induced degradation is still unknown. Interactions between the ETL materials and exciton-induced host molecular aggregates are examined, and whether the interactions are the factor behind the spectral shift in electroluminescence over time. Exciton-induced degradation in the HTL and its influence on device performance are

investigated. An approach to reduce the effect of exciton-induced degradation of HTL in device performance is also explored.

Exciton-induced degradation is comparatively investigated in solution-coated versus vacuum-deposited host:guest electroluminescent small-molecule material system, and whether the differences in initial film morphologies are responsible for the differences in the susceptibility to exciton-induced degradation. A number of studies have investigated the causes of the lower stability of solution-coated OLEDs; however, most of the studies have focused on neat material systems.

The influence of PEDOT:PSS HIL exposure to solvents during the HTL coating process on device performance is studied, and whether the changes play a role in the lower EL stability of solution-coated OLEDs than that of vacuum-deposited OLEDs. The solvent system utilized in making the coating solution can have a significant influence on the morphology of the film being coated and the underlying layers. However, the effects of solvents during the HTL solution on the underlying PEDOT:PSS HIL and the subsequent effects on device performance have not been addressed.

3.2 Methodology

In this work, the investigations of exciton-induced morphological changes in carbazole based PhOLEDs are performed experimentally by fabricating and testing organic small molecule electroluminescent materials and OLEDs utilizing them for the purpose of meeting the above objectives.

3.2.1 Materials and Device Configuration

Many organic compounds widely used considered as host materials for phosphorescent emitters are based on the carbazole group because high triplet energy (2.5-3.3 eV) can be obtained by simple synthesis and easy modification with other functional groups. The most prominent representative of carbazole-based host materials is 4,4'-Bis(N-carbazolyl)-1,1'-biphenyl (CBP), the photophysical properties listed Table 3.1. Because of its wide usage and relatively simple molecular structure, CBP has often been studied as a model compound for other carbazole-based host materials.

Table 3.1: Optical properties and energy levels obtained for CBP [65].

HOMO (eV)	LUMO (eV)	E_T (eV)	λ_{abs} (nm)	λ_{em} (nm)
-5.54	-2.23	2.66	293	366

As discussed above, state-of-the-art OLEDs consist of five functional layers: HIL, HTL, EML, ETL and, EIL. In many of the experiments performed in this work, the standard archetypical PhOLED structure ITO/MoO_3 /CBP/CBP: tris(2-phenylpyridine)iridium(III) ($Ir(ppy)_3$) (5%)/ 2,2',2"-(1,3,5-benzinetriyl)-tris(1-phenyl-1-H-benzimidazole) (TPBi)/LiF/Al is used. The schematic energy level diagram of the OLED is displayed in Figure 3.1. Here, MoO_3, which generally leads to longer lifetime, is chosen as the HIL material to facilitate hole injection. For the charge transport layer, the commonly used CBP and TPBi are chosen as HTL and ETL materials. The very stable phosphorescent material $Ir(ppy)_3$, which exhibits very high material quantum yield, is doped in the widely used CBP host. Lastly, LiF and Al are used in the EIL and cathode, respectively. In addition to CBP, TPBi, and $Ir(ppy)_3$, other organic materials used in this work are listed in Table 3.2 along with their molecular structures, chemical names, and abbreviations.

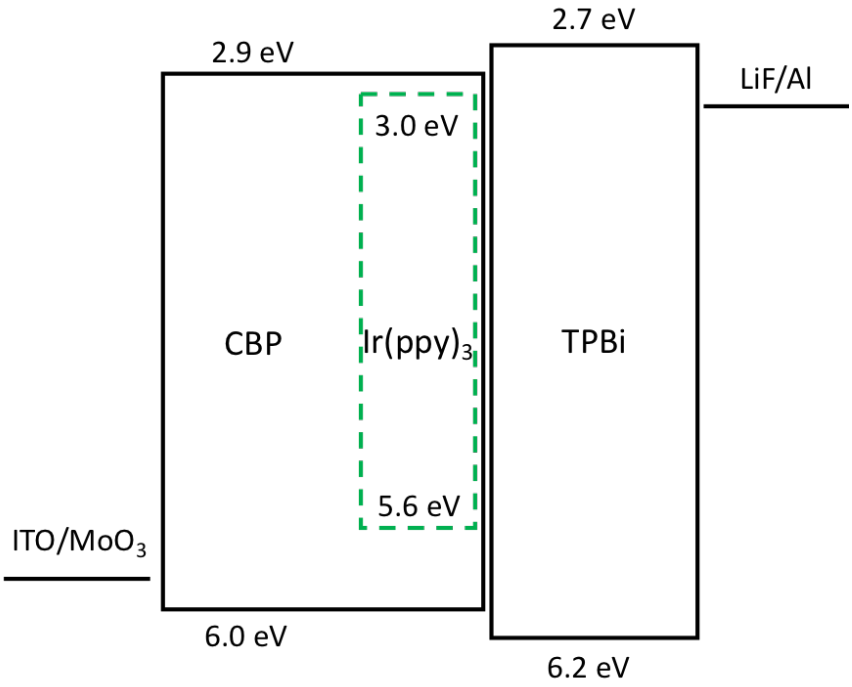

Figure 3.1: Energy level diagram of the standard PhOLED structure.

Table 3.2: List of organic materials that have been employed in this work.

Acronyms	**Chemical names**	**Chemical structures**	**Functions in OLEDs**
BmPyPb	1,3-Bis(3,5-dipyrid-3-ylphenyl)benzene	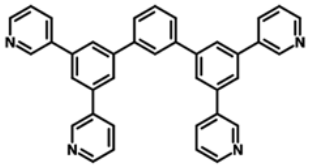	ETL

Bphen	4,7-Diphenyl-1,10-phenanthroline	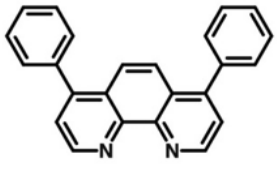	ETL
C545T	10-(2-Benzothiazolyl)-2,3,6,7-tetrahydro-1,1,7,7-tetramethyl-1H,5H,11H-(1)benzopyropyrano(6,7-8-I,j)quinolizin-11-one	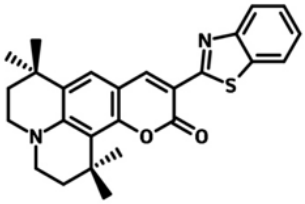	dopant
CBP	4,4'-Bis(N-carbazolyl)-1,1'-biphenyl	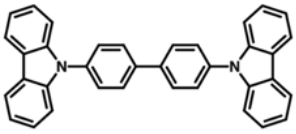	HTL & host
$Ir(piq)_3$	Tris(1-phenylisoquinoline)iridium(III)	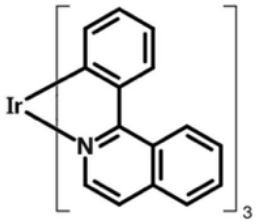	dopant

$Ir(ppy)_3$	Tris(2-phenylpyridine)iridium(III)	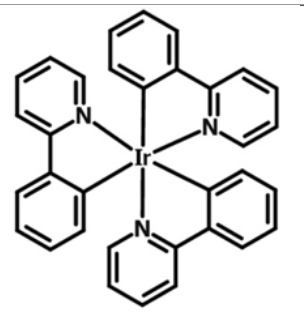	dopant
NPB	N,N'-Di(1-naphthyl)-N,N'-diphenyl-(1,1'-biphenyl)-4,4'-diamine	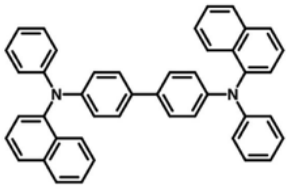	HTL
PEDOT:PSS	poly(3,4-ethylenedioxythiophene) polystyrene sulfonate	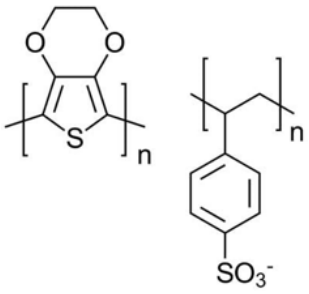	HIL
TaPc	1,1-Bis[(di-4-tolylamino)phenyl]cyclohexane	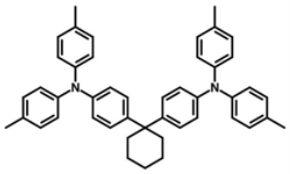	HTL

TPBi	2,2',2"-(1,3,5-Benzinetriyl)-tris(1-phenyl-1-H-benzimidazole)	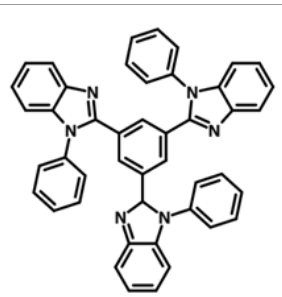	ETL

3.3 Device Characterization

The performance of an OLED is characterized by current density-voltage-luminance (J-V-L) characteristic, EL and device lifetime (EL stability), which are described below. The devices are kept in a N_2 environment during measurements.

3.3.1 Current Density-Voltage-Luminance characteristic

J-V-L characteristic is carried out using an Agilent 4155C semiconductor parameter analyzer connected to a silicon photodiode. When voltage is swept from 0 to 15 V, current density and luminance are recorded simultaneously. With the calculation of these experimental values, current efficiency and EQE can be derived.

3.3.2 EL Spectroscopy

The EL spectra of OLEDs are collected using an OceanOptics QE65000 spectrometer when the devices are driven at $20\,\mathrm{mA\,cm^{-2}}$.

3.3.3 Lifetime (EL Stability) Measurement

The changes in EL intensity and driving voltage versus time are recorded by the testing system from Botest. During the test, the device is continuously driven at a constant current density of $20\,\mathrm{mA\,cm^{-2}}$.

3.4 Material Characterization

The organic luminescence materials are characterized by atomic force microscopy (AFM), Fourier transform infra-red (FTIR) spectroscopy, PL spectrum, polarized optical microscopy (POM), and time resolve photoluminescence (TRPL). During the measurement, the organic films are kept in a N_2 environment.

3.4.1 Atomic Force Microscopy

AFM is used to study surface properties, such as morphology, size, surface roughness, and texture. In this work, AFM is used mainly for surface roughness measurements, and the images are obtained using a Veeco Dimension 3100 atomic force microscope in tapping mode.

3.4.2 Fourier Transform Infra-Red Spectroscopy

FTIR spectroscopy is a form of vibrational spectroscopy and a common technique to determine the chemical structures of organic materials. FTIR spectroscopy is performed using a Bruker Hyperion 3000 with a mercury cadmium telluride detector in the reflectance mode.

3.4.3 PL Spectroscopy

The PL spectra of organic films are collected under an excitation wavelength at 360 nm from a 200 W Hg lamp equipped with an Oriel-77720 monochromator and measured using an OceanOptics QE65000 spectrometer.

3.4.4 Polarized Optical Microscopy

POM is used for the identification of optical properties of crystallized materials. The images are obtained by placing two polarizers in a Leica Ergolux 200 microscope. In transmission mode, the first polarizer is located between the light source and the objective, and the second polarizer is placed between the objective and eyepiece.

3.4.5 Time-Resolved Photoluminescence Measurement

TRPL is performed to measure the exciton lifetime of organic films using an Edinburgh Instruments FLSP920 spectrometer from Edinburgh Instruments.

Chapter 4

Exciton-Induced Morphological Changes in Organic Luminescent Materials

The material in this chapters was published in H. Yu and H. Aziz, "Direct Observation of Exciton-Induced Molecular Aggregation in Organic Small-Molecule Electroluminescent Materials," J. Phys. Chem. C, vol. 123, no. 26, pp. 16424–16429, 2019 and reprinted here with the permission from publisher. Copyright 2019 American Chemical Society.

Exciton-induced material changes during electrical bias is now known to be one common cause of degradation that affects a wide range of OLED materials. We recently discovered that exciton stress can also lead to morphological changes in organic luminescent materials, and that the changes can be accelerated when positive polarons are also present [33, 34, 36, 58, 59]. This phenomenon causes a decrease in the luminescence quantum yield of the materials as well as in host-to-guest energy transfer efficiency, leading to a deterioration in OLED EL efficiency [36]. The occurrence of such exciton-induced molecular aggregation, however, has to date been inferred from indirect experimental observations, such as from changes in the EL and PL spectral characteristics and time-resolved decay rates of the materials involved or from the effects of intermixing a second material on modulating these intermolecular interactions.

In this work, we present direct observations of exciton-induced morphological changes in organic luminescent materials. 2-tert-Butyl-9,10-di(naphth-2-yl)anthracene (TBADN) and CBP are used as representative materials. Thin films of these materials were fabricated by vacuum-deposition or solution-coating and then irradiated by UV illumination as a means to create

excitons in them similar to those created by electrical bias during the normal operation of OLED. Results show that irradiation causes changes in the surface roughness in the TBADN films, giving direct evidence of exciton-induced morphological changes. Associated changes in PL spectral characteristics point to molecular aggregation and thus corroborate these observations. Further tests also show that the irradiated TBADN and CBP films are more susceptible to crystallization by thermal annealing in comparison to non-irradiated films, confirming that the exciton stress brings about morphological changes that facilitate crystallization in these materials later, and suggests the formation of aggregates that can act as nucleation sites for crystal growth. To the best of our knowledge, the results provide the first direct evidence of exciton-induced morphological changes and aggregation in these materials.

4.1 Experimental procedures

In this work, vacuum-deposited and solution-coated CBP and TBADN materials are used. The materials were purchased from Luminescence Technology Corp. and used as received without further purification. All films were fabricated on quartz substrates. For the vacuum-deposited films, the layers were thermally evaporated on the substrates at a rate of $1\,\text{Å}\,\text{s}^{-1}$ at a base pressure of 5×10^{-6} Torr using an Angstrom Engineering EvoVac system. For the solution-coated films, the materials were dissolved in toluene to form $10\,\text{g}\,\text{L}^{-1}$ solution and then were spin-coated on the substrates using a WS-400/500 series spinner from Laurell Technologies Corp. at a spin rate of 500/2000 rpm during 5/25 s. The coated films were then baked at 60 °C on a hot plate in a glove box to remove the solvent and complete the drying process. In all cases, a vacuum deposited MoO_3 interlayer, 5 nm thick, is used in between the quartz substrate and the film for the purpose of improving wetting and film uniformity.

4.2 Direct Observation of Exciton-Induced Molecular Aggregation

Anthracene derivatives are commonly used as blue emitters and host materials in OLEDs. Among them, TBADN is particularly widely utilized, owing to its high quantum yield and limited susceptibility to concentration quenching effects. OLEDs utilizing anthracene derivatives are known to exhibit a red-shift in their EL spectral characteristics over time, an effect that has been attributed to molecular aggregation and dimerization under electrical stress [66, 67, 68]. TBADN is therefore selected as a representative material for investigating exciton-induced morphological changes in organic luminescent materials. Neat TBADN films, 40 nm thick, are subjected to UV illumination of 365 nm peak emission and $2.3\,\mathrm{mW\,cm^{-2}}$ radiation power from a UV lamp for a period of 18 hours in a nitrogen environment. The sample temperature is maintained at room temperature during the illumination test using a cooling fan to ensure illumination-induced heating effects remain negligible. Subjecting TBADN to 365 nm illumination drives the $S_0 \rightarrow S_1$ transition and therefore the UV illumination produces singlet excitons in the similar fashion to those produced by electrical bias when the material is used in an OLEDs. Two groups of samples are fabricated and tested. In one group, the TBADN films are fabricated by vacuum-deposition whereas in the other group they are made by solution-coating. AFM is used to test the surface topography and roughness before and after the UV irradiation, referred to herein as "pristine" and "UV-irradiated" films, respectively. To ensure that any observed changes in film morphology are due to the exciton stress, and not due to temporal changes in the material over the span of the 18 hours or caused by any unintentional thermal effects from the illumination, scans from an adjacent area of the substrate that has been shielded from the UV using black masking tape is also collected in each case and used as a "non-irradiated" control sample. Figure 4.1 illustrates this process. As seen from the AFM scans in Figure 4.2, the surface roughness (Rms) in the case of the pristine and the non-irradiated vacuum-deposited TBADN films is 0.74 nm and 0.68 nm, respectively. By

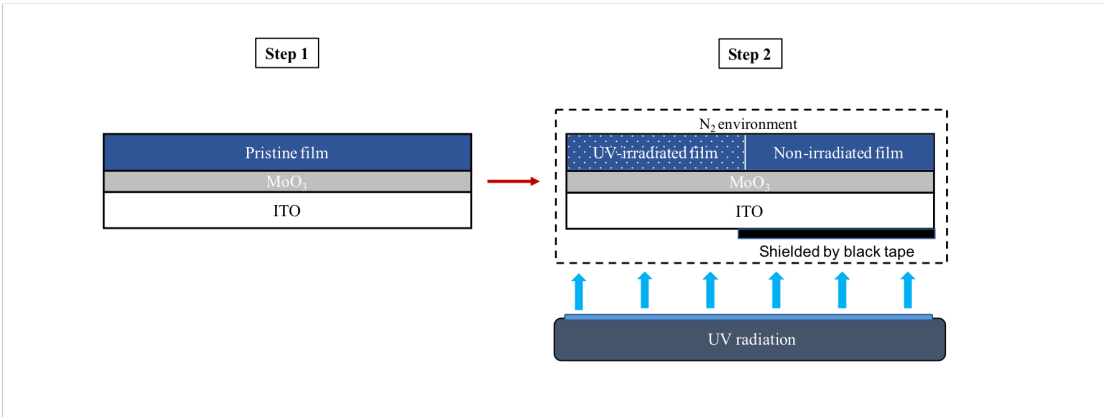

Figure 4.1: Schematic illustration depicting the differences between the "pristine", "UV-irradiated" and "non-irradiated" films described in the text.

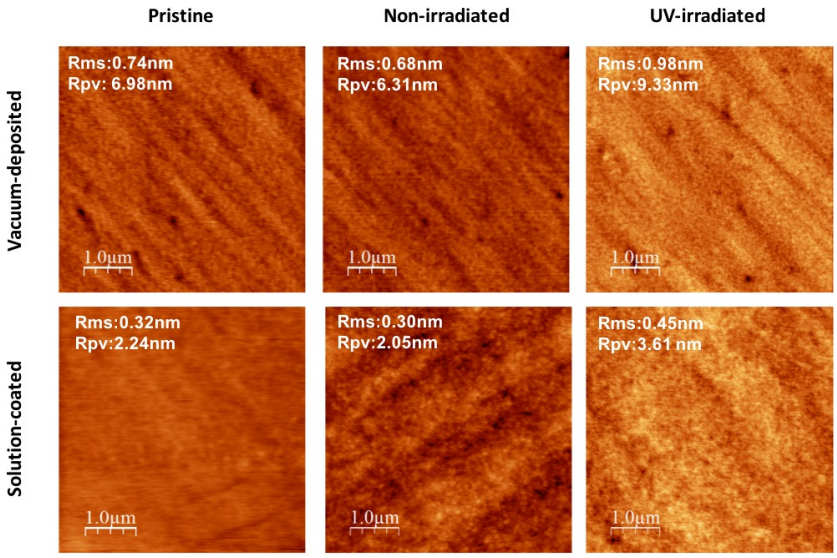

Figure 4.2: AFM surface scans collected from the pristine, non-irradiated and UV-irradiated vacuum-deposited, and solution-coated TBADN films. Rms and Rpv values are indicated on the AFM images.

contrast, the UV-irradiated areas show increased Rms of 0.98 nm. The solution-coated films show similar changes in surface topography under the UV irradiation (Rms of 0.32 nm and 0.30 nm vs. 0.45 nm in the pristine, the non-irradiated, and the UV-irradiated films, respectively). These results clearly show the UV irradiation brings about morphological changes in the films that lead to an increased surface roughness. An increase in roughness suggests that the changes are associated with increased molecular aggregation in the films [69]. The fact that a significant increase in roughness is observed only in the UV-irradiated films and not in the non-irradiated controls indicates that the phenomenon must be driven by the electronic excitation in TBADN molecules produced by the UV and not due to any thermal or temporal effects. These results therefore give direct evidence of exciton-induced molecular aggregation. Such morphological changes could perhaps be driven by the typically higher electronic dipole moment of excited molecules that could lead to increased intermolecular dipole-dipole interactions. One can also expect the increased access of molecules to higher vibrational modes during excitation to afford them more energy to move and thus to reorganize into more thermodynamically favorable, less-disordered molecular aggregates [34]. We also note that the vacuum deposited films have rougher morphologies compared to the solution coated films, probably due to the different morphological make-up of these systems [46, 47].

Seeing that exposure to UV leads to an increase in film roughness, we also investigate the PL characteristics of the pristine films and after the UV irradiation to further verify the hypothesis that the effect is due to exciton-induced aggregation. Figure 4.3 (a) shows typical PL spectra (collected under 330 nm excitation and normalized to max peak intensity) collected from the vacuum-deposited and solution-coated films. The films are denoted by (v) and (s), respectively. As the figure shows, in both cases the PL spectra of the pristine films exhibit the characteristic TBADN singlet emission band (arising from the $S_1 \rightarrow S_0$ transition) whereas the irradiated films show a red shift in their spectra. A similar red shift is usually observed in the EL spectra of TBADN based OLEDs with electrical aging and ascribed to emission from intermolecular

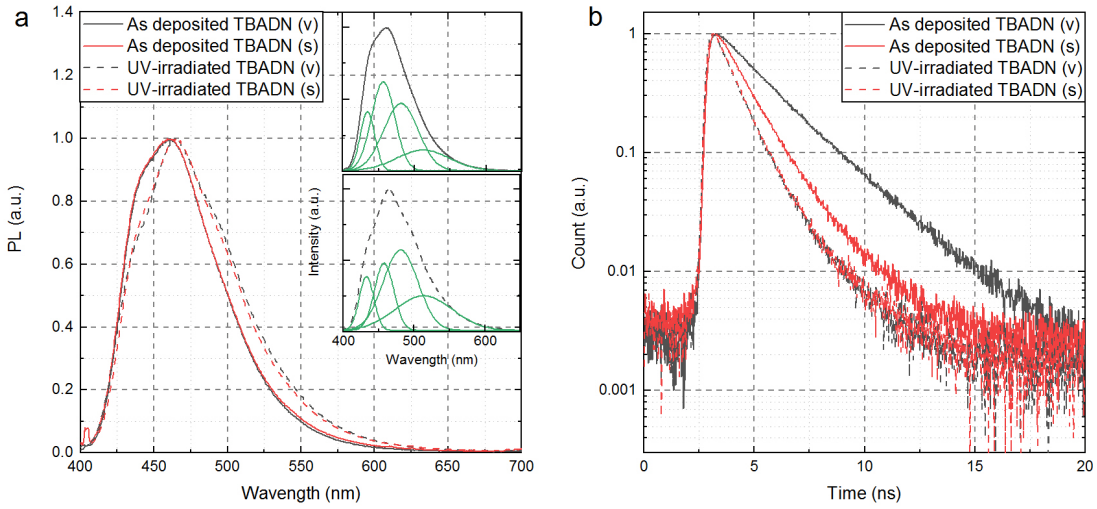

Figure 4.3: (a) Normalized PL spectra and (b) TRPL characteristics of pristine and UV-irradiated TBADN films fabricated by vacuum- deposition and solution-coating. The insets show multi-peak Gaussian fit analysis of the PL spectra of the vacuum-deposited TBADN film.

TBADN species associated with increased molecular aggregation under the electrical stress [68]. A Gaussian multi-peak fit analysis of the spectra produces four distinct bands with peaks at different wavelength, and also shows that the relative height of the two longer wavelength bands increases after the UV irradiation, consistent with the red shift observed in the spectra. This is shown in the insets in Figure 4.3 (a) for the case of the vacuum-deposited TBADN films.

We also collected spectra at 1 min intervals during the first hour and 30 min for the remainder of the 18 hours of the UV irradiation to monitor changes in the PL intensity over time. Figure 4.4 shows the PL intensity at max peak over that period of time normalized to the initial value. Clearly, PL intensity changes over time but not monotonically. After an initial decrease in the first 1 hour, PL intensity starts to increase significantly, before it gradually starts to decrease again relative yet at a much lower rate. Those changes were generally much larger in the case of the solution-coated film. Since a decrease in PL intensity under the same excitation power

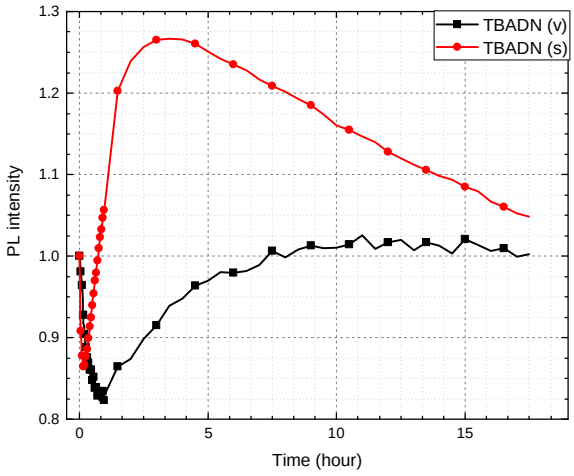

Figure 4.4: Relative PL intensity vs UV irradiation time of TBADN films fabricated by vacuum-deposition and solution-coating.

suggests a decrease in PL quantum yield of the materials, the initial decrease in PL over the first hour suggests a decrease in the PL qunatum yield of the TBADN and is consistent with the decreases in exciton lifetime in both cases. The increase in PL on the other hand can be attributed to increased light scattering due to the morphological changes.

We also carry out TRPL on the same films. Figure 4.3 (b) shows transient PL characteristics at 460 nm vs time under pulsed excitation at 380 nm. TBADN exciton lifetime is shorter in the solution-coated film as compared to the vacuum-deposited film in the case of pristine films, in agreement with previous observations [44, 51]. Remarkably, the TBADN exciton lifetime becomes significantly shorter after the UV irradiation in both cases. A decrease in exciton lifetime is indicative of an increase in exciton quenching rate. An increase in exciton quenching rate is consistent with morphological changes that promote increased bimolecular interactions, such as molecular aggregation and/or dimerization, hence make concentration quenching and/or other bimolecular quenching pathways become more efficient [70, 71]. The decrease in exciton lifetime

after the UV irradiation could also be due to the excess energy of molecules in the excited states that may cause bond cleavage and produce new chemical by-products that can act as quenchers [30, 31].

In order to verify that the red shift in the PL spectra is indeed associated with intermolecular TBADN species, we similarly test and compare between vacuum-deposited TBADN films in which CBP molecules are introduced at 0%, 50%, and 75% (by volume). In this system, the CBP molecules should act as molecular spacers that can separate TBADN molecules from each other and hence prevent their aggregation. At the same time, due to its wider bandgap relative to that of TBADN, energy transfer from TBADN to CBP is inefficient, and therefore excitons continue to be formed on TBADN molecules under UV excitation. Figure 4.5 shows PL spectra collected from these films before and after the irradiation for 40 hours (after being normalized to the max peak intensity). A longer UV irradiation time is used in this case in order to allow for PL spectral changes to become more pronounced and thus to allow seeing differences between the samples more clearly. As can be seen from the figure, introducing the CBP indeed impedes UV-induced spectral shift of TBADN, suppressing it almost completely in the case of 75% CBP. This observation further supports that the PL spectral shift observed in Figure 4.3 (a) is indeed associated with exciton-induced molecular aggregation.

Finding that exposure to UV leads to an increase in surface roughness suggesting that the effect is due to exciton-induced molecular aggregation, and that both PL and TRPL measurements give further credence to this notion, we further test this conclusion by studying the effect of thermal annealing on these films with the purpose of investigating and comparing between their crystallization behavior. Should the UV exposure indeed lead to molecular aggregation, one would expect the irradiated films to be more susceptible to crystallization by thermal annealing due to the likely role of such aggregate domains to function as nucleation sites for crystal growth and hence facilitate crystallization. Therefore UV-irradiated vacuum-deposited and solution-coated films, together with non-irradiated control samples of the same films, are tested by heating them

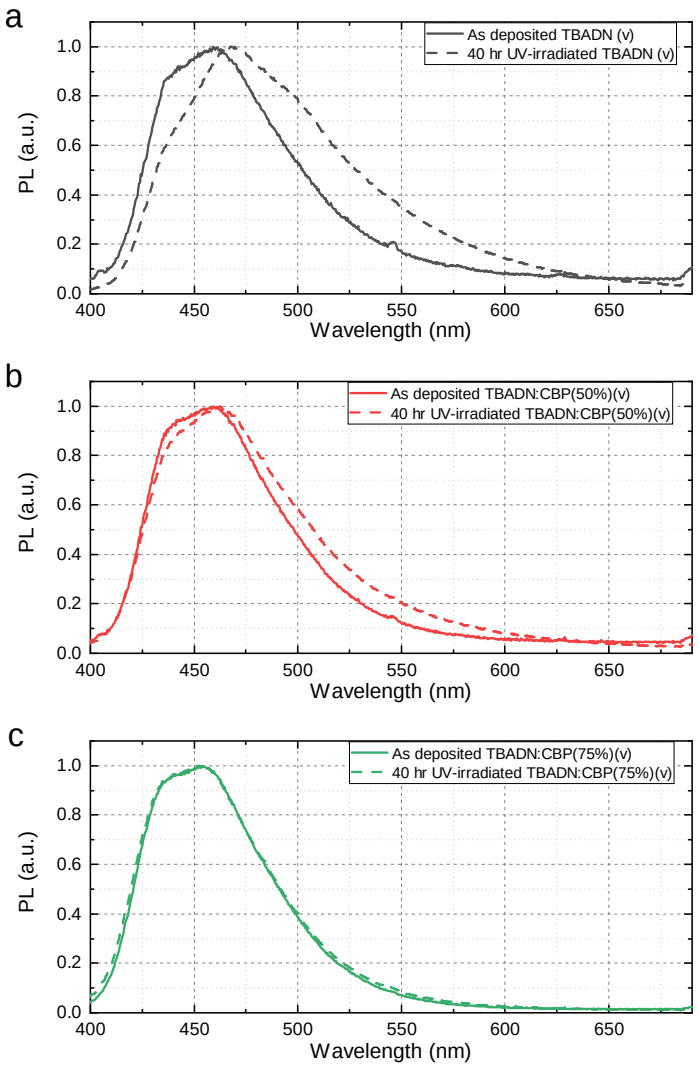

Figure 4.5: Normalized PL spectra of vacuum-deposited TBADN films containing (a) 0%, (b) 50%, and (c) 75% CBP (by volume).

to temperatures above the Tg in order to induce crystallization. Considering that the glass transition temperature (Tg) of TBADN is 110 °C [43]. the films are heated to various increasing temperatures starting at 100 °C in 20 °C steps and holding them at each temperature for 10

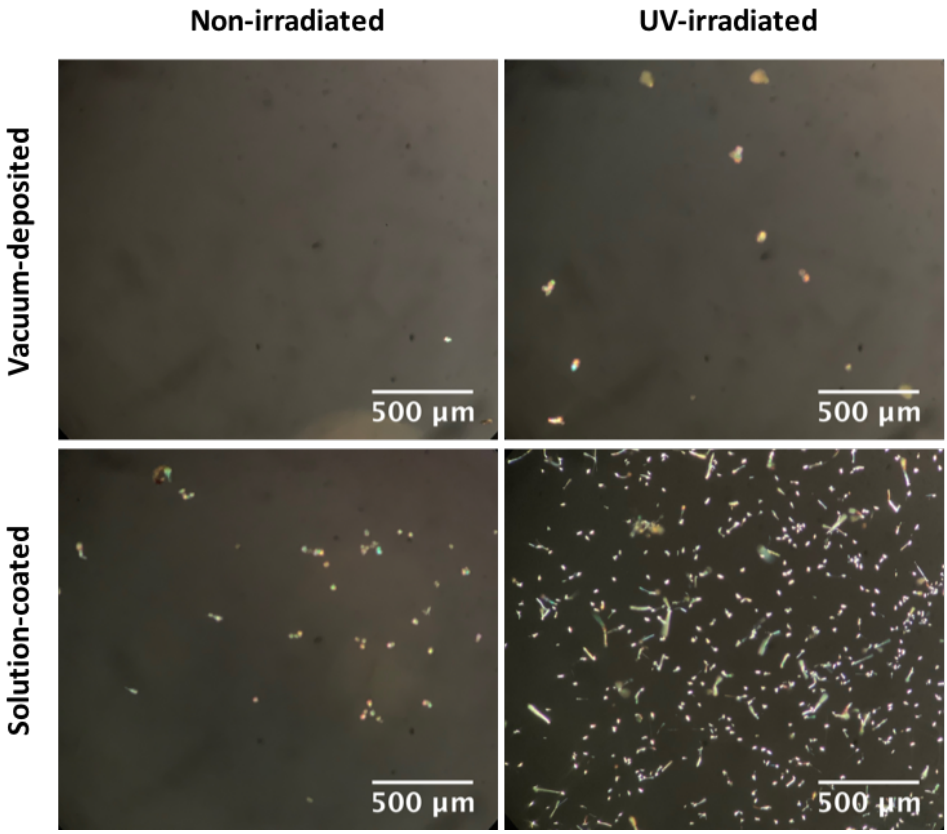

Figure 4.6: POM images of non-irradiated and UV-irradiated TBADN films fabricated by vacuum-deposition and solution-coating.

min. The films are examined for crystallization at the end of each step using POM. In POM, any crystalline phases (with sizes larger than the wavelength of light) will appear bright whereas other phases remain dark. Following this protocol, no crystallization was detected in the films until 240 °C was reached. Figure 4.6 presents the POM images collected from the films upon reaching 240 °C. As can be seen, crystalline domains can be seen in the films to different extents with the UV-irradiated films showing significantly more domains relative to their non-irradiated counterparts. These results conclusively prove that the exposure to UV alters the morphology of the films,

making them more susceptible to crystallization and indicate that the irradiated films must have some pre-existing cites or domains with higher level of molecular ordering (i.e., crystalline aggregates) that facilitate further molecular ordering and crystal growth when the films are heated. Such domains must have been formed due the UV exposure, again pointing to aggregation due to the exciton stress. We also note the much more significant crystallization observed in the case of solution-coated films vs their vacuum deposited counterparts, even in the non-irradiated films. The more significant crystallization not only shows that solution-coated layers are more susceptible to exciton-induced aggregation as was concluded from indirect observations in earlier studies [44] but also that solution-coating produces less uniform morphologies that include regions of localized aggregates among regions of lower molecular packing density as was hypothesized earlier [51, 72]. The results are also consistent with the generally accepted notion that solution-coated films have lower thermal stability relative to vacuum-deposited ones [50]. The results in this work therefore give direct evidence not only of molecular aggregation by exciton stress in organic materials, represented in TBADN, but also of the lower susceptibility of films fabricated to solution-coating to this phenomenon.

Having obtained direct evidence of exciton-induced molecular aggregation in TBADN, we investigate other organic luminescent materials to see if similar effects can be observed. We found out in a previous work that exposing CBP to exciton stress results in changes in their PL spectra and a decrease in exciton lifetime, and also that the effects are stronger in the case of solution-coated films (i.e., a similar behavior to what is observed in Figure 4.3 above with TBADN) [44, 51, 72]. It was hypothesized based on those observations that CBP undergoes exciton-induced molecular aggregation. We therefore similarly tested the effect of thermal annealing on UV-irradiated CBP films as well as non-irradiated control samples for comparison. Two groups of CBP films (30 nm thick) on quartz substrates, with an MoO_3 interlayer, again fabricated using vacuum deposition or solution-coating, are subjected to UV irradiation for 18 hours and the samples are maintained at room temperature using a cooling pan. Identical samples on the

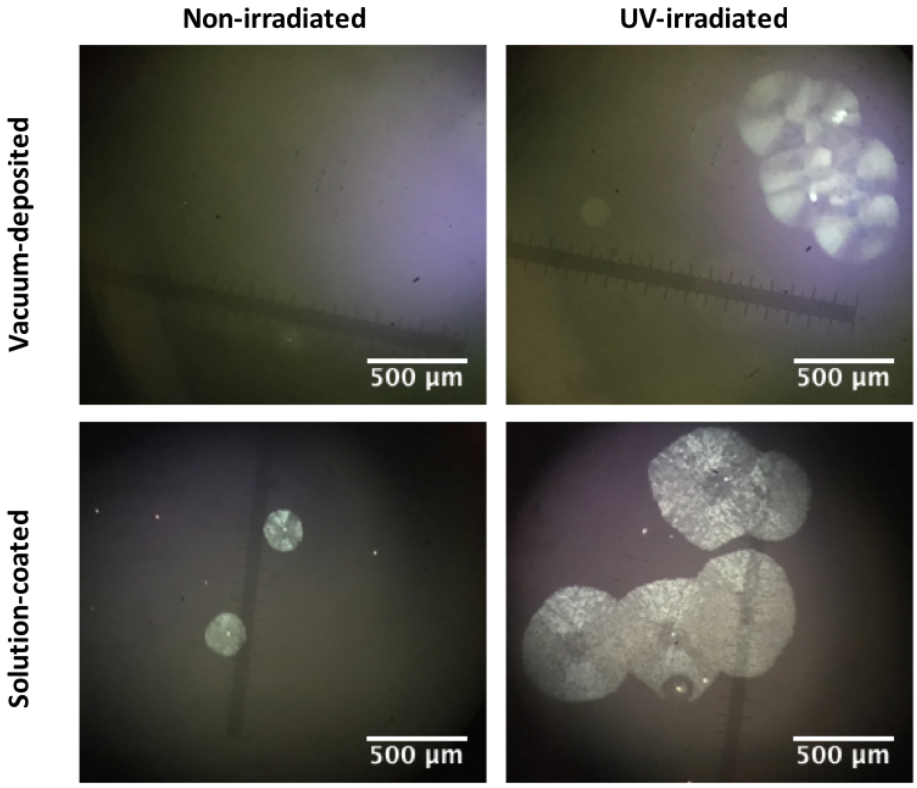

Figure 4.7: POM images of non-irradiated and UV-irradiated CBP films fabricated by vacuum-deposition and solution-coating.

same substrates are shielded from the UV illumination via black masking tape to be used as non-irradiated control films. The films are annealed at various temperatures starting at 60 °C, (the Tg of CBP is 62 °C) [73], until visible crystallinity is observed. Crystallization was first observed upon reaching a temperature of 100 °C and 80 °C in the vacuum deposited and solution-coated films, respectively, where the different onset of crystallization is in line with previous observations [70]. Figure 4.7 shows the POM images collected from the films upon reaching those temperatures. As can be seen, crystalline domains can be detected only in the irradiated samples in the case of the vacuum deposited films whereas all the solution coated films, whether irradiated or not,

showed crystalline domains, with the irradiated ones showing more and larger ones. Clearly this shows that the UV irradiated CBP films undergo crystallization more easily, again pointing to the presence of more nucleation cites for crystal growth. These results show that, like in case TBADN, the earlier exciton stress leads to some molecular aggregation in the CBP films, and hence the formation of these nucleation cites. The results therefore demonstrate that exciton-induced molecular aggregation is not limited to one specific material suggesting the common occurrence of this phenomenon in organic small molecule materials.

4.3 Conclusion

In conclusion, studies on TBADN and CBP films made by vacuum deposition and solution coating give direct evidence of molecular aggregation as a result of exciton stress. AFM measurements show that exposing TBADN films to UV illumination for a prolonged period of time leads to an increase in their surface roughness giving direct evidence of morphological changes and molecular aggregation as a result of excitation. PL measurements show that the exposure to UV leads to a red shift in the PL spectra of the materials and a decrease in exciton lifetime consistent with molecular aggregation. POM tests show that UV irradiated TBADN and CBP films crystallize more easily showing that the UV exposure leads to morphological changes in the films that facilitate their crystallization upon heating. Results also show that solution coated films are more susceptible to exciton-induced aggregation. The results give direct evidence of a phenomenon that has recently been suggested to play a major role in the degradation of OLEDs based on small molecule luminescent materials.

Chapter 5

Effect of Exciton Stress in the Electron Transport Layer

The material in this chapters was published in H. Yu, Y. Zhang, Y. J. Cho, and H. Aziz, "Exciton-Induced Degradation of Carbazole-Based Host Materials and Its Role in the Electroluminescence Spectral Changes in Phosphorescent Organic Light Emitting Devices with Electrical Aging," ACS Appl. Mater. Interfaces, vol. 9, no. 16, pp. 14145–14152, 2017 and reprinted here with the permission from publisher. Copyright 2017 American Chemical Society.

We recently discovered that interactions between excitons and polarons play a leading role in the degradation of these devices during electrical bias [33, 34]. We also found that the accompanying red shift that occurs in the EL spectra of the devices after aging is caused by the appearance of new longer wavelength emission bands that are likely the result of a molecular aggregation process caused by those interactions. The exact origin of those long wavelength bands is however still unclear. For example, long wavelength bands can arise from a variety of intermolecular species including various excimer, exciplex, electromer, and electroplex species [74, 75, 76, 77, 78]. Considering that the electron-hole recombination zone and exciton formation occurs in the vicinity of the EML/ETL interface in a PhOLED during operation, the role of the ETL materials should also be considered in this process.

In this study, we investigate the origin of those degradation-induced long wavelength bands that gradually emerge in the EL spectra of typical PhOLEDs on prolonged electrical bias. For

this purpose, we use devices with neat (i.e., un-doped) EMLs, utilizing the widely used CBP as a model host material. We find that these bands depend on the choice of the ETL material, revealing that the latter influences the EL spectral shifts that occur in PhOLEDs with aging. Results show that both ETL molecules and electrical driving-induced CBP aggregates participate in complex formation, leading to the observed spectral shifts.

5.1 Experimental procedures

In this work, we use CBP as the host and hole transport material, and TPBi, BmPyPb or Bphen as electron transport materials. The materials are purchased from EM Index and Luminescence Technology Corp., and used as received without further sublimation. All devices are fabricated on pre-patterned ITO substrates (purchased from Kintec) via thermal deposition in vacuum (at a base pressure of below 5×10^{-6} Torr) using an Angstrom Engineering EvoVac system. All layers are deposited at a rate of 0.1-1.0 $\text{Å}\,\text{s}^{-1}$. For UV irradiation, 365 nm illumination from a UV lamp at a power density of $2.3\,\text{mW}\,\text{cm}^{-2}$ was used.

5.2 Interactions between the ETL Materials and Exciton-Induced Host Molecular Aggregates

We first study the EL characteristics of a device of the structure ITO/MoO_3 (5 nm)/ CBP (30 nm)/TPBi (40 nm)/LiF (1 nm)/Al (80 nm). In this device, CBP and TPBi are used as EML and ETL materials, respectively. Figure 5.1(a) shows the EL spectra collected before and after electrically driving the device at $20\,\text{mA}\,\text{cm}^{-2}$ for 30 mins. The spectra are normalized to the same maximum height. The initial EL spectrum exhibits the characteristic CBP emission band with a peak at 410 nm, which is herein referred to as the "CBP monomer" band. The spectrum

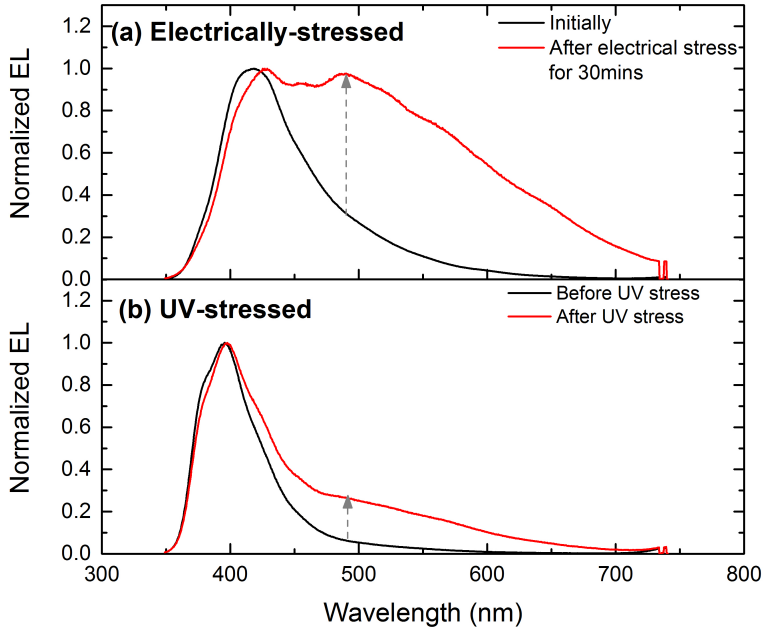

Figure 5.1: EL spectra (normalized to the CBP monomer band intensity) of CBP/TPBi devices subjected to (a) electrical stress through electrical driving at 20 mA cm^{-2} for 30 min and (b) UV stress for 72 hours, collected before and after the stresses.

of the same device after electrical stress shows a second band at 488 nm, which can be attributed to the changes induced by the electrical stress. As both polarons and excitons are created by the electrical bias and to understand which of these two species may be behind the mechanism producing this new band, the same device structure is subjected to UV irradiation for 72 hours (without any electrical bias). In this case, only excitons are present in the device. Figure 5.1 (b) shows the EL spectra before and after the UV irradiation. Similar to the electrically-stressed device, the initial EL spectrum shows the CBP monomer band at 400 nm, whereas a new band at 490 nm again emerges after the UV irradiation. The observation that both electrical stress and UV irradiation can induce the appearance of the new band suggests that excitons are the

primary stimulus behind its appearance. The fact that the intensity of the new band is higher in the case of the electrically stressed device may suggest that the underlying mechanism, although it is driven by excitons, is accelerated by the presence of polarons, possibly because of exciton-polaron interactions [33]. The higher intensity may also be simply due to the higher exciton density produced by the electrical bias in comparison with that produced by the UV irradiation.

According to Wang et al., the new longer wavelength band is likely associated with the molecular aggregation of CBP [33]. However, because excitons play a role in the EL spectra shift and CBP molecules may undergo chemical (photo) degradation, it is possible that the new band may instead be caused by species resulting from chemical decomposition of CBP. It has been shown by Kondokov et al. that C-N bond cleavage in CBP can occur under UV irradiation, resulting in a gradual decrease in its PL quantum yield [30]. At 50% loss in PL yield, the fraction of decomposed CBP molecules was estimated to be around 21% (estimated from changes in IR spectra in the 1300-1600 cm^{-1} range where C-N bond stretching modes exist) [79]. Therefore, to test for any chemical decomposition in our samples due to UV irradiation under the conditions used in Figure 5.1 (b), we use FTIR measurements. Figure 5.2 shows the IR absorption spectra from a 100 nm CBP film (coated on a KBr substrate) before and after UV irradiation for 72 hours (i.e., the same irradiation conditions as those used with the device shown of Figure 5.1 (b). The PL quantum yield of the CBP drops by around 80% after the irradiation, suggesting (based on the above studies) that the fraction of decomposed molecules would exceed 21% and should, therefore, be detectable using FTIR. The test results however show no detectable changes in the IR spectra. Particularly, no new peaks are detectable in the spectra after the UV irradiation. Thus, the FTIR results suggest that any chemical decomposition in CBP as a result of UV irradiation must be insignificant. It can, therefore, be concluded that the new emission bands in Figure 5.1 arise primarily from the morphological changes rather than due to chemical changes in the CBP films.

To further prove that the new band in Figure 5.1 is indeed associated with the CBP inter-

molecular interactions (i.e., aggregation), we test the effect of introducing TPBi into the CBP EMLs on the EL spectra of the devices and their evolution with time. Figure 5.3 exhibits the collected EL spectra during electrical driving at 20 mA cm^{-2} for 30 mins of devices of the structure ITO/MoO_3 (5 nm)/CBP:TPBi (x%) (30 nm)/TPBi (40 nm)/LiF (1 nm)/Al (80 nm) with TPBi concentrations of 0%, 5%, and 25% (by volume). As expected, the device without TPBi mixing shows the CBP monomer band in its initial EL (exact bands vary among devices in the range of 400-420 nm, which we can attribute to the changes in microcavity effects because of small variations in the device thicknesses). The new longer wavelength band at 488 nm emerged after 1 min and got stronger over time as given in Figure 5.3 (a). On the other hand, the new

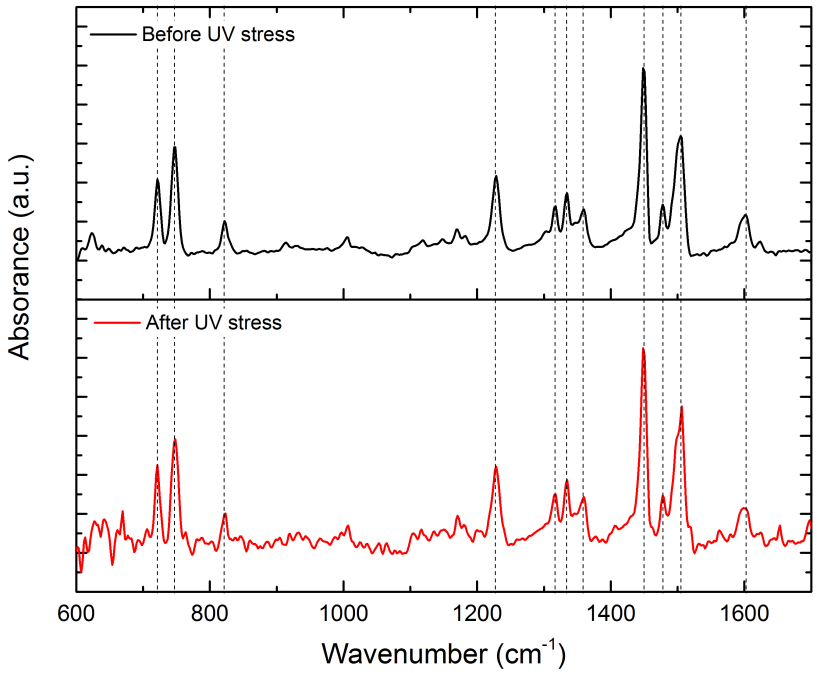

Figure 5.2: FTIR spectra of CBP film, collected before and after subjecting it to the UV stress for 72 hours.

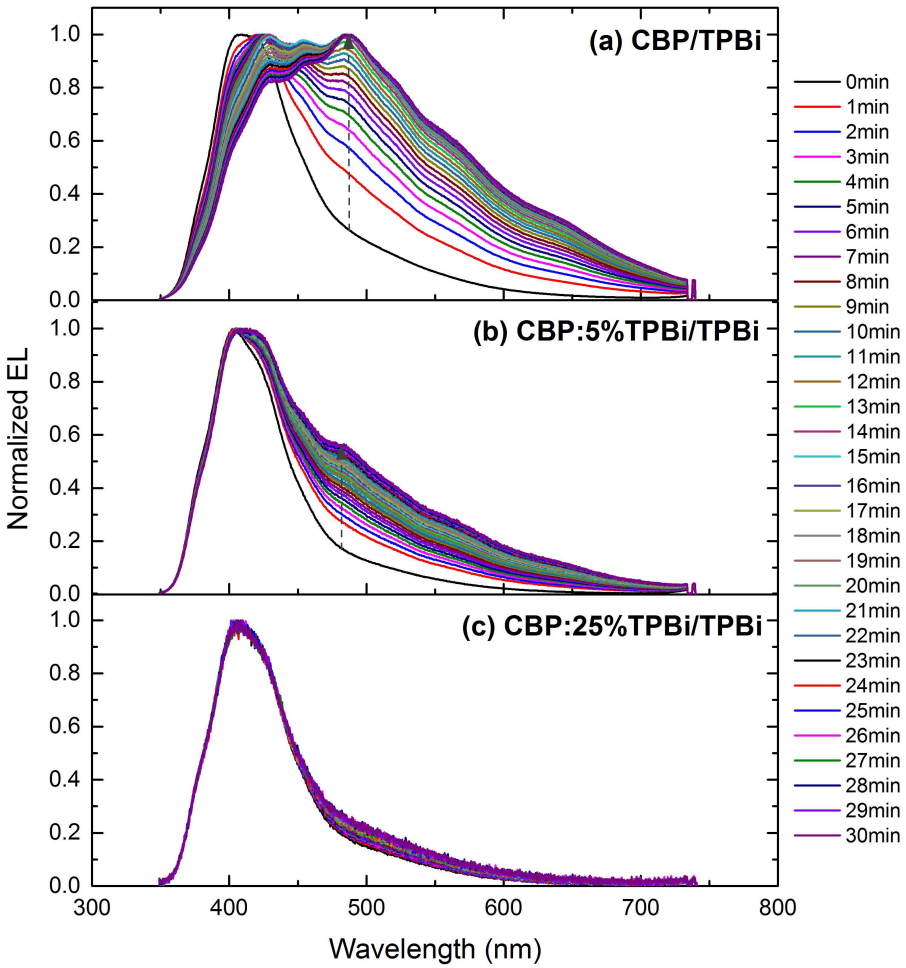

Figure 5.3: EL spectra of CBP/TPBi devices where CBP layers mixed with TPBi [(a) 0%, (b) 5%, and (c) 25% by volume], collected after electrical driving at 20 mA cm^{-2} for certain periods of time.

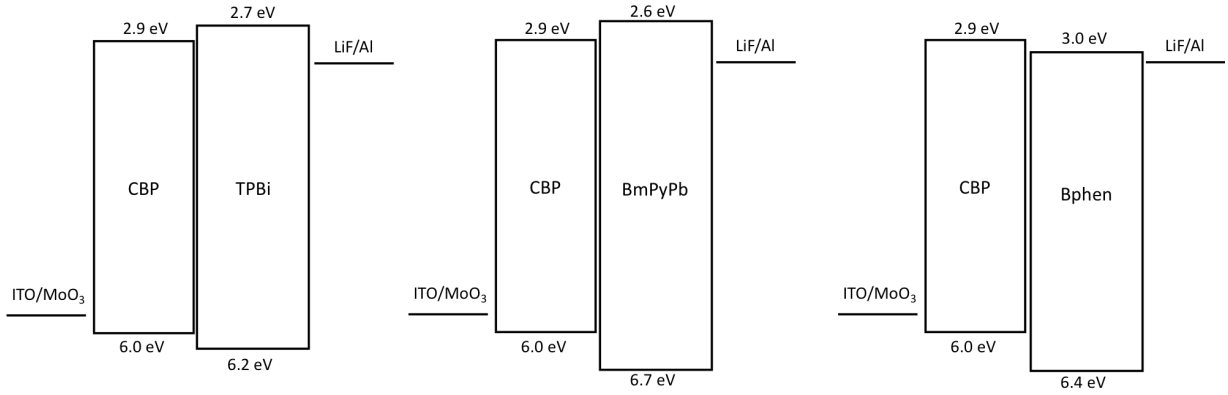

Figure 5.4: Energy level diagrams of the devices described in the text.

band is much weaker in the case of 5% TPBi mixing (Figure 5.3 (b)) and is completely suppressed with a 25% concentration (Figure 5.3(c)). The suppression of the new band can be attributed to the role of TPBi molecules in acting as molecular spacers that separate CBP molecules from each other and thus prevent their dimerization or aggregation. This observation further supports the conclusion that the new long wavelength band is associated with increased intermolecular interactions between CBP molecules.

We have now determined that CBP molecules aggregate and contribute to the emergence of the new band when they are exposed to excitons. Next, to gain more insights into the nature of the species behind the new band and whether ETL materials play a role in it, we study the effect of varying the ETL material on the changes in EL spectra of the devices during a prolonged electrical bias. For this purpose, we investigate devices that have the same EML material but three different ETL materials. The device structure is ITO/MoO_3 (5 nm)/CBP (30 nm)/ETL (40 nm)/LiF (1 nm)/Al (80 nm). In these devices, CBP is used as the EML material, and the three different ETL materials are TPBi, BmPyPb, and Bphen. The schematic energy diagrams of the devices are displayed in Figure 5.4. These devices are electrically driven at 20 $\mathrm{mA\,cm^{-2}}$ for a period of 30 mins and their EL spectra were collected periodically during that time. Figure

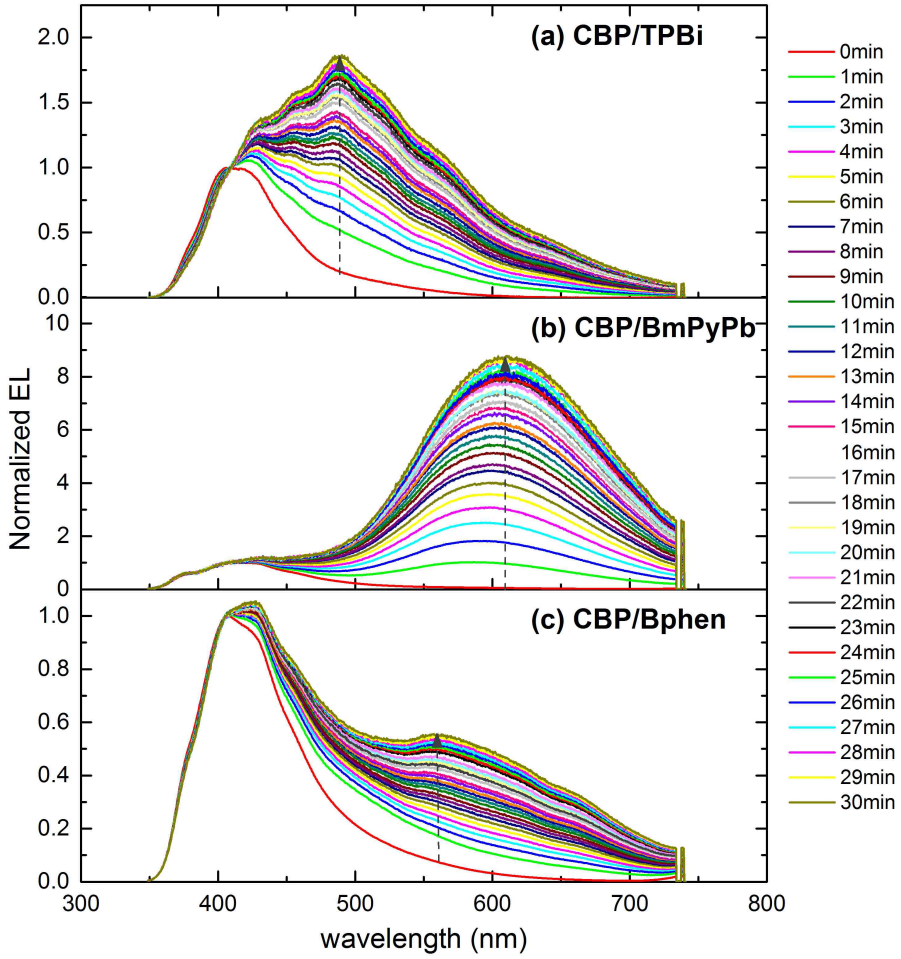

Figure 5.5: EL spectra (normalized to the CBP monomer band intensity) of CBP/ETL devices with (a) TPBi, (b) BmPyPb, and (c) Bphen ETLs, collected after electrical driving at 20 mA cm^{-2} for certain periods of time.

5.5 presents the collected spectra after being normalized to the CBP monomer emission band. As can be seen, the initial EL spectra of all devices are similar, with peaks at around 405 nm, which corresponds to the CBP monomer band. As time progresses, a new emission band emerges at a longer wavelength in each case. In the case of the device with the TPBi ETL, the new band had a peak at 488 nm as before and become stronger over time, resulting in significant EL spectra change with time. On the other hand, the peak wavelength of the new band was at 612 nm and 562 nm for devices with the BmPyPb and Bphen ETLs, respectively. The fact that the wavelength of the new band spectra does not correspond to any emission from either CBP or ETL materials and varied with ETL materials suggests that the new bands may originate from some complex species involving both CBP and ETL molecules [80]. We note that there is no clear correlation between the emission wavelength of such complex species and the LUMO level of these ETL materials. This suggests that factors other than the energy offset between the ETL LUMO and the CBP HOMO play a role in forming this complex. The geometry of the ETL material molecules and the intermolecular separation between the ETL and CBP molecules may perhaps be important factors in this regard.

To investigate whether these new bands indeed arise from CBP/ETL complex, the EL characteristics of devices without an ETL were studied. For this purpose, single organic layer devices with the structure ITO/MoO_3 (5 nm)/CBP (30 nm)/LiF (1 nm)/Al (80 nm) were fabricated and tested. These devices were driven at a constant current density of 125 $mA\,cm^{-2}$ for 18 hours. (a five times higher current density than that used for aging the bilayer CBP/ETL devices was used here because of the highly unbalanced electron/hole ratio in these devices which results in a significant fraction of hole current leakage to the counter electrode and a lower density of electron-hole recombination and thus both a lower EL efficiency and slower degradation under electrical bias.) Figure 5.6 shows the EL spectra collected from these devices after various intervals of time under electrical stress. As can be seen from the figure, the normalized EL spectra show only the CBP monomer band at 403 nm, but none of the long wavelength bands observed

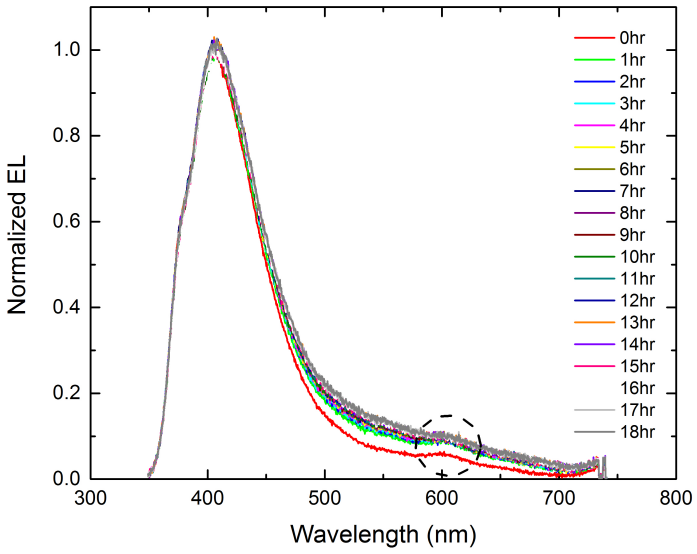

Figure 5.6: EL spectra (normalized to the CBP monomer band intensity) of single CBP organic layer device, collected after electrical driving at 125 mA cm^{-2} for certain periods of time.

in Figure 5.5. Moreover, the EL spectra show an additional emission band at 603 nm. The broad 603 nm band is a longer-wavelength band than that of the CBP monomer and does not appear in PL spectra, suggesting that the band corresponds to an electromer band associated with a dimer excited state that gets formed only under electrical bias [75]. The appearance of this band in single CBP-layered devices is consistent with the formation of CBP-CBP dimer species under electrical driving. Unlike the CBP/ETL devices, however, the EL characteristics do not show the 488 nm, 612 nm, or 562 nm bands observed in the bilayer devices with the TPBi, BmPyPb and Bphen ETLs, respectively, in the case of Figure 5.5, even after prolonged electrical driving, proving that the appearance of those bands requires the presence of the ETL materials. The results ,therefore, seem to further suggest, at least on first sight, that those bands indeed arose from the CBP/ETL complexes.

Seeing that those long wavelength bands emerge only in devices that contain ETLs and that their peak position varies depending on the choice of the ETL material, we further investigate whether they indeed arise from CBP/ETL material complexes. Toward this end, we investigate the effect of intermixing the ETL material with the CBP to see whether it would similarly induce the formation of such a complex (and hence the appearance of the same bands) as would be expected in such cases. We therefore fabricated and tested devices of the following structure: ITO/MoO_3 (5 nm)/CBP:TPBi(x%) (30 nm)/LiF (1 nm)/Al (80 nm) with TPBi concentrations of 0%, 5%, 25%, and 50% (by volume). The EL spectra collected after various time intervals of electrical driving at 125 mA cm^{-2} are shown in Figure 5.7 (a)-(d). Figure 5.7 (e) depicts the rate of growth of the new band in each device (defined as the ratio of the height of the new band to the height of the monomer in each device after the various driving times). Figure 5.7 (a) shows the EL spectra of the single CBP layered device without TPBi mixing. Similar to Figure 5.6, all EL spectra show the CBP monomer band at 403 nm and the electromer band at 603 nm. As can be seen from Figure 5.7 (b) and (c), the presence of TPBi molecules (at 5% and 25% by volume, respectively) in the single CBP layer grants the appearance of the 488 nm band after electrical driving, in agreement with that in Figure 5.1, pointing to the formation of the complex as expected. The increase in intensity of the new band with the TPBi concentration from 0% to 25% indicates that this new band grows faster as the number of TPBi molecules increases, as given in Figure 5.7 (e), demonstrating that the band indeed arises from the CBP/TPBi complex. Quite surprisingly, however, further increasing TPBi to 50% leads to an opposite effect and prevents this band from appearing, suggesting that the production of the CBP/TPBi complex is suppressed by the high TPBi concentrations. This can be seen in Figure 5.7 (d) where, in contrast to the low-TPBi concentration devices, the CBP:50% TPBi layer device exhibits only the 403 nm CBP monomer emission band. This unusual trend indicates that whereas TPBi is necessary for the appearance of this band, a high CBP concentration (>50%) is also necessary for the production of this complex, suggesting that the complex may in fact involve an aggregated (or dimerized) CBP species, that is, a CBP_{ag}/TPBi complex where CBP_{ag} represents the CBP

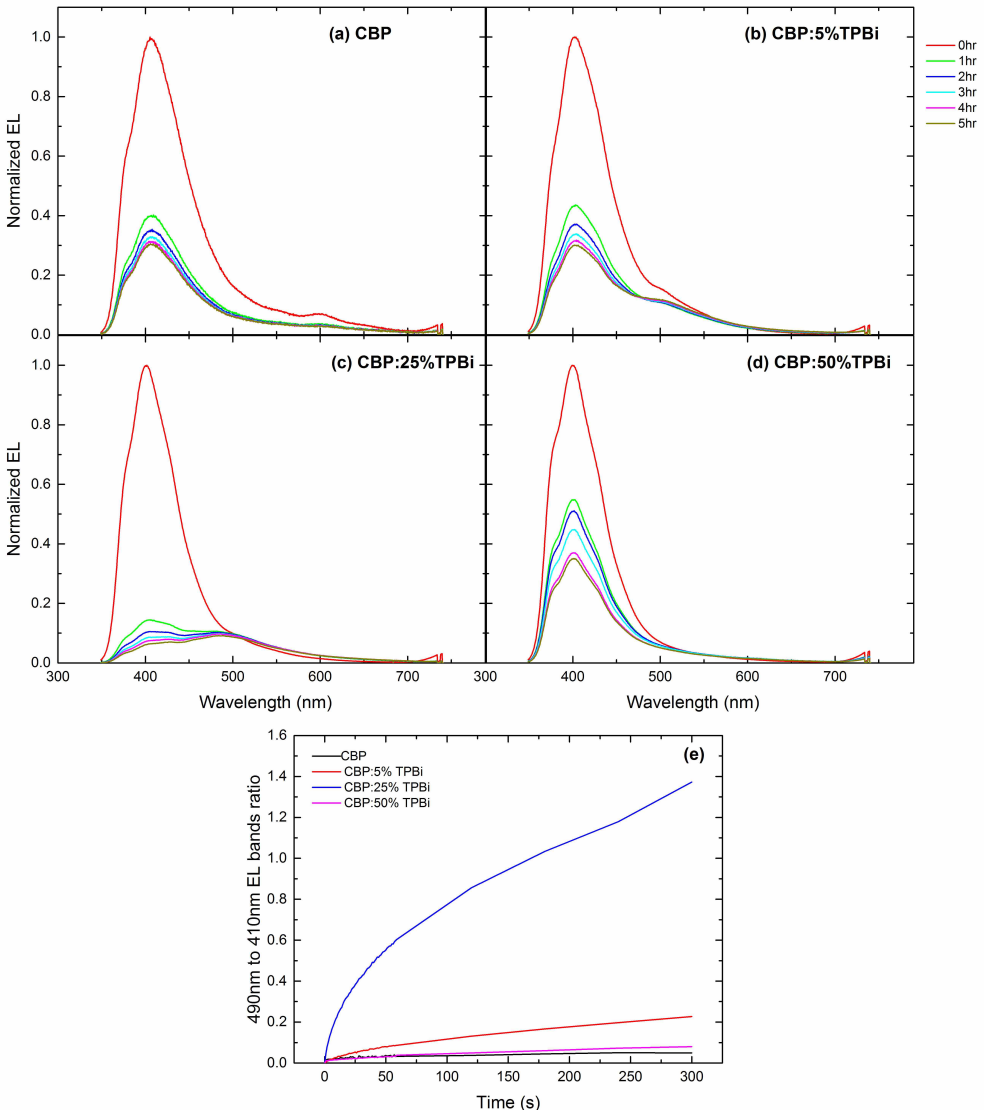

Figure 5.7: EL spectra of single organic layer devices with CBP mixed with TPBi [(a) 0%, (b) 5%, (c) 25%, and (d) 50% by volume], collected after electrical driving at 20 mA cm^{-2} for certain periods of time. (e) Change in 490 nm to 410 nm band ratio in the devices.

dimer or aggregate. In this context, increasing TPBi concentration inhibits the formation of the CBP_{ag} species, resulting in no complexation and no new band. Also, as can be seen from the four figures, the CBP electromer band at 603 nm disappeared completely upon introducing the TPBi (appears only in Figure 5.7 (a), the device with no TPBi), suggesting that the emission from the CBP-CBP electromer is replaced by an emission from the CBP_{ag}/TPBi complex as TPBi is introduced in low concentrations. This CBP_{ag}/TPBi complex band shows a time-increasing property, which is evident from the fact that it did not exist initially. The increase in its emission intensity with time reflects an increasing population of the complexes with time [81]. This may perhaps be attributed to the molecular reorganization and reorientation (which is necessary for the CBP_{ag} species formation) which is known to have a slow response time [82].

To further test the complexation behavior between the CBP_{ag} species and TPBi molecules and to investigate the influence of excitons in inducing it, neat CBP layers are subjected to excitons via either electrical stress or UV irradiation, using for this purpose single CBP layer devices of the structure ITO/MoO_3 (5 nm)/CBP (30 nm)/LiF (1 nm)/Al (80 nm). After the stress, the LiF/Al layers are peeled off using Scotch tape inside of a glove box (because the adhesion between organics and LiF/Al is the weakest among all device inter-layer interfaces of the device, the technique allows removal of the LiF/Al contact without compromising the underlying layers [83, 84].), and TPBi (40 nm)/LiF (1 nm)/Al (80 nm) layers are then deposited on the stressed CBP layers. Thus, the final devices are bilayer devices that comprise pre-stressed CBP layers and pristine TPBi layers. (A device in which the CBP layer was not pre-stressed was also included to be used as a reference.) The final devices are then electrically driven and their EL spectra are collected. Figure 5.8 (a) depicts the various steps of this experiment, whereas Figure 5.8 (b) shows the initial EL spectra collected from the final devices. The EL spectrum of the device with the pristine (i.e. un-stressed) CBP layer shows the usual CBP monomer band without any other new bands. In the devices with the pre-stressed CBP layers, however, significant spectral broadening in the 500 nm region is clearly visible. This indicates that excitons induce the formation of aggregate

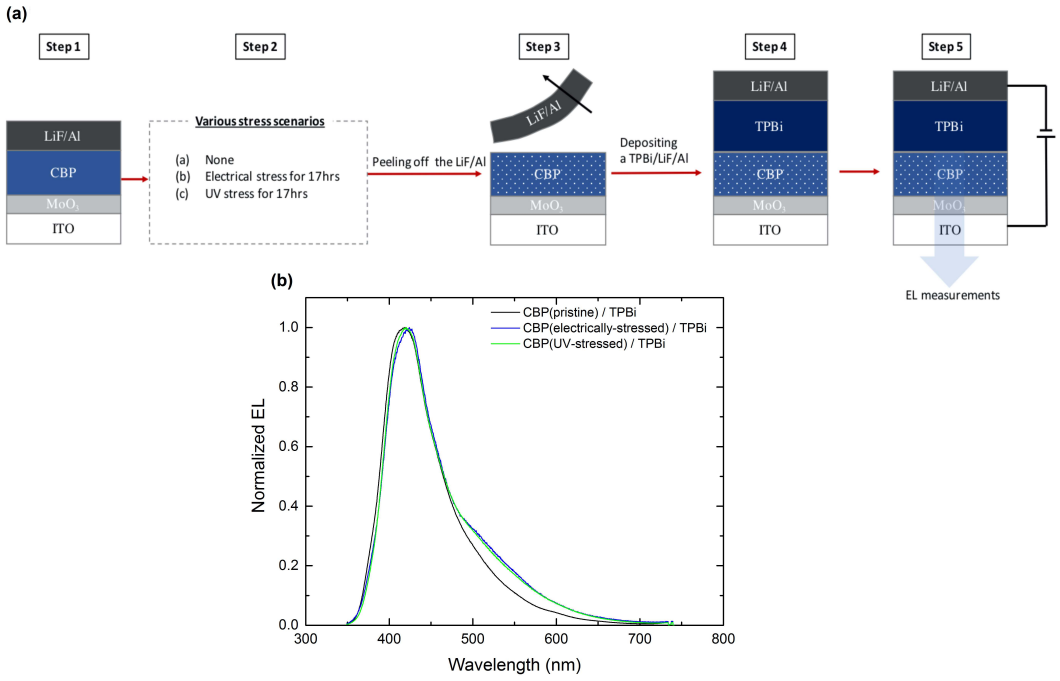

Figure 5.8: (a) Illustration of the conversion of single- to double-layer devices, in which single CBP-layer devices were subjected to various stress scenarios and then converted to double-layer devices with TPBi/LiF/Al layers. (b) Initial EL spectra of the double layer devices in step 5.

species within the CBP layer, that is, CBP_{ag} species (consistent with them being essentially CBP dimers or aggregates) but that the presence of such species becomes detectable (emissive) only when TPBi molecules are introduced (hence allows the emissive CBP_{ag}/TPBi complex species to be created, in this case across the CBP/TPBi interlayer interface). It should be noted that EL spectral measurements on the single layer devices (Figure 5.6) after electrical stress do not show such bands. That excitons can induce molecular dimerization or aggregation may perhaps be attributed to the increased electronic dipole moment of the excited molecules, which may promote intermolecular dipole-dipole interactions, which, in turn, may induce molecular reorientation and reorganization [34].

Knowing that excitons induce aggregation in CBP and that the latter leads to complexation with ETL material molecules, thermal stress was applied and compared with electrical stress and UV irradiation to verify whether they exhibit similar effects on the morphological changes of the CBP film. Single CBP layer devices with the structure ITO/MoO_3 (5 nm)/CBP (30 nm)/LiF (1 nm)/Al (80 nm) were treated under different stress scenarios: (a) no stress, (b) electrical stress under a current density of 125 mA cm^{-2} for 18 hours, (c) irradiation by UV light for 18 hours, and (d) thermal stress by heating at 100 °C for 1 hour (this temperature is above the Tg of CBP, 62 °C [73], and thus would lead to CBP aggregation). Devices with the three pre-stressed CBP layers were compared to one with a non-stressed CBP layer, denoted here as "pristine" CBP. As before, the LiF/Al layers were peeled off from the devices after the stress, and then TPBi (40 nm)/LiF (1 nm)/Al (80 nm) layers were deposited. Figure 5.9 shows the EL spectra collected from these devices under electrical driving of 20 mA cm^{-2} after different time intervals (as earlier, the spectra were normalized to the CBP monomer band). As expected, the pristine CBP/TPBi device showed a CBP monomer band at 420 nm initially, whereas the emergence of the 500 nm CBP_{ag}/TPBi complex band occurred over time (Figure 5.9 (a)). The EL characteristics of the UV and the electrically stressed devices were almost identical and had an EL trend similar to that of the pristine device (Figure 5.9 (b) and (c)) except that the CBP_{ag}/TPBi complex bands grew much faster. The rapid increase in the complex band in these devices is not surprising and can be attributed to the fact that CBP aggregation had already been initiated earlier during the stressing of the CBP film, and thus complexation with the TPBi occured relatively faster compared with that in the pristine CBP device. On the other hand, the EL spectra of the thermally stressed CBP/TPBi device (Figure 5.9 (d)) exhibited only a slight increase in the complex band, much less than that in the other devices. This suggests that thermal stress brings about certain morphological changes in CBP that may result in a decrease in its susceptibility to exciton-induced aggregation later. The different behavior in the exciton-stressed devices versus the thermally-stressed devices suggests that the aggregated species might be different in the two cases, where, for example, CBP aggregation induced by excitons is limited to short range

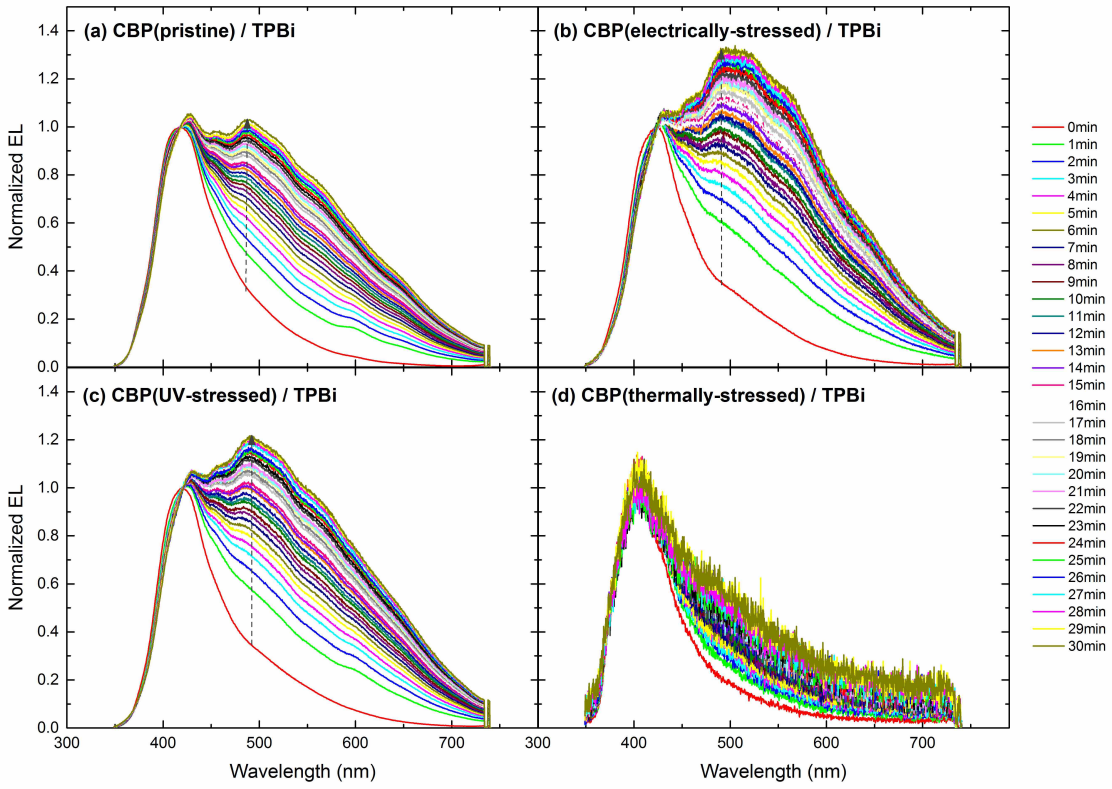

Figure 5.9: EL spectra (normalized to the CBP monomer band intensity) of pretreated CBP/TPBi devices [(a) pristine, (b) electrically stressed, (c) UV- stressed, and (d) thermally stressed CBP layers], collected after electrical driving at 20 mA cm^{-2} for certain periods of time.

molecular ordering or "pairing" that produces strongly interacting intermolecular species (e.g, dimer or trimer species), compared with the longer-range molecular ordering (crystallization) in the case of thermal stress.

For a better understanding of the CBP morphologies, the topographies of the CBP films under the same four different stress scenarios are given in Figure 5.10. As can be seen, the

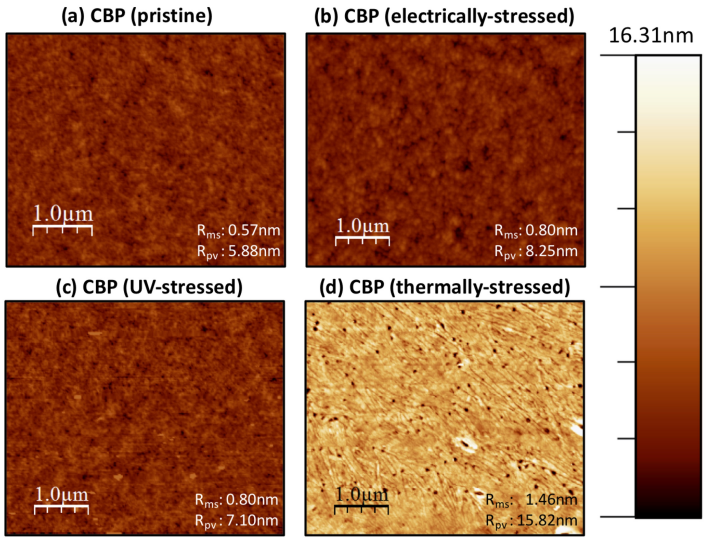

Figure 5.10: AFM images of the pretreated CBP layers [(a) pristine, (b) electrically stressed, (c) UV-stressed, and (d) thermally stressed] after peeling off the LiF/Al layers. Rms and Rpv values are indicated on the AFM image.

morphologies of the UV irradiation and the electrically stressed CBP films are almost identical to those of the pristine CBP film, whereas those produced by thermal stress are distinctly different. The Rms 0.7 ± 0.1 nm and peak-to-valley roughness (Rpv) 7.0 ± 1.0 nm are obtained for the pristine, the UV irradiated and the electrically stressed CBP films. By contrast, the thermally stressed CBP film presents crystalline features with many pin holes in it. Hence, the Rms value of 1.5 nm and Rpv value of 15.8 nm are doubled, compared with those of the other CBP films. Clearly, the thermal stress clearly leads to long-range crystallization in CBP, whereas both UV irradiation and electrical stress do not. This is consistent with a scenario where the CBP_{ag} species induced by excitons have only a short-range order, perhaps consisting of only a few CBP molecules each and thus are below what can be detected by AFM. The EL characteristics and

the AFM images, therefore, show that CBP aggregation induced by excitons differs from that induced by the thermal stress.

5.3 Conclusion

In conclusion, the long wavelength bands that appear in the emission spectra of CBP are found to be caused primarily by molecular aggregation in the material, induced by excitons. Although the aggregation occurs primarily in the host material, complexation between these aggregates and the ETL material occurs and influences the location of this band and hence the spectral shifts that occur. Comparisons between the effects of exciton and thermal stress suggest that exciton-induced aggregation may be limited to short-range molecular ordering or pairing (e.g., dimer or trimer species formation) versus longer range ordering (crystallization) in the case of thermal stress. The findings provide new insights into exciton-induced degradation in wide band gap host materials and its role in limiting the stability of PhOLEDs.

Chapter 6

Effect of Exciton Stress in the Hole Transport Layer

The material in this chapters was published in H. Yu and H. Aziz, "Exciton-Induced Degradation of Hole Transport Layers and Its Effect on the Efficiency and Stability of Phosphorescent Organic Light-Emitting Devices," Adv. Opt. Mater., vol. 7, no. 5, p. 1800923, Mar. 2019 and reprinted here with the permission from publisher. Copyright 2018 WILEY-VCH Verlag GmbH & Co. KGaA, Weinheim.

A proper management of excitons within the EML has been found to be crucial for realizing long OLED lifetimes [60, 85]. Aside from the EML where most excitons are created in an OLED, a non- negligible fraction of excitons can also be present in other device layers, especially those adjacent to the EML such as the HTL and the ETL. And although it is generally known that device stability is strongly influenced by the choice of hole transport layer materials [61, 62, 86], the influence of excitons in those layers on device performance and stability has received little attention. Interactions between excitons and positive polarons can also lead to morphological changes in various OLED materials [33, 34, 58] suggesting that they may also affect charge transport layers, especially HTLs where a high concentration of positive polarons is normally present during device operation. However, the effect of excitons on the HTLs and their influence on device efficiency and stability has not been studied.

In this work, we investigate the effect of exciton-induced degradation of HTLs and its influence on the efficiency and stability of PhOLEDs, using for that purpose the archetypical PhOLED hole

transport material CBP. In order to be able to determine and isolate contributions from only the HTLs, we use UV illumination during device fabrication as a means to expose only certain parts of the HTLs to exciton stress. The results reveal that exciton stress of only the HTLs can lead to a significant deterioration in the EL EQE and stability of PhOLEDs, revealing the detrimental role of exciton-induced degradation of HTLs in limiting device performance.

6.1 Experimental procedures

In this work, we use CBP as the host and hole transport material, TPBi as the electron transport material, TAPC as the electron blocking material. For emitter materials, $Ir(ppy)_3$, $Ir(piq)_3$ and C545T are used. The materials are purchased from Shanghai Han Feng Chemical Co. and Luminescence Technology Corp. and used as received. All devices are fabricated on ITO substrates (purchased from Kintec) via thermal deposition at a rate of 0.1-1.0 $\text{Å}\,\text{s}^{-1}$ at a base pressure of below 5×10^{-6} Torr using an Angstrom Engineering EvoVac system. For UV radiation, a 365 nm illumination from a UV lamp at a power density of $2.3\,\text{mW}\,\text{cm}^{-2}$ was used.

6.2 Exciton-Induced Degradation in the HTL and Its Influence on Device Performance

Zhang et al. have shown that extending the doping to the entire HTL of a PhOLED can lead to significant improvements in EL stability [60]. The effect was attributed to a lower exciton density due to an extended exciton formation zone, hence a reduction in degradation by bimolecular exciton-exciton and exciton-polaron interactions [60]. In order to further investigate this effect, we first study and compare between the EL stability of PhOLEDs in which the HTL was undoped, partially-doped or fully doped. For this purpose, we fabricate green PhOLEDs of the general

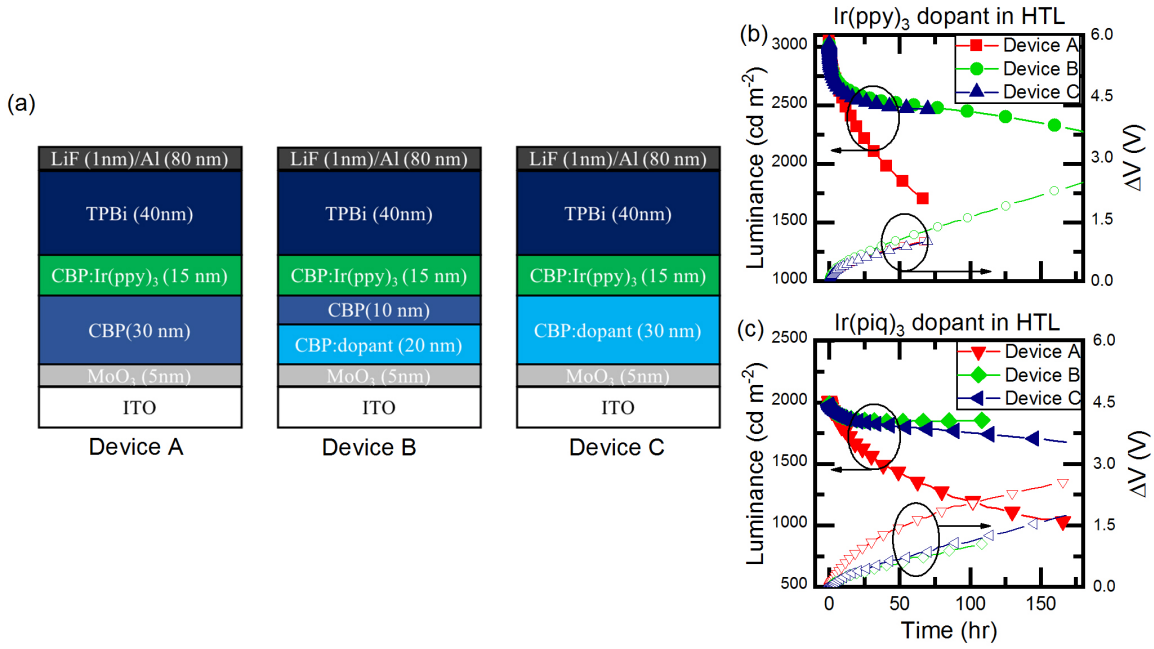

Figure 6.1: (a) Schematic illustrations of the three device configurations described in the text.The dopant in the HTL is either $Ir(ppy)_3$ or $Ir(piq)_3$ at 5% (by volume).(b) and (c) changes in EL intensity and driving voltage (= driving voltage-initial driving voltage) versus time for devices using $Ir(ppy)_3$ dopant in the HTL and $Ir(piq)_3$ dopant in the HTL, respectively, under a constant current density.

structure ITO/MoO_3 (5 nm)/HTL (30 nm)/CBP:$Ir(ppy)_3$ (5%) (15 nm)/TPBi (40 nm)/LiF (1 nm)/Al (80 nm), in one of three different HTL configurations, as depicted in Figure 6.1 (a). In device configuration A, the entire HTL was made of neat (i.e., undoped) CBP, and the device is used as a control device. In device configuration B, the HTL consisted of two layers; CBP: dopant (5%) (20 nm)/CBP (10 nm). In device configuration C, the entire HTL was doped at 5% by a dopant. $Ir(ppy)_3$ was used as the dopant in one set of devices whereas $Ir(piq)_3$ was instead used in a second set of devices. The EL characteristics of these devices under electrical driving at a current density of $20\,mA\,cm^{-2}$ are summarized in Table 6.1. Figure 6.1 (b) and (c)

Table 6.1: (a) Voltage, luminance, CIE coordinates, and EQE at a current density of 20 mA cm^{-2} of the devices described in the text.

Device	$Ir(ppy)_3$ dopant in HTL				$Ir(piq)_3$ dopant in HTL			
	Voltage (V)	Luminance (cd m^{-2})	CIE (x,y)	EQE (%)	Voltage (V)	Luminance (cd m^{-2})	CIE (x,y)	EQE (%)
A	5.70	8900	(0.281, 0.627)	12.03	5.92	8610	(0.283, 0.628)	11.54
B	7.92	4280	(0.290, 0.626)	5.72	8.85	1490	(0.485, 0.477)	3.67
C	8.15	3930	(0.290, 0.626)	5.23	7.49	1900	(0.495, 0.468)	4.53

present the EL intensity and changes in driving voltage (= V-V_0 where V and V_0 represent the driving voltage at any time t and the initial driving voltage, respectively) versus driving time at a constant current density that gives an initial luminance L_0 of 3000 cd m^{-2} and 2000 cd m^{-2} from these two sets of devices, respectively. In these measurements, the same initial luminance (as opposed to the same current density) is used in order to obtain a comparable initial exciton population among the devices of each set. Clearly from the figure it can be seen that device configuration C leads to much more stable EL performance in comparison to the control device configuration (device A), in line with observations by Zhang et al. [60]. Interestingly, the same effect was observed irrespective of the dopant used in the HTL. More notably and surprisingly however, device configuration B demonstrates a similar stability to device C despite the presence of an undoped layer in between the EML and the doped portion of the HTL. Although at first glance one might attribute the higher stability of device C relative to device A to an extended exciton formation zone, the fact that device B also displays a comparable stability despite the presence of an undoped layer, which would expectedly lead to an interrupted, and hence a less extended exciton formation zone relative to device C, suggests that other factors may be involved in the increased stability of devices with doped HTLs.

We have recently found that a significant fraction of excitons is often present in the HTLs

of OLEDs, and that their presence there can induce additional degradation modes that shorten device EL lifetime [87, 88, 89]. In general excitons can exist in the HTL of an OLED via one of two pathways: (i) the formation of excitons in the HTL via recombination of leaked electrons from the EML and injected holes from the anode; or (ii) the diffusion of excitons from the EML. Considering that such pathways would expectedly be affected by the introduction of dopants in the HTL, it is reasonable to suspect that these excitons (i.e., the ones in HTL) may play a role in the different stability behavior of the devices above.

Therefore, to investigate if the presence of excitons in the HTL may induce changes that influence device EL performance and stability, we test the effect of subjecting various portions of the HTL to exciton stress for various periods of time, using optical excitation as a means for creating these excitons. For this purpose we use devices of the structure: ITO/MoO_3 (5 nm)/CBP (x nm)/*UV*/CBP (30-x nm) /CBP:$Ir(ppy)_3$ (5%) (15 nm)/TPBi (40 nm)/LiF (1nm)/Al (80 nm). In making these devices, the MoO_3 and the first CBP layer (of thickness x nm) are deposited on the ITO substrate. The device fabrication process is then interrupted, and the deposited layers are exposed to UV radiation of 365 nm peak emission and 2.3 $mW\,cm^{-2}$ radiation power from a UV lamp for a given period of time in a nitrogen environment (denoted by *UV* in the above device structure description). Afterwards, the deposition of the remaining layers (including, if applicable, a second CBP layer (of thickness 30-x nm)) is resumed in order to complete device fabrication. Figure 6.2 (a) illustrates this process. This approach allows not only to isolate and study the effect of exciton stress in HTLs alone (i.e. without it being confounded by the effect of exciton stress on EMLs as well as is always the case with electrical driving) on device performance but also to investigate the effect of exciton stress, selectively, in certain parts of the HTLs. First, we study the effect of forming excitons in the entire HTL for various periods of time on device performance. For this, a series of devices in which the entire HTL is exposed to UV (i.e. x=30 nm), but for various periods of time (1, 3, 14, 21 or 40 hours) are fabricated and tested. To ensure that any changes in device performance are caused by the photoexcitation and

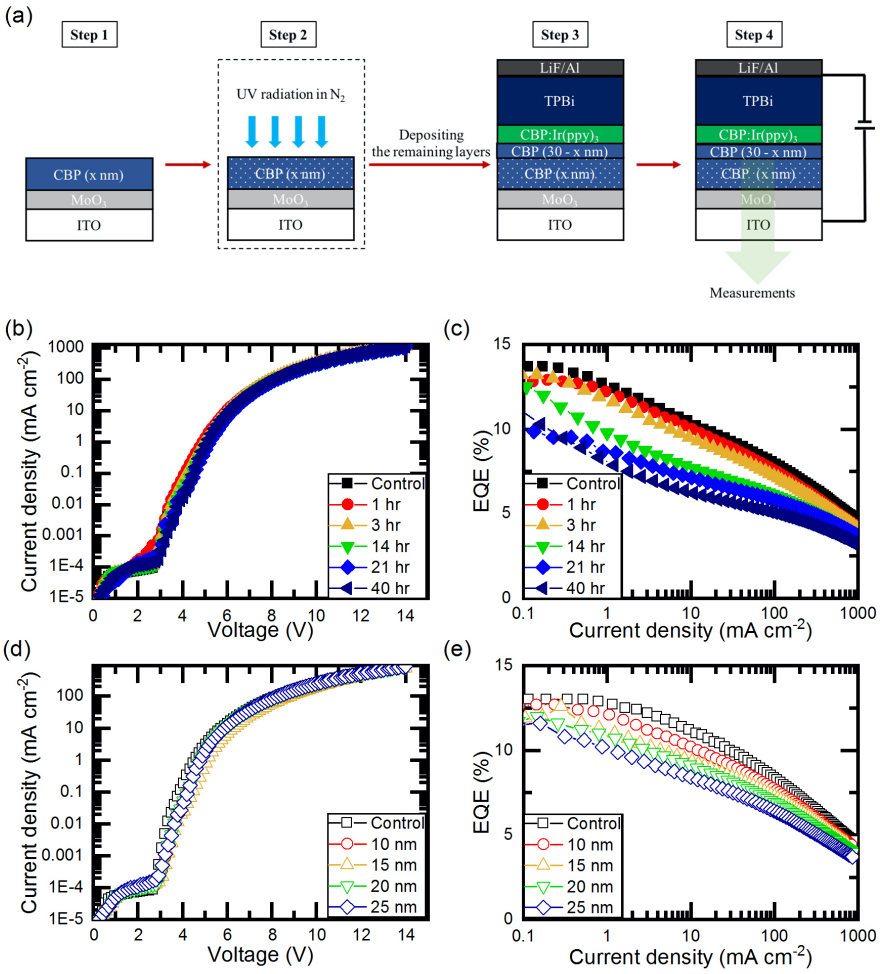

Figure 6.2: Schematic illustrations of the device fabrication and testing sequence including the UV exposure step. (b) J–V and (c) EQE characteristics of devices in which the entire HTL is exposed to UV for various periods of time (1, 3, 14, 21, or 40 hours). (d) J–V and (e) EQE characteristics of devices in which various portions of the HTLs are exposed to UV (x = 10, 15, 20, or 25 nm). Data from control devices with unexposed HTLs are also included.

not simply due to confounding factors associated with breaking the vacuum and/or fabrication interruption, a device with the same fabrication interruption step but without the UV exposure is also fabricated and tested to serve as a control device. Figure 6.2 (b) shows the J-V characteristics of these devices. It can be seen that the characteristics of the devices are very similar, indicating that the exciton stress of the HTL does not significantly alter charge injection or transport in it. In contrast, EQE also shows a significant decrease with UV exposure time in Figure 6.2 (c). Since the only difference among the devices is the UV exposure time, it follows that the decrease in EQE must be caused by the earlier exposure of the HTLs to the UV (i.e. by some change or degradation in the HTL caused by the exciton "stress").

In general, two factors could lead to such a decrease in EQE; (1) a change in hole injection or transport in the HTL that leads to a deterioration in charge balance, and, as a result, in exciton formation efficiency; or (2) an increase in luminescence quenching in the organic stack due to the creation of non-radiative quenching sites. The similar J-V characteristics suggests that charge injection and transport is not significantly altered by the exciton stress as pointed out earlier, in turn suggesting that the second factor must play a more dominant role in the decrease in EQE. Therefore, in order to verify this hypothesis, we measure PL from the control device and the device in which the entire HTL is exposed to UV for 40 hours. Figure 6.3 shows the PL spectra under 365 nm excitation, showing the characteristic $Ir(ppy)_3$ emission as expected. The relative peak heights are proportional to the PL output intensity in each case and show that the PL was 18% lower in case of device with the UV-exposed HTL in comparison to the control. As both spectra are collected under the same excitation power density, the lower PL intensity of the device with the UV-exposed HTL reflects a lower quantum yield, pointing to increased luminescence quenching in this device and verifying that the exciton stress of the HTL leads to the formation of quenching sites that subsequently reduce the PL yield of the EML, and hence the EQE. The inset of Figure 6.3 presents the EL spectra of the same devices, showing no significant spectral shifts.

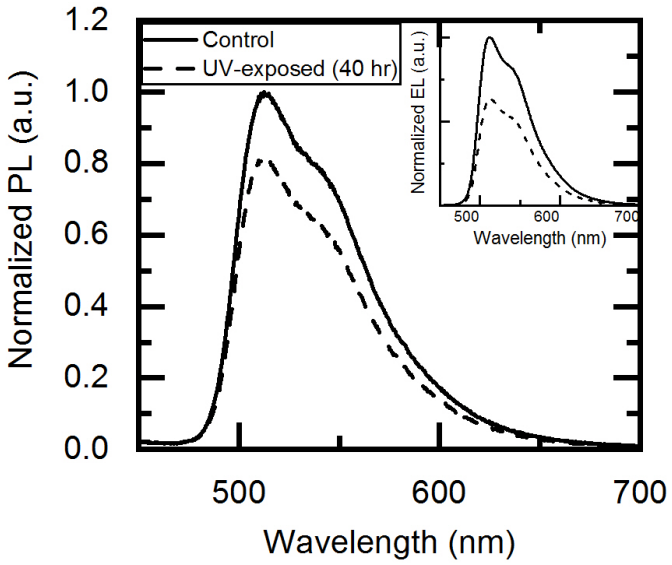

Figure 6.3: PL spectra collected under 365 nm excitation from a device with an HTL exposed to UV for 40 hours and from an unexposed control device. The peak highs are proportional to the PL output intensity each case. The inset shows EL spectra collected from the same devices at 20 mA cm^{-2}.

Next, we study the effect of exposing only the lower portion of the HTL to exciton stress. For this experiment, another series of devices in which x=10, 15, 20 or 25 nm are fabricated and tested following the same approach (where again x represents the thickness of the CBP portion exposed to the UV, with the balance of the 30 nm overall HTL thickness deposited after the UV exposure). In this case, the UV exposure is done for the same amount of time (42 hours) in all devices. Figure 6.2 (d) and (e) show the results from these devices. As with the previous set, these devices again have similar J-V characteristics. As can be seen, their EQE decreases as the thickness of the UV-exposed portion of the CBP layer increases. The results clearly indicate that exposing the HTL to UV, thereby to exciton-stress, causes some changes (i.e., degradation) in them, which in turn leads to a decrease in device EQE.

Finding that exciton-induced degradation of the HTL can reduce device EQE and PL efficiency, identifying the mechanism by which changes in the HTL can impair device efficiency becomes both crucial and interesting. Given their less efficient PL and at the same time similar J-V characteristics, the decrease in EQE can be primarily attributed to increased luminescence quenching as opposed to differences in charge balance among the devices as pointed out earlier, and suggests that the exciton-stress must lead to the formation of non-radiative quenching sites (which could be physical, such as the creation of non-radiative states due to morphological changes like aggregation or grain boundary formation, or chemical by-products, as a result the exciton-stress) in the HTL, and that these quenchers are capable of reducing the EML luminescence. It is known that exciton-stress can lead to both morphological and chemical changes in OLED materials resulting in a decrease in their quantum yield [51, 58]. Because in our devices both the HTL and EML host are made of the same material (i.e., CBP), there is no energy barrier at the HTL/EML interface to prevent the drift of electrons from the EML into the HTL or the diffusion of excitons between the two layers. It is therefore possible that a significant fraction of electrons drift into the HTL during the normal operation of an OLED where they can recombine with holes to form excitons. These excitons can subsequently diffuse to the EML and contribute to device EL output. In this context, the formation of quenchers in the HTL can cause the non-radiative deactivation of some of these excitons, thereby reduce the number supplied to the EML, and, as a result, reduce OLED EQE. Alternatively, it is possible that a fraction of excitons that are created on the EML host molecules diffuse back and forth between the two layers before they eventually get harvested, radiatively, on guest sites in the EML. The creation of quenchers in the HTL would provide non-radiative deactivation pathways for some of these excitons, hence reduces the fraction that will diffuse back to the EML to contribute to device EL, and, as a result, cause EQE losses. Regardless of which of these two scenarios plays a more dominant role in the observed EQE loss, they both involve the diffusion of excitons from the HTL to the EML. This may explain how degradation in the HTL, even in "remote" regions that are not in direct contact with the EML, can lead to OLED EQE losses. Therefore, in order to verify

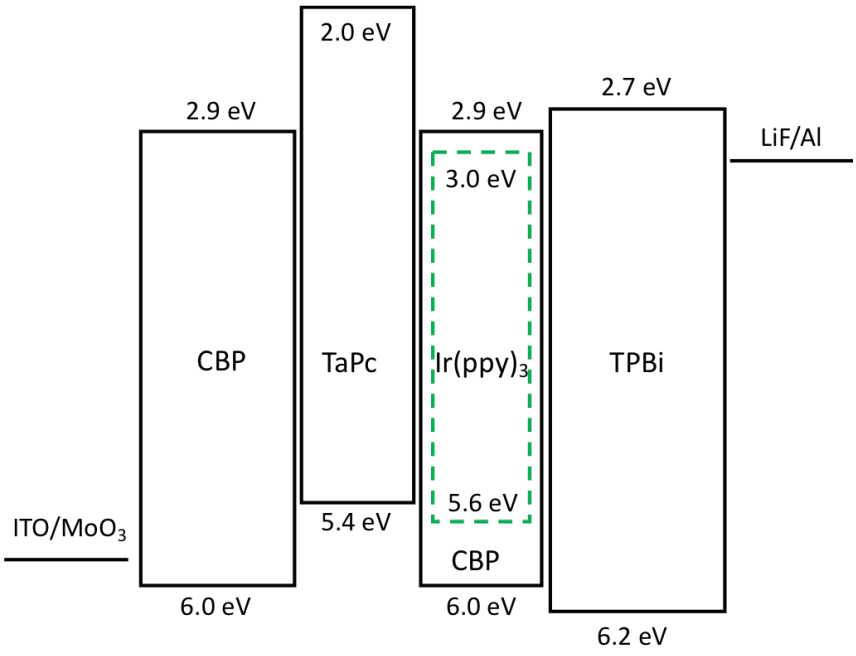

Figure 6.4: Energy level diagram of the device described in the text.

whether the diffusion of excitons from the HTL to the EML indeed plays a role in the observed EQE loss, we insert an exciton blocking layer (EBL) between the two layers. In such case, one would expect the presence of quenchers in the HTL to no longer have a significant effect on device EQE. TAPC is selected for the EBL due to its wider energy band gap than those of both the host and guest materials which makes it effectively block the diffusion of excitons in between the HTL and EML. The structure of this device is ITO/MoO_3 (5 nm)/CBP (20 nm)/*UV*/TAPC (10 nm)/ CBP:Ir(ppy)$_3$ (5%) (15 nm)/TPBi (40 nm)/LiF (1 nm)/ Al (80 nm). The schematic energy level diagram of the device containing a TAPC exciton blocking layer are displayed in Figure 6.4. As with the previous device, fabrication was interrupted after depositing the 20 nm CBP HTL deposition, and the deposited layers are exposed to UV radiation for 42 hours. Once again, a control device fabricated using the same process but without the UV exposure step is tested for comparison. Figure 6.5 (a) presents J-V characteristics of those devices again show-

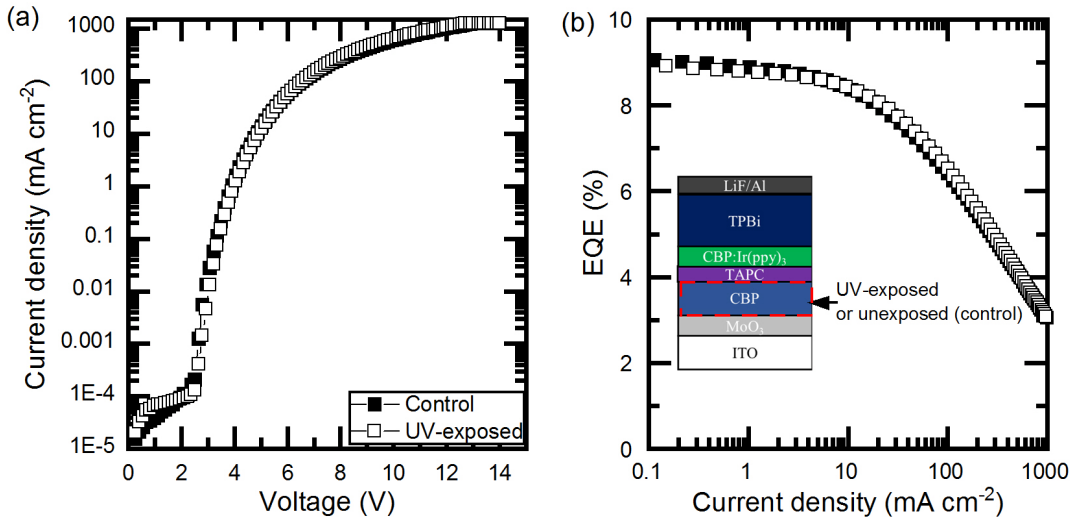

Figure 6.5: (a) J–V and (b) EQE characteristics of a control device and a device with a UV-exposed HTL, both containing a TAPC exciton-blocking layer. Device schematic is provided in (b).

ing the almost identical traces for the exciton-stressed and the control devices. A look at their EQE characteristics (in Figure 6.5 (b)) indeed shows that, contrary to the previous cases, the two devices exhibit almost identical EQE characteristics. These results confirm that stopping exciton diffusion from the HTL to EML indeed prevents the decrease in device EQE from HTL degradation (by the earlier exciton stress) proving that the diffusion of excitons from the HTL to EML indeed contributed significantly to device electroluminescence output when the EBL was absent, and hence to the EQE losses observed in the earlier cases.

Having established that the diffusion of excitons plays a key role in allowing degradation in the HTL to negatively impact device EQE, and seeing that degradation in relatively "remote" regions of the HTL, as far as 20 nm away from the EML, can still impact device EQE, it follows that excitons with relatively long diffusion lengths (>20 nm) must be involved. As the diffusion length of singlet excitons is typically limited to 5-10 nm whereas that of triplet excitons can be

orders of magnitude longer [89, 90], it is possible that triplet excitons play a leading role in this efficiency loss mechanism. To investigate whether this might be the case, we conduct similar tests on OLEDs in which a fluorescent guest is used in the EML instead of the phosphorescent guest. As triplet excitons do not contribute to device EL in the case of fluorescent OLEDs; any quenching of triplet excitons due to HTL degradation should have minimal impact on device EQE. We therefore fabricate and test devices of the following structure: ITO/MoO_3 (5 nm)/CBP (20 nm)/*UV*/ CBP (10nm)/ CBP: C545T (5%) (15 nm)/TPBi (40 nm)/LiF (1 nm) /Al (80 nm), where C545T is the fluorescent guest material. As with the previous cases, the device fabrication is interrupted after depositing the first CBP layer (20 nm thick) and the layers are exposed to UV radiation for 42 hours, after which the device fabrication is completed. Figure 6.6 (a) and (b) show J-V and EQE

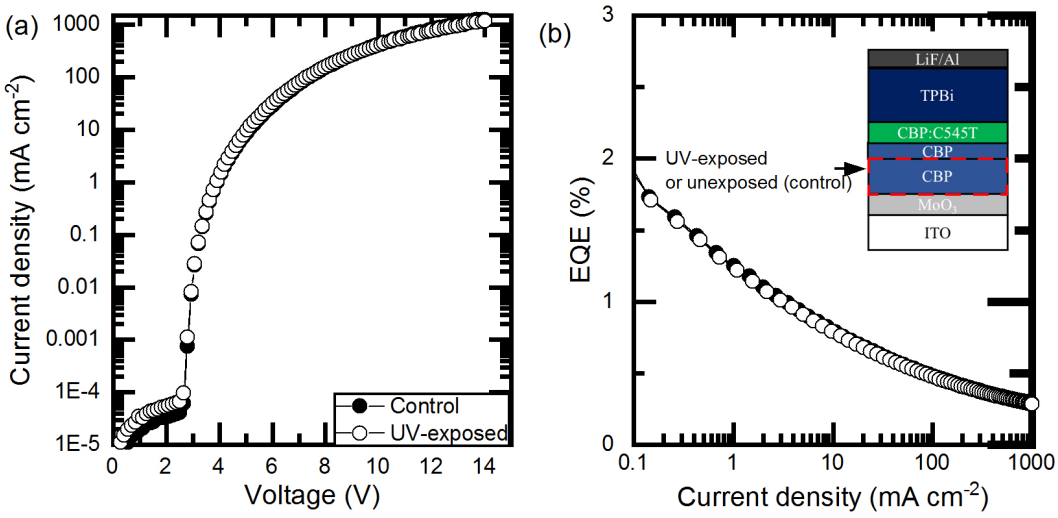

Figure 6.6: (a) J–V and (b) EQE characteristics of a control device and a device with a UV-exposed HTL, in which C545T is used as the guest emitter in the EML. Device schematic is provided in (b).

characteristics collected from one of these devices and its non UV-exposed control counterpart. Again, J-V characteristics show no detectable changes. Quite remarkably, the devices show no

detectable differences in EQE characteristics in this case. As both singlet and triplet excitons must still exist in the HTL of this device during electrical driving, either due to their migration from the EML or due to the recombination of holes with leaked electrons, and therefore must, as before, be quenched in the 20 nm UV degraded portion of the HTL, the fact that they have no bearing on device EQE in this case suggests that excitons in HTL do not contribute significantly to device EL output in the case of fluorescent OLEDs. One can attribute this behavior to the fact that only singlet excitons can contribute to device EL output in the case of fluorescent OLEDs. Due to their much shorter diffusion lengths, the diffusion of singlet excitons from the EML to HTL and from the HTL to EML is rather limited and therefore the presence of any quenchers in the HTL will have no significant effect on the electroluminescence efficiency of the EML. This is clearly different from the case of phosphorescent OLEDs where triplets contribute significantly to device EL output. Due to their longer diffusion lengths, triplet excitons created by electron-hole recombination in the HTL can diffuse to the EML and thus contribute to device EL output in the case of phosphorescent OLEDs. In this case any quenching of these triplet excitons in the HTLs (such as due to exciton-induced damage of the HTL itself) would have a more significant negative impact on device EQE. These results therefore also reveal that any degradation in the HTL (be it due to exciton-stress or other factors) will be more detrimental to device EQE in the case of phosphorescent OLEDs than in the case of their fluorescent counterparts.

We should point out that exciton stress of HTLs also affects the EL stability of phosphorescent devices and not only their EQE. Figure 6.7 presents normalized changes in EL intensity (=L/L_0 where L and L_0 represent luminance at any time t and initial luminance, respectively) and changes in driving voltage versus driving time at a constant current density for devices of structure: ITO/MoO_3 (5 nm)/CBP (20 nm)/*UV*/CBP (10nm)/CBP:$Ir(ppy)_3$ (5%) (15 nm)/TPBi (40nm)/LiF (1nm)/Al (80 nm). As before, the UV exposure time was 42 hours. Data from a control device (i.e., with CBP not exposed to UV) is again included for comparison. The devices are driven at a constant current density and had an initial luminance of 3000 $\mathrm{cd\,m^{-2}}$ at the

driving current. It can be seen that device lifetime LT50 (time taken for luminance to decrease to 50% of its initial luminescence) is only about 5 hours in the case of the device with exciton-stressed CBP; versus 20 hours in the case of the control device. This clearly shows that the exciton stress that the HTL was exposed to earlier also accelerates EL degradation, pointing to the role of exciton-induced degradation of HTLs in shortening device lifetime. Interestingly, the driving voltage rise trends show no marked differences between the two devices, consistent with the earlier conclusion that the exciton stress does not lead to significant charge trap formation in the HTL, again indicating that the decrease in efficiency and stability is not primarily the result of changes in charge balance.

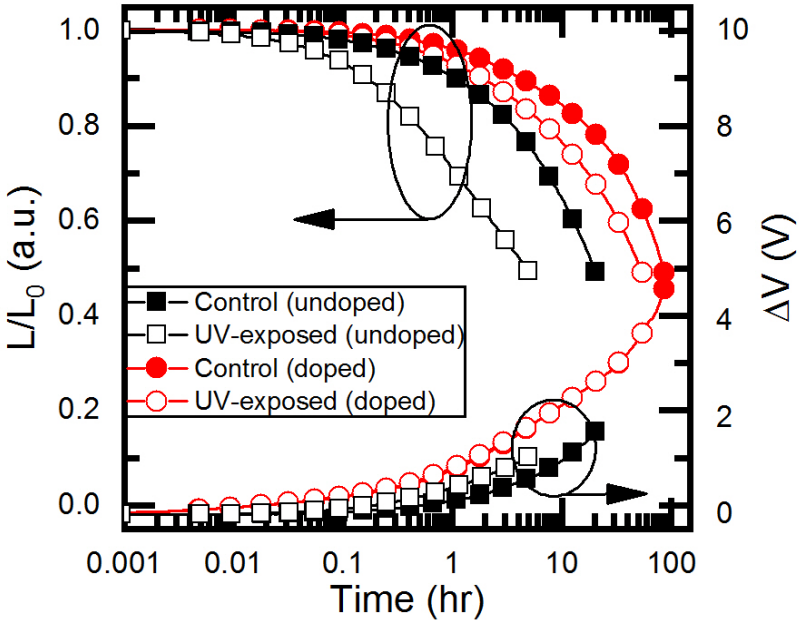

Figure 6.7: Normalized luminance and changes in driving voltage versus time for devices with a UV-exposed HTL (doped or undoped) and of control devices with unexposed HTL (doped or undoped), under constant current density.

In order to understand the role that dopants in the HTL play in increasing device stability, we also fabricate and test devices of the structure: ITO/MoO_3 (5 nm)/CBP:Ir(ppy)$_3$ (5%) (20 nm)/*UV*/CBP (10 nm)/CBP:Ir(ppy)$_3$ (5%) (15 nm)/TPBi (40 nm)/LiF (1 nm)/Al (80 nm) following the same approach. As before, the UV exposure time was 42 hours. Data from a control device (i.e. with the fabrication interrupted for 42 hours but without the first CBP:Ir(ppy)$_3$ layer being exposed to UV) is again included for comparison. The devices are driven at a constant current density and had an initial luminance of 3000 $\mathrm{cd\,m^{-2}}$ at the driving current. Results from these devices are also included in Figure 6.7. As can be seen from the figure, the lifetimes for the device containing the UV-exposed doped HTL is significantly longer than that of the device with the undoped HTL. Furthermore, the difference in lifetime between the device with the UV-exposed doped HTL and its non UV-exposed counterpart is smaller (only about 1.5× versus 4× times in the earlier case). These results show that having dopants in the HTL reduces their degradation by photogenerated excitons, suggesting that the increase in device EL lifetime upon introducing dopants in the HTL may very well be due to a similar effect, i.e., a reduction in exciton-induced degradation of HTLs. That the presence of dopants in the HTLs can reduce their exciton-induced degradation may be attributed to their role in acting as energy acceptors that allow for fast energy transfer from the HTL material, hence reduces the lifetime of excitons on it (i.e., on the host material), and creating additional pathways for their deactivation, and thus reduces their harmful effects [33, 34].

Having established that exciton-induced degradation of the HTL reduces device EQE and accelerates its EL degradation, and finding that the primary role of doping the HTL in increasing device stability might be associated with reducing this degradation mode, we investigate the effect of using alternative approaches for increasing the exciton stability of HTLs on device EL stability. It has been observed for polymers that a higher degree of crystallinity and/or film density film leads to shorter exciton lifetime and increased exciton stability [91, 92, 93]. Similar results should occur with small molecules. We therefore investigate the use of thermal annealing

as a way to increase HTL crystallinity on both their exciton stability and device EL stability. First, we test the effect of thermal annealing on the morphology and exciton stability of CBP films. A 30 nm thick CBP film is deposited on glass and annealed at 100 °C for 30 mins in a nitrogen environment. The annealing temperature exceeds the Tg of CBP (62 °C) [73]. Figure 6.8 (a) and (b) show typical PL spectra (collected under 330 nm excitation) and AFM surface scans collected from the annealed film and from an un-annealed film used as control, respectively. Clearly, the annealing leads to the appearance of well resolved vibronic bands in the PL spectra and a more granular morphology with a much higher surface roughness (Rms of 38.31 nm versus 1.40 nm in the annealed and control film, respectively) indicative of crystallization. Exciton lifetime also becomes shorter as indicated from TRPL characteristics collected at 400 nm, which correspond to CBP emission peak, in Figure 6.8 (c). The decrease in exciton lifetime can be attributed to exciton quenching at grain boundaries that appear in as a result from the transition from a more amorphous to a more crystalline film morphology [89, 94]. We also test the effect of exposing the films to UV continuously for 48 hours. The dotted traces in Figure 6.7 (a) and (b) represent the PL spectra collected from the same films after they have been exposed to the UV radiation, showing a decrease in PL intensity. The decrease was only about 30% in the case of the annealed film versus 50% in the case of the control film, indicating that the annealing slows down the deterioration in CBP quantum yield by exciton stress, which may be attributed to the higher crystallinity and shorter exciton lifetime.

Next, we test the effect of using an annealed HTL on device EL stability. For this we fabricate and test devices of the structure ITO/MoO_3 (5 nm)/ annealed CBP (20 nm)/ un-annealed CBP (10 nm)/ CBP:Ir(ppy)$_3$ (5%) (15 nm)/TPBi (40 nm)/LiF (1nm) /Al (80 nm). To do this, device fabrication is interrupted after depositing the first CBP layer, and the ITO/MoO_3/CBP (20 nm) stack is annealed at 100 °C for 30 mins in a nitrogen environment. Afterwards, the deposition of the second CBP layer and subsequent layers is resumed in order to complete device fabrication. A control device without the annealing step is also tested for comparison. Figure 6.9 (a) presents the

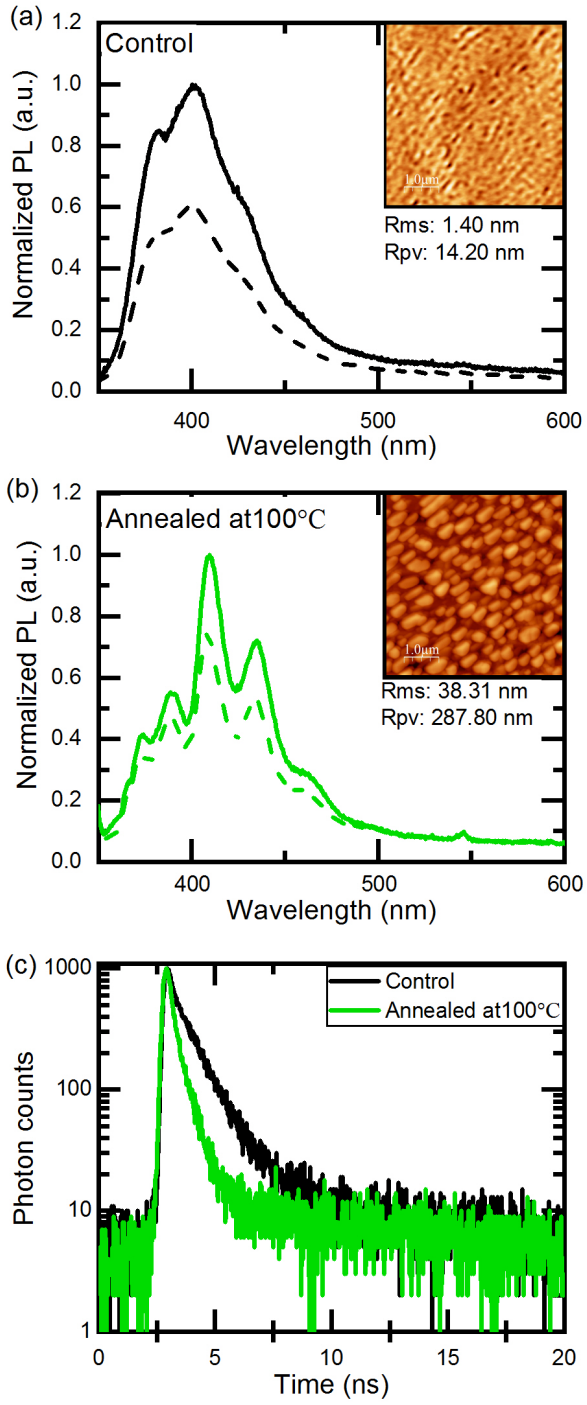

Figure 6.8: PL spectra collected under 365 nm excitationfor : (a) a control film and (b) an annealed film. The dotted lines represent the PL spectra collected from same films after UV exposure for 48 hours. The insets show the AFM surface scans collected from the same films. (c) TRPL characteristic collected at 400 nm for the control film and the annealed film. AFM and TRPL measurements are done before the UV exposure step in both cases.

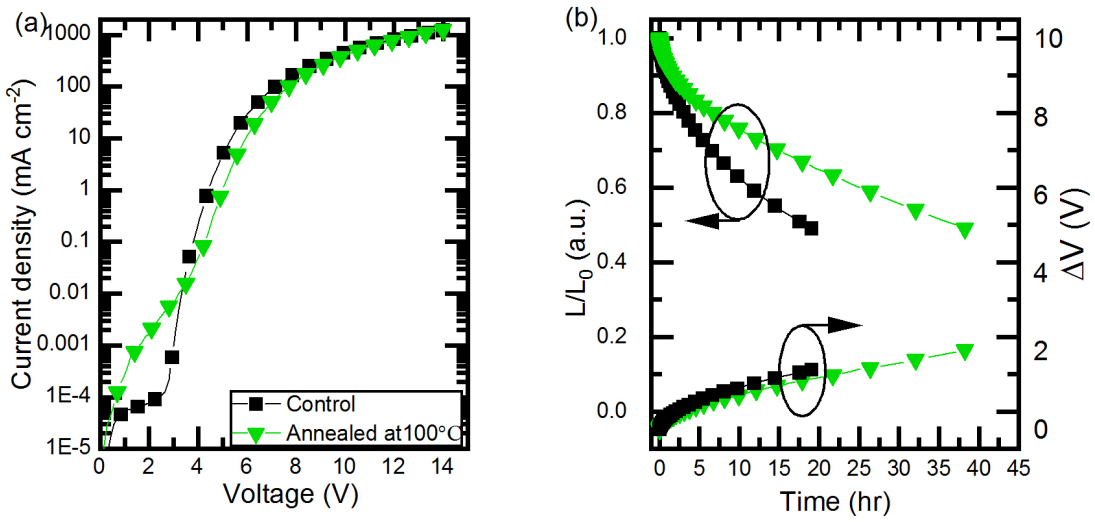

Figure 6.9: (a) J–V characteristics. (b) Normalized luminance and changes in driving voltage versus time, under a constant current density, for a control device and a device with an annealed HTL.

J-V characteristics of these devices, showing a slightly lower drift current and a higher leakage current of the device with the more crystalline HTL which can respectively be attributed to increased charge trapping at grain boundaries and to the higher film roughness. Figure 6.9 (b) shows EL stability test results and driving voltage under a constant current density driving of $20\,\mathrm{mA\,cm^{-2}}$. As can be seen from the figure, the device with the annealed HTL displays $2\times$ longer lifetime than the control device. Although it is not possible to ascertain that the increased stability is primarily or exclusively due to the higher exciton stability of the annealed HTL, the fact that these devices exhibit increased stability despite their coarser and less homogenous HTL morphology, which should have a negative effect on stability, suggests that the increased exciton stability may indeed be a factor in that.

6.3 Conclusion

In summary, we demonstrate the effect of exciton-induced degradation of HTL on device efficiency and stability. Results show that exciton stress of only the HTLs can lead to a significant deterioration in the electroluminescence external quantum efficiency and stability of PhOLEDs, revealing the detrimental role of exciton-induced degradation of HTLs in limiting device performance. The creation of quenchers in HTLs and the diffusion of excitons from the HTL to the EML appear to play roles in this degradation mechanism.This phenomenon affects PhOLEDs more significantly than their fluorescent counterparts because of the relatively longer exciton diffusion length of triplet excitons which allows a larger fraction of triplets to reach the EML, and thus makes their quenching by quenchers in the HTL to more negatively impact EQE. Increasing the exciton stability of HTLs such as by means of introducing dopants in them or altering their morphology reduces this degradation mode, and therefore helps increase device EL stability. The findings uncover a new degradation mode in PhOLEDs and provide key insights for device design for realizing better performance and stability.

Chapter 7

Influence of Deposition Rate on Exciton-Induced Degradation

The material in this chapters was published in H. Yu and H. Aziz, "Influence of deposition rate on hole transport layer morphology and its effect on the electroluminescence stability of phosphorescent organic light emitting devices," in Organic and Hybrid Light Emitting Materials and Devices XXIII, 2019, vol. 4360, no. September, p. 84 and reprinted here with the permission from publisher.

The exciton stability the organic thin layers is considerably affected by the film morphology. The finding of the dependence of the morphology of the organic layer on the deposition rates suggested that a lowering of the deposition rate would decrease the degree of disorder in the organic layer [12]. In addition, Kearns et al have shown that lowering the deposition results in a better kinetic and thermodynamic stability as the low deposition time enhances surface mobility of molecules allowing higher-ordered packing configuration [19]. This higher-ordered alignment would increase exciton quenching due to structural defects and therefore decrease exciton lifetime [89], implying that the effect of deposition rate on the morphology in the HTL could play an important role in device performance and stability.

In this work, the effects of the deposition rate of HTLs and its influence on the EL stability of PhOLEDs are studied and compared with respect to the morphologies of these HTL, using for that purpose the archetypical PhOLED hole transport material CBP. The results show that

the morphologies and exciton lifetime of CBP films vary with different deposition rates range from 0.1 to 10.0 $\text{Å}\,\text{s}^{-1}$. The correlation between the observed morphology and exciton stability variations in the HTL and the performance of the corresponding PhOLEDs is presented. The finding shows that the deposition rate of HTLs can lead to a significant deterioration in the stability of PhOLEDs, revealing the detrimental role of morphology and exciton lifetime of HTLs in PhOLED performance.

7.1 Experimental procedures

In this work, the following device structure was used: ITO/MoO_3 (5 nm)/HTL (30 nm)/CBP: $Ir(ppy)_3$ (5%) (5 nm)/TPBi (40 nm)/LiF (1 nm)/ Al (80 nm), where CBP, TPBi and $Ir(ppy)_3$ were used as the host and hole transport material, the electron transport material and the emitter material, respectively. In order to eliminate the different conditions of the HTL/EML interface, the HTL consisted of two layers - a 20 nm thick CBP layer with the various different deposition rates of 0.1, 1.0, and 10.0 $\text{Å}\,\text{s}^{-1}$ and a 10 nm thick CBP layer with the deposition rate of 1 $\text{Å}\,\text{s}^{-1}$. To study the effect of the deposition rate on the films in environments that closely simulate the conditions in OLEDs, a 30 nm thick CBP films were deposited on an ITO/MoO_3 (5 nm) substrate with three different deposition rates aforementioned.The devices were fabricated on ITO substrates (purchased from Kintec) via thermal deposition at a rate of 0.1-10.0 $\text{Å}\,\text{s}^{-1}$ at a base pressure of below 5×10^{-6} Torr using an Angstrom Engineering EvoVac system. For UV radiation, a 365 nm illumination from a UV lamp at a power density of $2.3\,\text{mW}\,\text{cm}^{-2}$ was used.

7.2 Influence of Deposition Rate on the Hole Transport Layer Morphology and Its Effect on Device Performance

In order to further evaluate the device performance as a function of the deposition rate of HTL, we need to determine the surface morphology and exciton stability of the HTL. First, we examine the correlation of the morphology of CBP layer with the deposition rate. Figure 7.1 shows the surface morphology and roughness of the 30 nm CBP film on ITO/MoO_3 (5 nm). The Rms values of the pristine films deposited at 0.1, 1.0, and 10.0 $\text{Å}\,\text{s}^{-1}$ rates are 0.58, 0.57, and 0.61 nm, respectively. No detectable changes are observed for each of the films. By contrast, the Rpv show increased Rpv of 5.23 nm in the case of the low deposition rate. This may show that the low deposition rate brings about a slightly higher structural order in the film. From a morphology stability perspective, the higher-ordered molecular configuration leads to morphological changes and therefore increased surface roughness overtime [95]. This would show larger crystalline features. One can expect the higher structural order to display a large increase in roughness and large grains on the films. To systematically study the structural order of all the films with the different deposition rates, all films were stored at room temperature in a nitrogen atmosphere and then examined again. Five days after fabrication, films started to exhibit increased surface roughness and crystals. These results clearly show the different morphology evolution and crystalline morphology. For the films with the low deposition rate of 0.1 $\text{Å}\,\text{s}^{-1}$, the surface roughness becomes much rougher and bigger crystalline features with a larger lateral correlation length are observed. The dependence of the morphology on the deposition rate can be explained by the fact that a lower deposition rate enabled the CBP molecules to settle into the higher structural ordered alignments which in turn accelerated the crystallization process.

Knowing that the morphology dependence on the deposition rate would be reflected in the exciton stability of the organic layer, we also investigate the PL characteristics of the CBP films before and after UV irradiation to further verify that lowering the deposition rate may increase

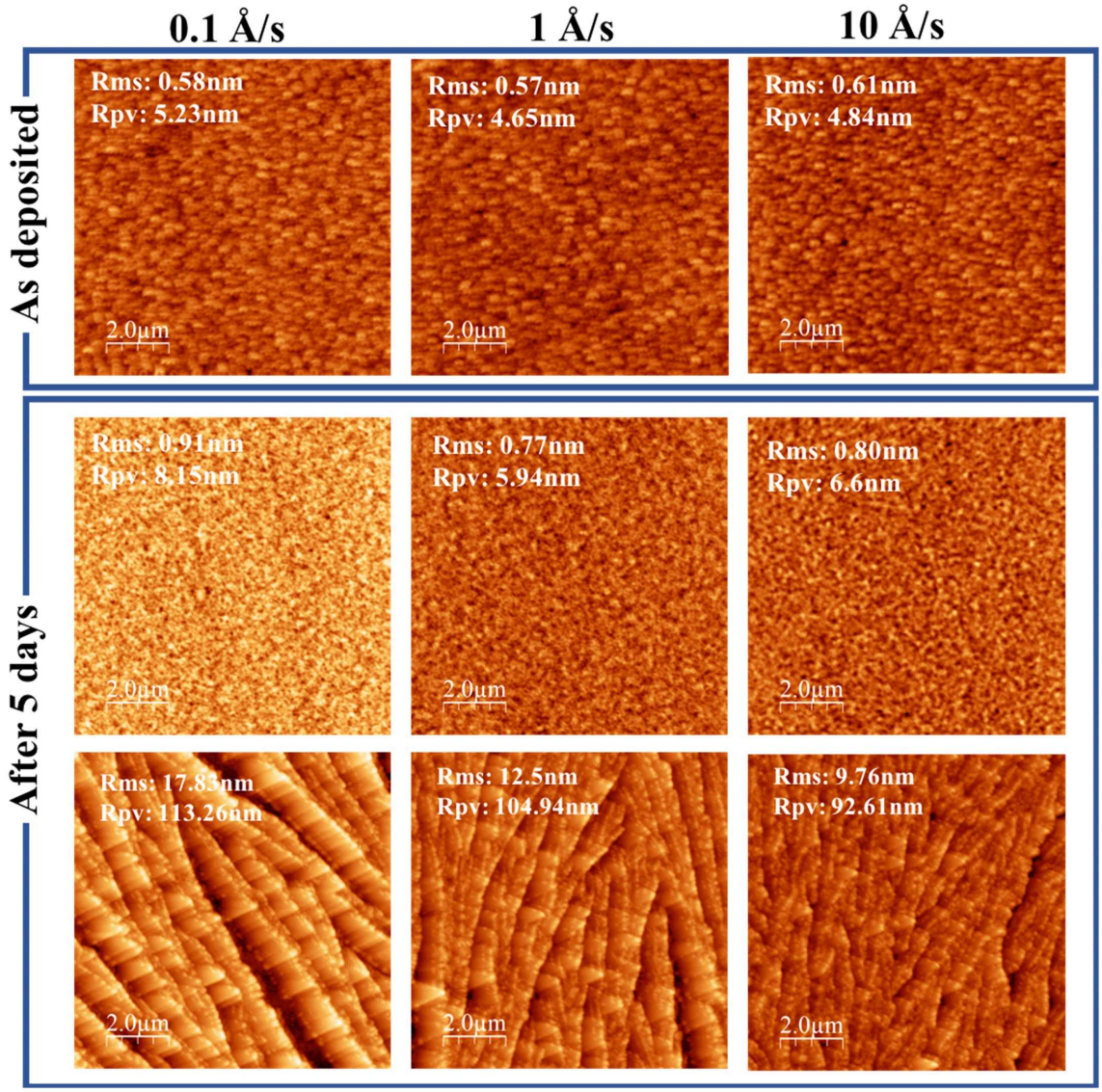

Figure 7.1: AFM surface scans taken at the different periods of time after fabrication; pristine ((a), (b), and (c)) and after 5 days of storage ((d), (e), and (f)) in the amorphous area and ((g), (h), and (i)) in the crystalline area. The films are deposited at various rates (0.1, 1.0, and 10.0 $\text{Å}\,\text{s}^{-1}$). Rms and Rpv values are indicated on the AFM images.

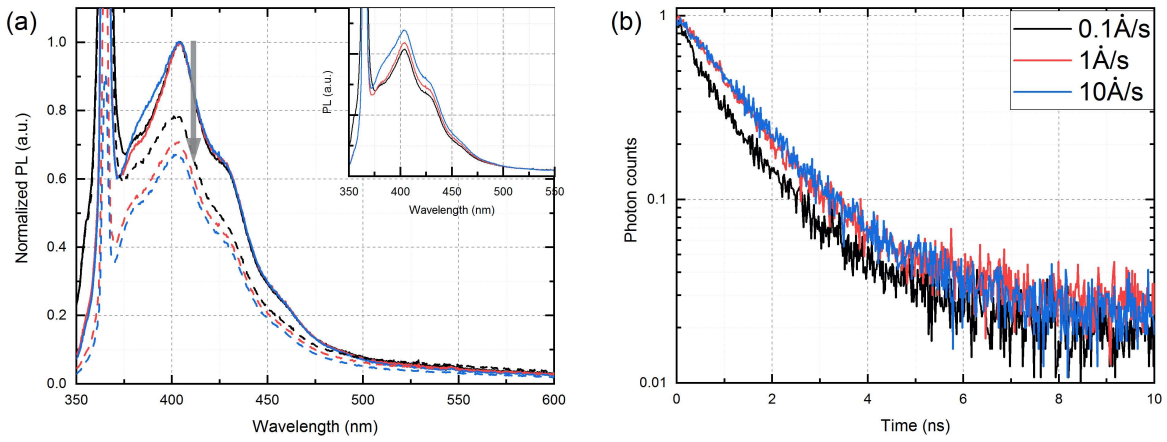

Figure 7.2: (a) PL spectra collected under 365 nm excitation. The dotted lines represent the PL spectra collected from same films after UV exposure for 18 hours. (b) TRPL characteristic collected at 400 nm for the film before the UV exposure step.

the exciton stability of the organic layer. For this experiment, 30 nm CBP films on ITO/MoO_3 deposited at 0.1, 1.0, and 10.0 $\text{Å}\,\text{s}^{-1}$ rates are fabricated and subjected to 2.3 $\text{mW}\,\text{cm}^{-2}$ radiation power from a UV lamp for a period of 18 hours in a nitrogen environment. Figure 7.2 (a) a shows the typical PL spectra (collected under 365 nm excitation) corresponded to the characteristic CBP singlet emission band with a peak at around 400 nm. The sharp peak at around 365 nm is from the Hg lamp. The dotted traces represent the PL spectra collected from the same films after they have been exposed to UV irradiation. The PL intensity decayed by 21, 30 and 34% for the CBP deposited at 0.1, 1.0, and 10.0 $\text{Å}\,\text{s}^{-1}$, respectively. Clearly, reducing the deposition rate increases the exciton stability of the film. The reason the lowest deposition rate leads to better exciton stability is that the more ordered configuration may increase exciton quenching at structural defects and encourage faster exciton dissociation. It may also be associated with reducing voids and pores within the film which allow for larger molecular rotation and thereby increased molecular reactivity. As a result, the deterioration in CBP quantum yield by exciton

stress is reduced. This is shown in the insets in Figure 7.2 (a). In the case of the films without irradiation, the lowest relative PL quantum yield is observed in the film with the lowest deposition rate. In a similar manner, the exciton quenching at the structural defects coincided in the higher structural order may lead to the lower PL quantum yield. We also tested the TRPL characteristics of the films. Figure 7.2 (b) shows the TRPL characteristics at 400 nm collected under pulsed excitation at 380 nm. The PL decay rate is faster in case of the film deposited at the lowest deposition rate relative to other counterparts. A decrease in exciton lifetime is indicative of an increase in exciton quenching. The increase in the exciton quenching can be attributed to easier exciton diffusion which facilitates exciton quenching by bimolecular effects. This implies that the formation of the high ordered molecular configuration resulted in higher exciton stability and exciton lifetime and that the molecular ordering could be achieved through controlling the deposition process.

Having established that lowering the deposition rate increases the exciton stability and decreases exciton lifetime, we investigated the use of deposition rate as a way to increase the exciton stability of HTL as well as device EL stability. We found in a previous work that exciton induced degradation of HTL reduces device stability and that this degradation mode can be suppressed by decreasing exciton lifetime of HTL. For this, we deposited the 20 nm CBP HTL at three different rates (0.1, 1.0, and 10.0 $\text{Å}\,\text{s}^{-1}$ rates). Figure 7.3 (a) shows the current density-voltage-luminance characteristics of the OLEDs. It can be seen that the devices show very similar characteristic, indicating that differences in HTL morphology do not significantly alter charge injection or transport in them. This suggests that although the morphological characteristics of the films are different, the difference might be too small to influence the charge transport properties. A look at their EQE in Figure 7.3 (b) indeed shows that the EQE diminishes as the deposition rate decreases. This could be attributed to an increase in luminescence quenching in the organic stack, due to a large number of nonradiative quenching sites in the HTL.

Figure 7.4 (a) shows normalized changes in EL intensity (=L/L_0 where L and L_0 represent

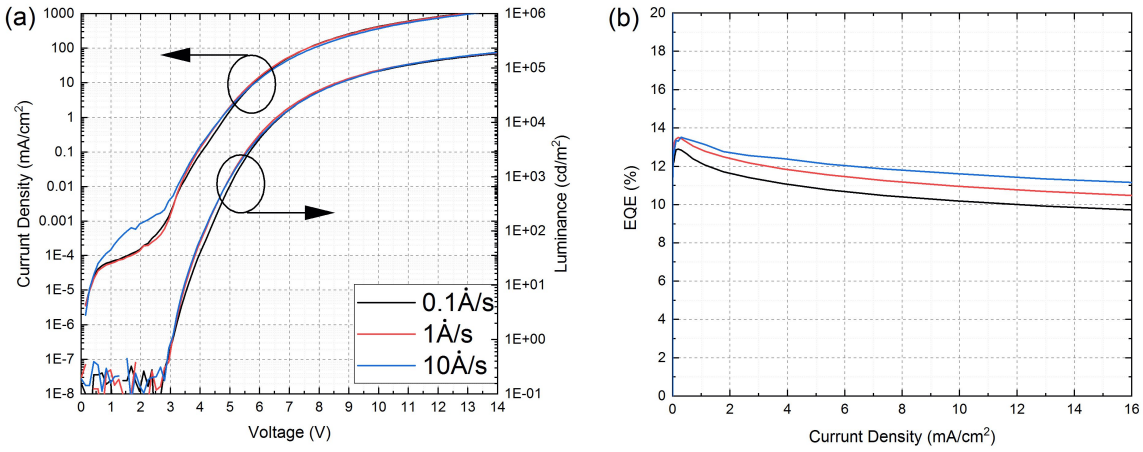

Figure 7.3: (a) J-V and (b) EQE characteristics of devices with HTL deposited at various rates (0.1, 1.0, and 10.0 Å s^{-1}).

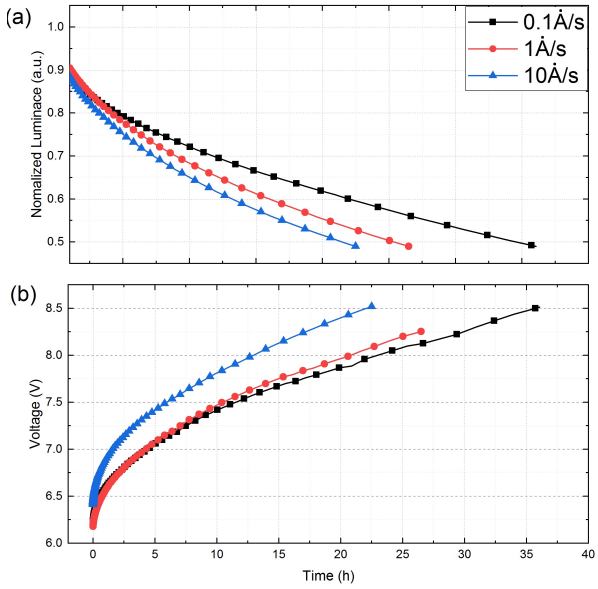

Figure 7.4: (a) Normalized luminance and (b) changes in driving voltage versus time for devices with HTL deposited at various rates (0.1, 1.0, and 10.0 Å s^{-1}).

luminance at any time t and the initial luminance, respectively) versus driving time at a constant current density driving of 20 mA cm^{-2} for the devices with the three different deposition rates. It can be seen that the device lifetime somewhat increases with decreasing deposition rate. Figure 7.4 (b) shows the changes in driving voltage (=V/V_0 where V and V_0 represent voltage at any time t and initial voltage versus driving time at the same current density. Again, the devices with the lowest deposition rate exhibited the smallest increase in the driving voltage. Since the only difference among devices is the deposition rate of HTL and their exciton lifetime, it follows that the increase in EL stability must be caused by the shorter exciton lifetime of HTL material. This is consistent with previous work that showed that a shorter exciton lifetime in HTLs reduces the exciton-induced degradation of the HTL and therefore leads to an increase in device EL stability.

7.3 Conclusion

In summary, we demonstrate the effect of changing the deposition rate of the CBP HTL on device stability. Firstly, a lower deposition rate is found to enhance the exciton stability and to shorter exciton lifetime. This result can be attributed to the higher morphological order in the film. Secondly, the device stability is found to increase upon decreasing the HTL deposition rate, which could be attributed to the higher morphological order in HTL that reduces exciton-induced degradation in them. Our study shows that changing the deposition rate of the organic films can vary the morphology and exciton stability, hence provide direct correlations between material deposition rate, HTL morphology and PhOLED electroluminescence performance.

Chapter 8

Exciton-Induced Degradation in Solution-Coated versus Vacuum-Deposited Host:Guest Material Systems

The material in this chapters was published in H. Yu and H. Aziz, "Differences in Photoluminescence Stability and Host-to-Guest Energy Transfer in Solution-Coated Versus Vacuum-Deposited Electroluminescent Host:Guest Small-Molecule Materials," J. Phys. Chem. C, 2020 and reprinted here with the permission from publisher. Copyright 2020 American Chemical Society.

A number of studies have investigated the causes of the lower stability of solution-coated OLEDs [43, 44, 46, 47, 51, 72]. However, the underlying mechanisms are still not clearly understood. In addition, most of the studies so far have focused on neat material systems. In particular, an investigation of this behavior in small molecule host:guest (H:G) material systems, the systems typically used in the EL layers of OLEDs, has not been adequately investigated. In case of vacuum-deposited OLEDs, a number of degradation mechanisms were reported in the past [25, 30, 61, 96, 97, 98]. Zhang and Aziz [36] reported that host aggregation by exciton-polaron interactions can occur even in H:G systems and can lead to phase segregation between the host and guest materials, in turn leading to a change in energy transfer rate from the host to guest. This study, however, focused on vacuum-deposited systems. Because solution-coated films are known to have a considerably different morphology, the question of whether solution-processed

H:G systems could be more susceptible to host aggregation and phase segregation arises.

In this study, we study and compare between changes in the PL characteristics in H:G electroluminescent small-molecule material systems made by solution-coating versus vacuum deposition. CBP, one of the most widely utilized OLED host materials is used as a representative host material. Two commonly used green-emitting and red-emitting phosphorescent emitters, $Ir(ppy)_3$ and $Ir(piq)_3$, are used as guest materials, doped into the CBP. Thin films of these H:G systems are fabricated by vacuum-deposition or solution-coating. PL spectral measurements and time-resolved PL measurements are used for comparing between the two systems and in changes in them after prolonged UV irradiation as well as thermal stress. Results show that solution-coated H:G systems have a lower PL stability relative to their vacuum-deposited counterparts, and that they also have a lower host-to-guest (H$\rightarrow$ G) energy transfer efficiency. UV and thermal stress are both found to cause host-guest (H-G) phase separation more readily in case of solution-coated films, further degrading host-to-guest energy transfer. Findings from thermal stress tests suggest that the differences in behavior arise from differences in initial film morphologies because of the different coating methods.

8.1 Experimental procedures

Thin films of neat CBP and of CBP:$Ir(ppy)_3$ and CBP:$Ir((piq)_3$ H:G mixtures made by either vacuum-deposition or solution-coating were fabricated on quartz substrates. The materials were purchased from Luminescence Technology Corp. and used as received without further purification. For the vacuum-deposited films, the layers were thermally evaporated on the substrates at a rate of 1 $\text{Å}\,\text{s}^{-1}$ at a base pressure of 5×10^{-6} Torr using an Angstrom Engineering EvoVac system. For the solution-coated films, the materials were dissolved in toluene to form 10 $\text{mg}\,\text{mL}^{-1}$ solutions and then were spin-coated on the substrates using a Laurell spin coater. The coated films were

then baked at 60 °C on a hot plate in a glove box to remove the solvent and complete the drying process. In all cases, a vacuum deposited MoO_3 interlayer, 5 nm thick, was used in between the quartz substrates and the films for the purpose of improving wetting and film uniformity. For UV irradiation tests, a 365 nm illumination from a UV lamp at a power density of $2.3\,\mathrm{mW\,cm^{-2}}$ was used. During the irradiation tests, the films were kept in a nitrogen environment and their temperature was maintained at room temperature using a cooling fan in order to minimize any illumination-induced heating effects.

8.2 Differences in Photoluminescence Stability and Host-to-Guest Energy Transfer

We first study and compare between changes in the PL characteristics of 30nm thick films made by vacuum deposition versus solution-coating of neat CBP and of CBP:$Ir(ppy)_3$ and CBP:$Ir(piq)_3$ H:G mixtures because of prolonged UV irradiation. The UV irradiation leads to exciton formation in these materials and thus allows studying their behavior after exciton stress. The guest concentration in the H:G films was 5% by volume, typical of concentration levels used in phosphorescent OLEDs for complete host to guest energy transfer to occur. The films are subjected to 365nm illumination from a UV lamp at a $2.3\,\mathrm{mW\,cm^{-2}}$ radiation power for a period of 18. Figure 8.1 shows the PL spectra collected from the films before and after the UV irradiation, referred to herein as "pristine" and "UV-irradiated" films, respectively. The letters "v" and "s" are used to denote films made by vacuum deposition and solution-coating, respectively. The peak highs are normalized proportionally to the initial (i.e., pristine) PL intensity in each case. The PL spectra of the neat CBP films in Figure 8.1 (a) exhibit the characteristic CBP singlet emission band which can be ascribed to the S1 $\rightarrow$ S_0 transition. As expected, the UV irradiation leads to a decrease in PL intensity, and the decrease was more significant in case of the solution-coated films, consistent with previous observations [51, 72]. The PL spectra of

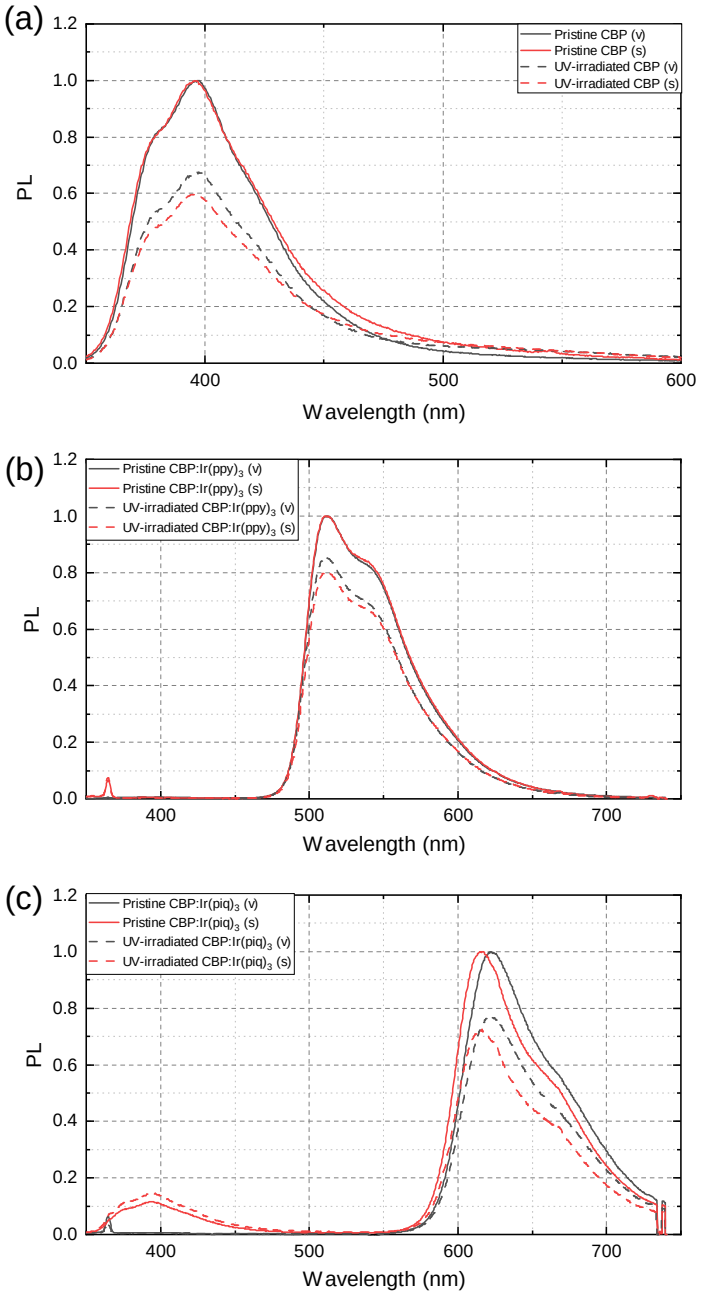

Figure 8.1: PL spectra collected under 330 nm excitation from (a) neat CBP films (b) CBP:Ir(ppy)$_3$ (5%) films and (c) CBP:Ir(piq)$_3$ (5%) films fabricated by vacuum-deposition and solution-coating before and after exposure to the UV irradiation for 18 hours.

the H:G films, presented in Figure 8.1(b) and 8.1(c), show the characteristic emission bands of their respective guest materials with peaks at around 510 nm and 620 nm for the CBP:Ir(ppy)$_3$ and CBP:Ir(piq)$_3$ films, respectively. Given the concentration of the guest is only 5%, most of this luminescence will result primarily from guest excitation by energy transfer from the host, similar to what takes place under electrical bias in OLEDs made with the same materials. As with the neat CBP films, the PL intensity of the solution-coated H:G films decreased after the UV irradiation and the decrease was larger in case of the solution-coated films. Considering that the excitation power used in the PL measurements was kept constant, such decrease in the PL intensity points to a decrease in the PL quantum yield of the materials. A deterioration in the quantum yield in H:G systems can generally be because of a degradation (1) in the host material, which affects the H$\rightarrow$G energy transfer rate and therefore guest luminescence, and/or (2) in the guest materials themselves that leads to a decrease in their PL quantum yield.

Interestingly, aside from the larger degradation in the PL quantum yield as a result of the UV irradiation in case of the solution-coated films, one can also see from Figure 8.1 (c) that while the PL spectra of the vacuum-deposited films exhibit only the Ir(piq)$_3$ emission band, their solution-coated counterparts additionally show a second emission band with a peak at 400 nm which corresponds to emission from the CBP host. The relative intensity of this band is also found to increase after the UV irradiation. In an ideal H:G system, the guest molecules will be well dispersed among the host molecules, allowing for efficient energy transfer from the host to the guest molecules to occur and thus the suppression of any luminescence from the host molecules. The appearance of a host luminescence band in the PL spectra therefore indicates that energy transfer from the host to guest molecules in the solution-coated CBP:Ir(piq)$_3$ film is incomplete. Such incomplete energy transfer, despite using the same guest concentration suggests that the molecular organization morphology in case of the solution-coated films is somewhat different from that in their vacuum-deposited counterparts with the earlier having a significant fraction of host molecules not sufficiently close to guest molecules for efficient energy transfer to occur.

This suggests that solution-coating may produce film morphologies with some initial H-G phase separation into guest-rich and guest-deficient (i.e., host-only) domains. Although, in principle, this effect may alternatively be simply because of incomplete solubility of the host and/or guest materials in the solvent solution used for making the films, the fact that the relative intensity of the host emission band increases after the UV irradiation suggests that this H-G phase separation can occur or at least proceed in the solid state and be accelerated by the UV stress. Such partial H-G phase separation even in the pristine films can be expected to play a role in their faster PL degradation under UV stress that is because the formation of guest-deficient domains makes it more difficult for excited host molecules in these domains to lose their excitation energy as quickly, in turn making them more susceptible to exciton-induced degradation and aggregation citeZhang2016a. Such aggregation will expectedly further increase the H-G phase separation and may therefore be a factor in the decrease in H→G energy transfer after the UV stress, as reflected in the relative increase in the host emission band intensity.

To further investigate the possibility of different molecular organization morphologies in solution-coated vs vacuum-deposited systems and their influence on the H→G energy transfer rate, we tested the PL characteristics of a similar set of films in which the guest concentration is only 0.25%. Such a low guest concentration allows us to obtain PL from both the host and the guest materials because of incomplete energy transfer and thus to study differences in H→G energy transfer rates in the two groups of films. The lower guest concentration also allows mitigating any factors associated with possible solubility limitations as was questioned earlier. Figure 8.2 shows the PL spectra from these samples, again normalized proportionally to the initial (i.e., pristine) PL intensity in each case. As expected, all PL spectra in this case show some emission from CBP, in addition to the guest emission bands because of incomplete H→G energy transfer. It can also be seen from the figure that here again the UV irradiation brings about a larger decrease in the guest PL band intensity in case of the solution-coated films, pointing to their faster degradation under UV stress. Interestingly, the CBP PL bands do not exhibit a similar decrease.

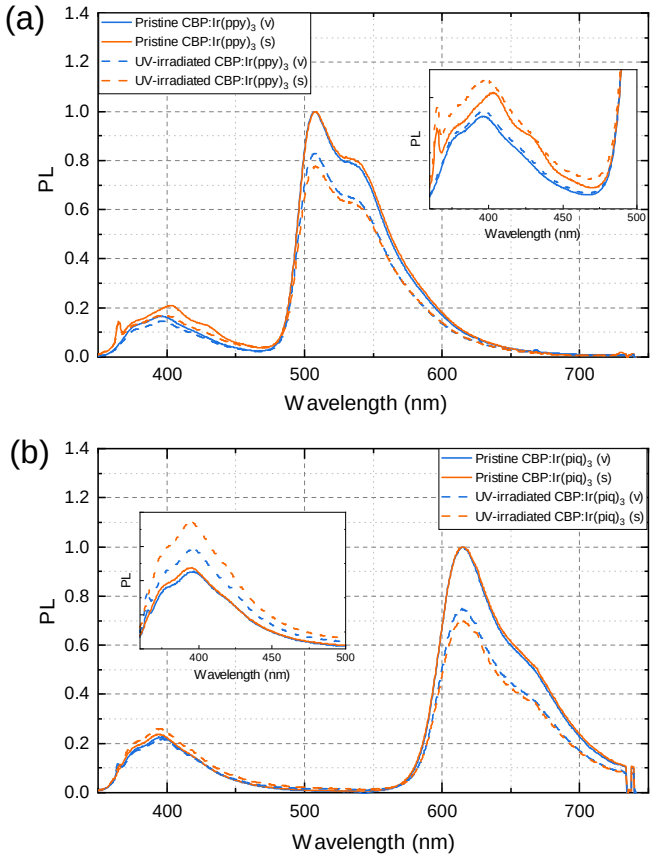

Figure 8.2: PL spectra collected under 330 nm excitation from (a) CBP:Ir(ppy)$_3$ (0.25%) films and (b) CBP:Ir(piq)$_3$ (0.25%) films fabricated by vacuum-deposition and solution-coating before and after being exposed to UV for 18 hours. The peak highs are proportional to the PL output intensity in each case. Insets: The PL spectra normalized to the guest emission peak intensity in each case.

No decrease in host PL bands is observed in this case, despite the fact that UV irradiation generally leads to a deterioration in host PL in the neat films. (Figure 8.2 (a)), suggesting that a second mechanism, that offsets the effect of the first, could be behind this observation, again

pointing to H-G phase separation [33, 36, 99]. The effect of this phase separation can perhaps be better visualized in the relative heights of the CBP bands when compared to the heights of the guest bands which clearly become relatively higher after the UV irradiation, especially in case of the solution-coated films. (the enlarged views show the PL band region of the same spectra after normalizing the spectra to the guest peak intensity to facilitate comparing the relative heights.) In this regard, the faster deterioration in guest PL stability under UV illumination in case of the solution-coated films may indeed be becuase of - at least in part - a faster deterioration in H→G energy transfer in these systems as a result of increased phase separation under the exciton stress. The faster H-G phase separation in the solution-coated films versus their vacuum-deposited counterparts can be attributed to their morphological differences where the earlier generally have less homogenous morphologies with domains of increased molecular aggregation [50, 36].

We also tested the TRPL characteristics of 30 nm thick neat CBP, CBP:Ir(ppy)$_3$ (0.25%) and CBP:Ir(piq)$_3$ (0.25%) films made by vacuum-deposition and solution-coating. Figure 8.3 presents the CBP fluorescence decay characteristics at 400 nm of the films collected under excitation at 380 nm. The fluorescence decay from the solution-coated neat film exhibits a faster decay rate relative to its vacuum-deposited counterpart, indicating that the exciton lifetime is shorter. This is in agreement with our previous observations and attributed to increased aggregation in solution-coated films [44, 36]. With guest-doping, exciton lifetime decreases unsurprisingly because of H→G energy transfer. The magnitude of the decrease in exciton lifetime upon doping is, however, much larger in case of the vacuum-deposited films, suggesting more efficient H→G energy transfer compared to the solution-coated ones. This observation is consistent with the results in Figure 8.1 and 8.2 and suggest that H→G energy transfer in solution-coated films may generally be less efficient in comparison to that in vacuum-deposited ones. This can again be ascribed to their morphological differences and the fact that solution-coated films tend to have less homogenous morphologies and contain more molecular aggregates that may reduce uniform inter-mixing with guest molecules and therefore reduce H→G energy transfer.

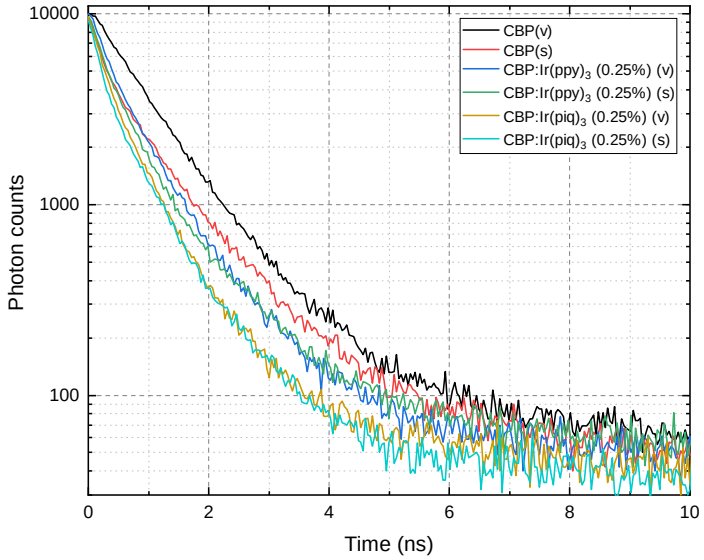

Figure 8.3: TRPL characteristics collected at 400 nm for CBP, CBP:Ir(ppy)$_3$ (0.25%) and CBP:Ir(piq)$_3$ (0.25%) films fabricated by vacuum-deposition and solution-coating.

Seeing that UV irradiation generally brings about a more significant deterioration in H→G energy transfer in case of solution-coated films, likely because of a more severe H-G phase separation, we investigate if thermal annealing may lead to a similar effect. Heating the materials to a temperature above their glass transition will increase molecular mobility and facilitate molecular reorganization in them and would therefore allow investigating and comparing between their phase segregation behavior. We therefore fabricated CBP films doped with the same guest materials at 0.25% and 5% and heated them to 130 °C [sufficiently above the Tg of CBP (62 °C [73])] for 10 min. Figure 8.4 (a)-(d) shows PL spectra (normalized to the guest emission peak intensity) of these films collected before and after the thermal annealing, and the fluorescence microscopy images of the films provided in Figure 8.4 (e). As can be seen, significant increases in PL band intensity in the 350-450 nm range, corresponding to the CBP band, are observed after the heating. The bands also show well-resolved vibronic features. The appearance of vibronic

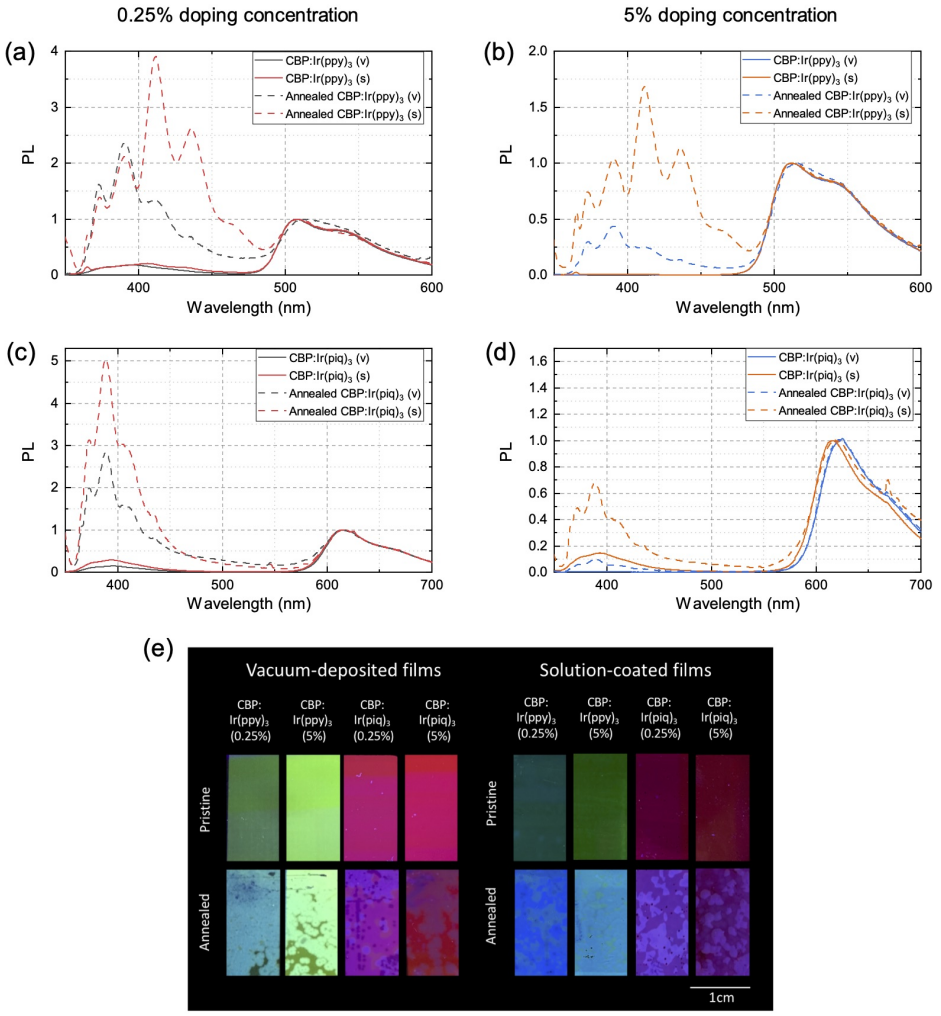

Figure 8.4: PL spectra collected under 330 nm excitation from CBP:guest films with the following guest materials and concentrations fabricated by vacuum-deposition and solution-coating, and collected before and after thermal annealing: (a) $Ir(ppy)_3$ at 0.25%; (b) $Ir(ppy)_3$ at 5%; (c) $Ir(piq)_3$ at 0.25%; and (d) $Ir(piq)_3$ at 5%. All spectra are normalized to the guest emission peak intensity. (e) Fluorescence microscopy images of the films before and after thermal annealing. All films were thermally annealed at 130 °C for 10 min.

details points to increased molecular ordering and crystallinity in the host material, which, in turn, indicates that H-G phase separation must indeed be occurring, producing larger and more molecularly-ordered host-only (i.e., guest-deficient) domains. Most notably, these PL bands are much stronger in case of the solution-coated films pointing to their greater susceptibility to H-G phase separation and consequent deterioration in H→G energy transfer (we note some variations in the peak positions of the more intense vibronic bands in case of solution-coated vs vacuum-deposited CBP:Irppy$_3$-doped films. Although the origin of this behavior is unclear at this point, it may perhaps be because of differences in molecular orientation of CBP molecules). The higher susceptibility to host crystallization also indicates that the initial molecular organization morphology of the solution-coated films must be more capable of promoting this behavior suggesting it has CBP aggregates initially that can act as nucleation sites for host crystallization to proceed from more efficiently. The presence of such guest-deficient aggregates in the initial morphology of solution-coated H:G systems and the less efficient H→G energy transfer may, therefore, indeed then be a factor behind their lower stability under exciton stress and their susceptibility to further H-G phase separation as noted earlier. It can also be seen that the films with higher doping concentration (e.g., 5%) are generally much more stable morphologically and show only smaller reductions in the H→G energy transfer rate after heating. The increased morphological stability with a higher doping concentration may be because of the presence of a large portion of the guest molecules dispersed within the host matrix and therefore the host molecule reorganization may be restricted by the guest molecules.

Knowing that solution-coated films are more susceptible to exciton-induced aggregation [99], we also used fluorescence microscopy to investigate and compare between crystallization in films fabricated by vacuum-deposition vs solution-coating after UV irradiation stress. The films were thermally annealed after the UV irradiation in order to enhance the aggregation and make the crystalline domains large enough to be visible under the microscope. Because UV irradiation leads to exciton-induced aggregation, one can expect the irradiated films to be more susceptible

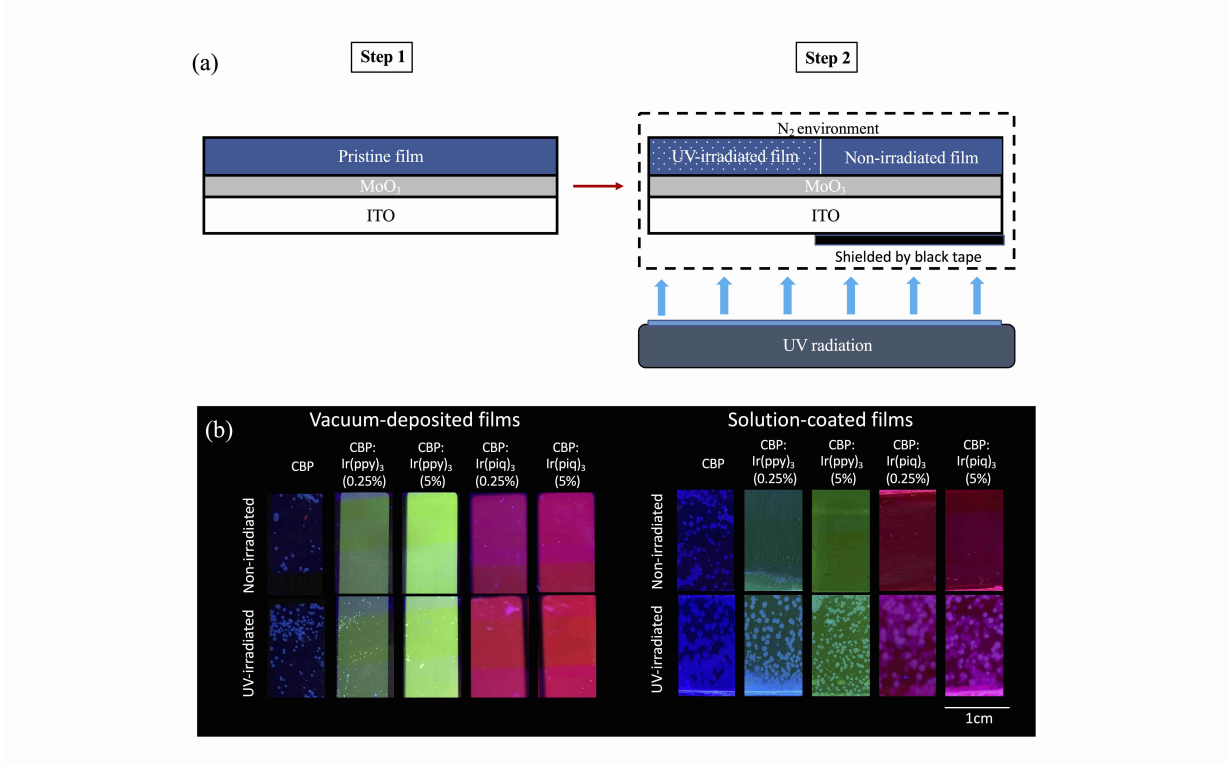

Figure 8.5: (a) Schematic illustration depicting the experimental procedure and differences between the "UV-irradiated" and the "Non-irradiated control" films referred to in the text. (b)Fluorescence microscopy images of neat and guest-doped CBP films subjected to UV irradiation for 18 hours and of non-irradiated controls. All films were thermally annealed at 100 °C for 10 min to enhance crystallization.

to crystallization by thermal annealing because of the presence of UV-induced aggregates that can act as nucleation sites for further aggregation and crystallization by the heat treatment to proceed. Neat and guest-doped CBP films, again made by vacuum deposition and solution-coating, were therefore subjected to UV irradiation for 18 hours. For comparison, another group of identical films were made on the same substrates but were shielded from the UV illumination via a black masking tape to be used as non-irradiated controls.

Figure 8.5 (a) illustrates this process. All films of both groups (both the UV-irradiated ones and the non-irradiated controls) were then heated to 100°C for 10 min. Figure 8.5 (b) presents fluorescence microscopy images of these films. Although the non-irradiated control films show no detectable crystallization, all the UV-irradiated films show crystalline features. The features are clearly much more extensive, in the case of solution-coated films. These results convincingly verify that the UV stress induces host aggregation and H-G phase separation in H:G systems, and that the phenomenon is much more severe in the case of solution-coated systems. The higher susceptibility of solution-coated films to H-G phase separation and deterioration in H→G energy transfer by exciton stress is likely because of less-homogenous morphologies of solution-coated films and the presence of a larger number of initial aggregates of host materials that help accelerate exciton-induced aggregation in these systems.

8.3 Conclusion

In conclusion, a comparison between H:G films fabricated by vacuum-deposition and solution-coating reveals differences in their PL stability and H→G energy transfer. Results show that exciton stress brings about larger loses in the PL quantum yield and in H→G energy transfer in the case of solution-coated H:G systems. The faster H-G phase separation in the solution-coated films is attributed to their less homogenous morphologies that include guest-deficient aggregates of host molecules, which makes H→G energy transfer less efficient in them in comparison to their vacuum-deposited counterparts. The less efficient energy transfer accelerates degradation and further aggregation of the host material under exciton stress, which in turn further increases the H-G phase separation and decreases the H→G energy transfer even further. The findings bring to light one of the fundamental causes of the lower stability of solution-processed OLEDs.

Chapter 9

Influence of PEDOT:PSS Hole Injection Layer Exposure to Solvents

Recent studies reveal that the solvent system utilized in making the coating solution can have a significant influence on the morphology of the film being coated and other device layers, especially the underlying (i.e., pre-coated) ones, and change their surface properties such as work function, sheet resistance and roughness [53, 54, 55]. For example, Yun et al have shown that exposure to solvents can alter the electrical and physical properties of PEDOT:PSS [55]. PEDOT:PSS is widely used in HIL because of its high conductivity, good film-forming property, and high thermal stability [56, 57]. During the solution-coating process of HTLs, the underlying PEDOT:PSS HILs are inevitably exposed to solvents in the HTL solution. It is therefore reasonable to suspect that the exposure to these solvents may lead to changes in the PEDOT:PSS that can influence device performance.

In this study, we investigate the influence of PEDOT:PSS exposure to toluene, a commonly used solvent in HTL coating solutions, on OLED performance. To test the effect of exposure to the solvent, toluene is spin-coated on PEDOT:PSS HILs and the layers are then thermally annealed to remove the solvent. Results show that exposure of PEDOT:PSS to solvents leads to a significant decrease in device EL stability, revealing that the phenomenon plays a role in the lower stability of devices with solution-coated HTLs. The solvent exposure is found to reduce hole injection efficiency, possibly due to changes at the PEDOT:PSS/HTL interface.

9.1 Experimental procedures

In this work, we use CBP as the hole transport and host material, $Ir(ppy)_3$ as the green phosphorescent and TPBi as electron transfer material. The materials were purchased from Luminescence Technology Corp. and used as received without further purification. PEDOT:PSS and LiF are used as a hole injection and electron injection materials. PEDOT:PSS solution is prepared by diluting the PEDOT:PSS dispersion (Sigma Aldrich, 2.8 wt% in H_2O) with 2-propanol in a 1:5 vol ratio and the solution was spin-coated at 5000 rpm for 60 s and then annealed at 130 °C on a hot plate under ambient conditions. For the vacuum-deposited layers, they were thermally evaporated on the substrates at a rate of 1 $\text{Å}\,\text{s}^{-1}$ at a base pressure of 5×10^{-6} Torr using an Angstrom Engineering EvoVac system. For the solution-coated layers, the materials were dissolved in toluene to form 10 $\text{mg}\,\text{mL}^{-1}$ solution and then the solution was spin-coated on the substrates using a Laurell spin coater. The coated films were then baked at 60 °C on a hot plate in a glove box to remove the solvent and complete the drying process. X-ray photoelectron spectroscopy (XPS) measurements were performed by Thermo-VG Scientific ESCALab 250 Microprobe equipped with a monochromatic Al Kalpha X-ray source (1486.6 eV) at a base pressure of 10^{-9} Torr using samples of the structure ITO/PEDOT:PSS. Thermo Scientific Avantage software was used for generating the spectra and estimating the atomic concentrations.

9.2 Effect of Toluene on PEDOT:PSS HIL Surface Property and Its Effect on Device Performance

First, we compare the performance of archetypal phosphorescent OLEDs using HTL fabricated via vacuum-deposition and solution-coating processes. Devices with the following structure were fabricated: ITO/PEDOT:PSS (40 nm)/CBP (either vacuum-deposited or solution-coated) (30 nm)/CBP (10 nm)/CBP:$Ir(ppy)_3$ (5%) (15 nm)/TPBi (40 nm)/LiF (1 nm)/Al (80 nm). In

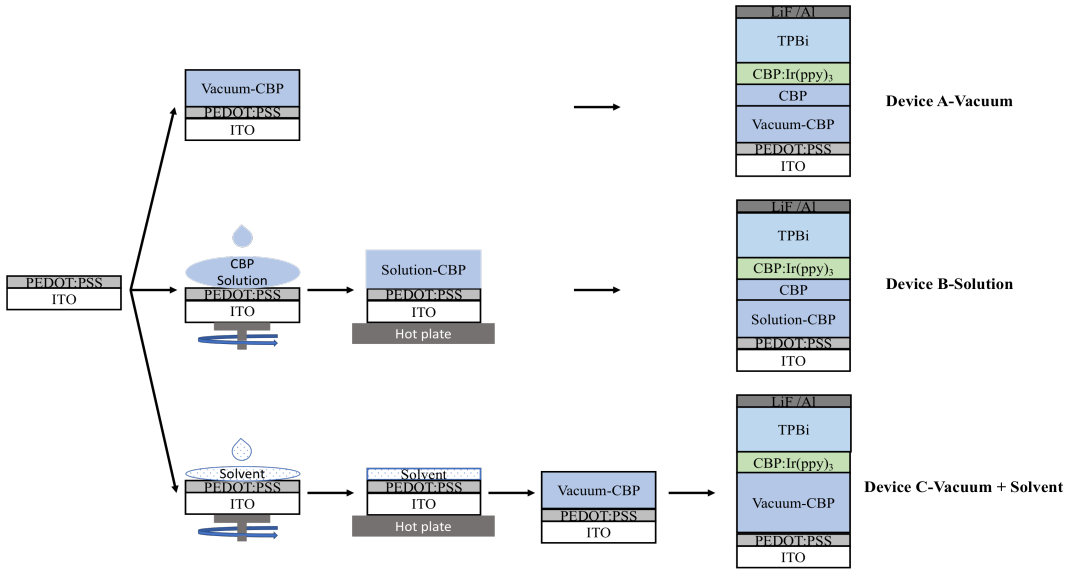

Figure 9.1: Schematic illustrations of the device fabrication sequence including the solvent exposure process.

making these devices, the first 30 nm thick CBP HTL was either vacuum-deposited (device A, used as a control device) or spin-coated (device B). Then, the remaining layers, including the second 10 nm thick CBP layer, were vacuum-deposited to complete the device fabrication process. Figure 9.1 illustrates the fabrication steps of these devices. The 10 nm CBP layer was used for the sake of separating the HTLs from the EMLs and hence limit any effects arising from differences in the HTL fabrication processes on overall device performance to only the HTLs and HILs (without also affecting the EMLs). The EL performance metrics of these devices under electrical driving at a current density of 20 $\mathrm{mA\,cm^{-2}}$ are summarized in Table 9.1. Figure 9.2 (a) shows the J-V-L characteristics of these devices. As seen, device B shows slightly lower charge injection and transport properties in comparison to device A, seen in a slightly higher threshold voltage and a slightly lower current density at any given voltage especially at higher voltages. Figure 9.2

Table 9.1: Driving voltage, luminance, EQE and LT 50 at 20 mA cm^{-2} for devices utilizing vacuum-deposited HTL (device A), solution-coated HTL (device B) and vacuum-deposited HTL (device C) with solvent exposed PEDOT:PSS.

	Voltage [V]	Luminance [cd m^{-2}]	EQE [%]	LT50 [h]
Device A	7.84	12 400	16.80	0.74
Device B	8.40	9 420	12.86	0.12
Device C	8.50	11 900	16.23	0.17

(b) presents the EQE vs current density characteristics of the devices showing a lower EQE in the case of device B in comparison to device A. Figure 9.2 (c) and (d) present the normalized EL decay (=L/L$_0$) and voltage rise (=(V-V$_0$)/V$_0$) versus driving time t at a constant current density of 20 mA cm^{-2} where L and L$_0$ represent the luminance at any time t and the initial luminance, respectively, and V and V$_0$ represent the driving voltage at any time t and the initial driving voltage, respectively. Although the initial luminance is higher in device A than device B, it can be clearly seen that device B shows a more rapid decrease in luminance and increase in voltage in comparison to device A. The luminance LT50 lifetime (time taken for luminance to decay to 50% of its initial luminescence) is 0.74 hours and 0.12 hours for device A and device B, respectively. Although differences in charge injection and transport between the two devices may lead to differences in electron/hole charge balance and in the location/or and width of electron-hole recombination zone within their EMLs, which can be behind the differences in their efficiency and stability, their identical EL spectra in Figure 9.2 (e) indicate that microcavity effects must be very similar in the two devices suggesting that any differences in the recombination zones must be insignificant. The lower EQE and device stability of the solution-processed OLEDs can therefore be primarily attributed to differences in film morphology, in agreement with previous reports [43, 44, 100]. Considering that the stability of device B is about 83% lower than that of device A

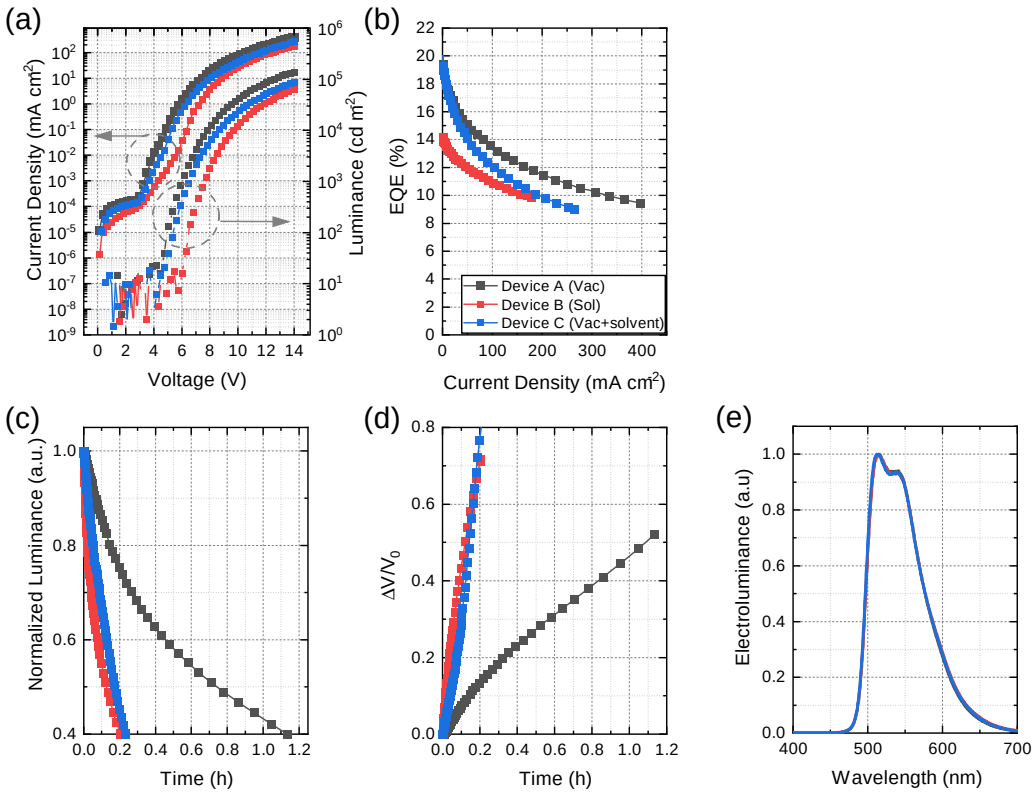

Figure 9.2: (a) J-V-L (b) EQE characteristics (c) normalized luminance and (d) driving voltage versus time under a constant current density of devices utilizing vacuum-deposited HTL (device A), solution-coated HTL (device B) and vacuum-deposited HTL that has been exposed to solvent (device C).

whereas its EQE is only 23% lower, an additional mechanism that has a more significant impact on device stability than it being primarily due to differences in charge balance must exist in the case of device B. It is therefore crucial to identify the underlying causes of the lower stability of device B. Since the only difference between these two devices is the fabrication process of the HTL, it follows that the reduced stability must be related to that aspect. Knowing that morphology

and surface electronic properties of PEDOT:PSS can be affected by exposure to solvents [55], it becomes important to investigate the extent that this stability reduction may be due to the HIL exposure to the HTL solvent.

Yun et al. have shown that exposure to water-immiscible solvents such as the toluene used in the HTL solution can lead to a change in the work function of PEDOT:PSS layer due to its partial adsorption on the surface [55]. As can be seen in Figure 9.2 (d), the voltage rise is significantly faster in device B than device A. Since a progressive increase in driving voltage is required for maintaining the same current density, the trend reflects a rapid deterioration in charge injection and/or transport with time in the device [32, 36]. which may indeed be due to changes at the PEDOT:PSS/CBP interface that arose from the exposure of the PEDOT:PSS surface to the toluene in the HTL solution. Therefore, to further investigate this possibility, we fabricated and tested a device in which only the PEDOT:PSS layer was exposed to toluene and all other device layers are made by vacuum deposition (device C). The device structure is: ITO/PEDOT:PSS (40 nm)/solvent exposure process/CBP (40 nm)/CBP:Ir(ppy)$_3$ (5%) (15 nm)/TPBi (40 nm)/LiF (1 nm)/Al (80 nm). The solvent exposure step was done by spin coating only solvent on the PEEDOT:PSS in a way similar to that used in fabricating a solution-coated HTL, and was followed by annealing at 60 °C for 5 min. Toluene was used for that purpose being a widely used solvent for solution-coated HTLs and the one used in device B. Afterward, the deposition of subsequent layers was resumed. Figure 9.1 illustrates the fabrication steps of device C. Exposing only the PEDOT:PSS layer to the solvent makes it possible to isolate and study the influence of HIL exposure to solvents on device performance without the effects of other confounding factors that take place when the HTL is made by solution coating such as differences in HTL bulk morphology. The EL performance metrics of device C are provided in Table 9.1, whereas the full characteristics are provided in Figure 9.2. A comparison of the EL characteristics shows that the EQE of device C at 20 mA cm^{-2} is similar to that of device A indicating that the solvent exposure of the PEDOT:PSS does not significantly impact efficiency. Surprisingly, and in

stark contrast to the EQE behavior, the LT50 of device C is only 0.17 hours, significantly lower than that of A and comparable to that of B. The EL and voltage versus time trends of C are also very similar to those of B. These results clearly indicate that the PEDOT:PSS exposure to the HTL solvent may indeed be the leading factor behind the lower stability of device B vs device A. A close examination of the J-V characteristics suggests that device C may have a slightly poorer charge transport than A (as can be inferred from a slightly lower current density at any given voltage versus device A). Although device A and device C have a similar maximum EQE, device C exhibits a stronger efficiency roll-off behavior. Since both devices have essentially identical EMLs, the larger efficiency roll-off is likely the result of a more severe deterioration in charge balance at the higher currents, again pointing to less efficient hole transport in the case of device C. Such less efficient hole transport, which can expectedly play a role - at least in part - in the lower stability, must be the result of the solvent exposure step, the latter being the only difference between the two devices. The observations also suggest that the significantly lower EQE of device B versus both A and C is likely due to changes in the CBP HTL bulk properties impacted by the fabrication processes.

In order to further examine the effect of the HTL solvent on the PEDOT:PSS layers and its possibly negative influence on charge transport, we studied the electrical performance of hole-only devices that have the following structure: ITO/PEDOT:PSS (40 nm)/CBP (20 nm)/MoO_3 (5 nm)/Al (80 nm). Under forward bias (i.e., when the ITO contact is held at a more positive potential relative to the Al contact), holes are easily injected from the ITO into the stack and then collected at the Al contact, whereas electron injection from Al is suppressed by the presence of the MoO_3 layer. Current flow under forward bias therefore occurs primarily via holes. Two groups of these hole-only devices were fabricated and tested. In one group, the PEDOT:PSS was exposed to solvent, whereas in the other group, the PEDOT:PSS was not exposed to solvent, and served as control. The solvent exposure was again done by spin coating toluene on the PEDOT:PSS layer followed by thermal annealing. The devices were subjected to a constant current density

of 20 mA cm^{-2} for 1 hour. The J-V characteristics of these devices before and after electrical aging are shown in Figure 9.3 (a). A comparison between the J-V curves before electrical aging shows that the solvent-exposed device exhibits a substantially decreased hole current relative to the control device, confirming that the solvent exposure indeed reduces hole conduction across the HIL and/or into the HTL. This result is consistent with the previous observation that solvent exposure of PEDOTLPSS layer increases hole injection barriers which can be ascribed to the change in the work function of PEDOT:PSS layer [54, 55]. After electrical aging, a shift in the J-V curves is observed in both devices, suggesting that hole conduction becomes more difficult. Notably, the shift is much larger in the case of the solvent-exposed device. Figure 9.3 (c) shows the changes in the driving voltage of the hole-only devices over one hour of electrical driving under a constant current density of 20 mA cm^{-2}. The figure clearly shows that a much larger voltage rise occurs in the case of the solvent-exposed device indicating a faster degradation in hole conduction when the PEDOT:PSS layer is exposed to the solvent. To test if this behavior might be specific to systems where CBP is used as HTL in combination with PEDOT:PSS we also study hole-only devices in which NPB, another widely used HTL is used instead of CBP. The structure of the hole-only devices in this case is ITO/PEDOT:PSS (40 nm)/solvent exposure process/NPB (20 nm)/MoO_3 (5 nm)/Al (80 nm). The J-V curves of these devices are presented in Figure 9.3 (b), whereas the voltage changes over time under electrical stress trends are shown in Figure 9.3 (c). From the results it can be seen that the NPB devices exhibit a very similar behavior. These observations therefore convincingly indicate solvent-induced degradation of the PEDOT:PSS layer is responsible for the rapid increase in driving voltage during device operation and therefore for the rapid device degradation in the solution-coated OLEDs.

We also investigate the effect of exposing PEDOT:PSS to the solvent on its surface morphology as well as that of the subsequently coated HTLs. Knowing that water-immiscible solvents like toluene mainly get adsorbed on PEDOT:PSS layers surface [55], one can expect it may have an effect on the morphology of the HTL. Indeed, a study by Nie et al. has found that exposing

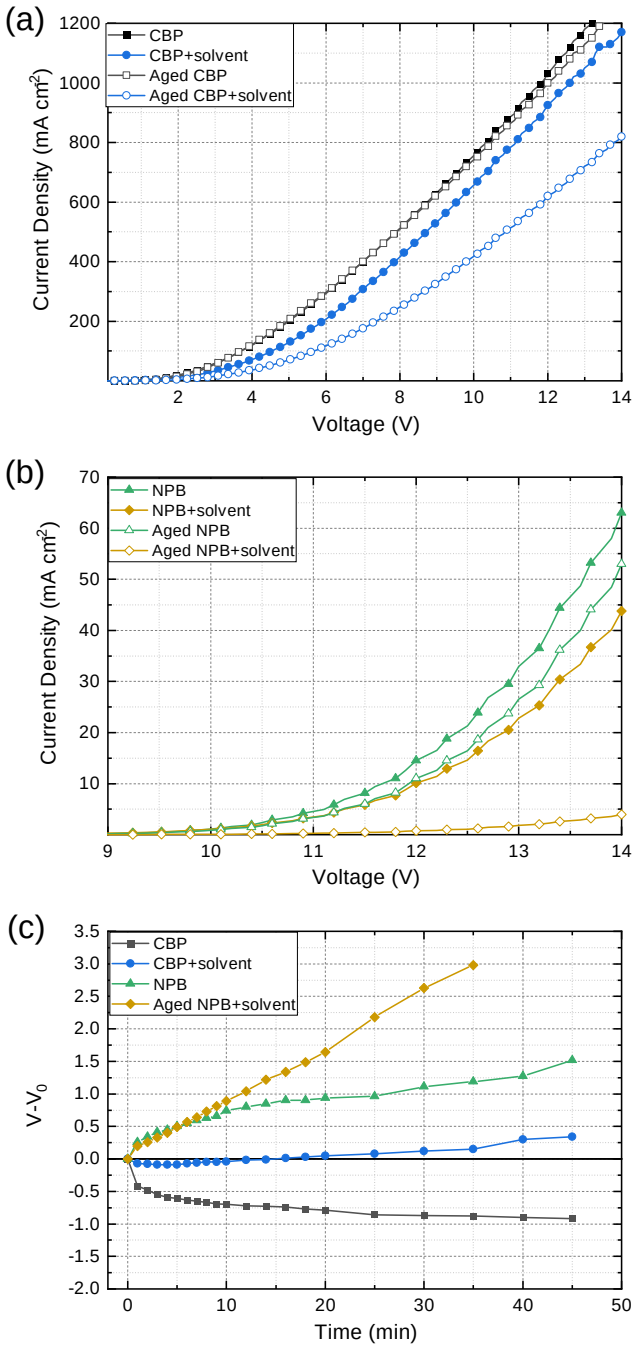

Figure 9.3: J-V characteristics of (a) CBP based hole only devices and (b) NPB based hole only devices before and after electrical driving. (c) Changes in driving voltage of the hole only devices over time at a constant current density of 20 mA cm^{-2}.

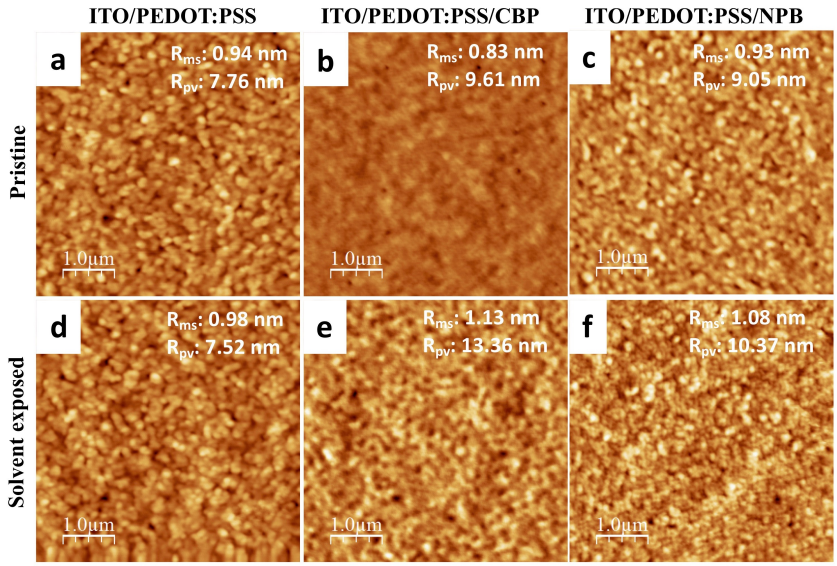

Figure 9.4: AFM images of the pristine (a) PEDOT:PSS film, (b) CBP/PEDOT:PSS film, and (c) NPB/PEDOT:PSS film, and the solvent exposed (d) PEDOT:PSS film, (e) CBP/PEDOT:PSS film, and (f) NPB/PEDOT:PSS film. Rms and Rpv values are indicated in the AFM images.

PEDOT:PSS layers to solvents does not appreciably affect their surface morphology but can alter that of layers coated on them [101]. We therefore used AFM measurements to investigate this behavior in our material system. For this purpose, solvent-exposed and pristine (i.e., un exposed) PEDOT:PSS 40nm thick films, with and without HTLs (CBP or NPB, 30 nm thick) coated on top of them were tested and compared. The same solvent-exposure and subsequent annealing protocol used earlier was used again here. The HTLs were all made by vacuum-deposition. Figure 9.4 (a) and (d) show surface topologies of the pristine and the solvent-exposed PEDOT:PSS films. The AFM images show that the solvent exposure does not lead to any detectable changes in surface morphology or film roughness. The negligible change is consistent with previous observations and can be attributed to the fact that toluene, being water immiscible, will not lead to significant conformational changes between PEDOT and PSS moieties [55, 101]. In contrast, the surface

morphology of the CBP film on the solvent-exposed PEDOT:PSS film exhibits slightly higher surface roughness than the CBP film on the pristine PEDOT:PSS film (Figure 9.4 (b) and (e)). Similarly, the NPB films on the solvent-exposed vs the pristine PEDOT:PSS show a difference in surface roughness, although much smaller in this case (Figure 9.4 (c) and (f)). These observations suggest that the HTL morphology becomes altered when coated on solvent-exposed PEDOT:PSS even if the surface topography of the PEDOT:PSS film remains unchanged.

According to a previous report [51], differences in morphology can influence the photophysical properties of a material and, as a result, its stability under electronic excitation, thus OLED EL stability. We however wish to note that we tested the PL stability under continuous UV illumination (365 nm at 2.3 $\mathrm{mW\,cm^{-2}}$ radiation power for 18 hours in a nitrogen atmosphere) of CBP films coated on solvent-exposed vs pristine PEDOT:PSS films and found no significant differences between their photostability behavior. These test results therefore rule out the possibility that the lower EL stability of device C vs A might be due to a negative effect of solvent exposure on the CBP layer stability. This further suggests that the lower EL stability of device C vs A is primarily due to the detrimental effect of the solvent exposure of PEDOT:PSS on charge conduction.

One possible explanation for the fact that the solvent-exposure of PEDOT:PSS affects the morphology of the subsequent HTL without it affecting the morphology of the PEDOT:PSS layer is that the solvent is adsorbed on the PEDOT:PSS surface and some of it remains even after the thermal annealing. According to Wang et al. complete solvent removal from film surface by thermal annealing is difficult [53]. The presence of residual traces of solvent molecules on the surface can be expected to alter the electronic properties of the PEDOT:PSS/HTL interface, which can affect charge injection and lead to the faster rise in driving voltage observed in these devices. The presence of residual solvent at the interface may also influence HTL morphology due to changes in nucleation and/or surface wetting properties or even due to its subsequent diffusion into the HTL bulk and lead to solvent-mediated aggregation, resulting in the increased roughness

of the HTL surface. We therefore use XPS to investigate the chemical and electronic properties of solvent-exposed PEDOT:PSS layers surface. The core level binding energy XPS spectra of the C 1s, O 1s, and S 2p orbitals from the solvent-exposed and pristine (i.e., unexposed) controls are shown in the upper and lower panels of Figure 9.5 (a),(b) and (c). The C 1s spectrum shows a main band with a peak at 284.2 eV and a shoulder band at 286.0 eV. The 284.2 eV band can be attributed to the C-C and C=C bonds, corresponding to the saturated and conjugated carbon atoms from PEDOT and PSS, respectively, whereas the 286.0 eV shoulder band can be attributed to C-O bonds [55, 102, 103]. The S 2p spectrum can be deconvoluted into two bands. In general, the lower binding energy band can be assigned to sulfur atoms in PEDOT, whereas the higher binding energy band can be assigned to sulfur in the sulfonic acid in PSS [55, 104]. Because the relative peak intensities of the PEDOT and PSS bands correspond with their relative proportions in the PEDOT:PSS matrix, the almost identical relative intensity values of the pristine and solvent-exposed films indicate that the solvent exposure did not alter the PEDOT/PSS ratio. This confirms that the solvent does not lead to significant conformal changes between PEDOT and PSS moieties, and thus does not alter the bulk electrical conduction properties of PEDOT:PSS. The asymmetric O 1s peak results from the overlapping of two separate bands at 531.8 and 533.3 eV, which could be assigned to the oxygen atoms in the PSS and PEDOT moieties, respectively [104]. Unlike the C 1s and S 2p, the O 1s peak in both films shows differences in peak positions, in the form of a peak position shift of 0.3 eV toward higher binding energy in the solvent-exposed film relative to the pristine film. While a shift of this magnitude could simply be due to experimental noise, it might also be due to some modification in the electron charge distribution in the oxygen bonds as a result of the solvent exposure, which could be associated with interactions between the oxygen atoms within PEDOT:PSS and solvent molecules. That is because while, overall, the C 1s and S 2p bands show no change in their peak positions, indicating that the solvent exposure does not lead to chemical changes in PEDOT:PSS in general, their peak intensities are slightly decreased in the solvent-exposed films, while that of the O 1s peak conversely increased. (Fig 9.5 (d), (e) and (f) show the relative intensities of these bands in the solvent-exposed films and

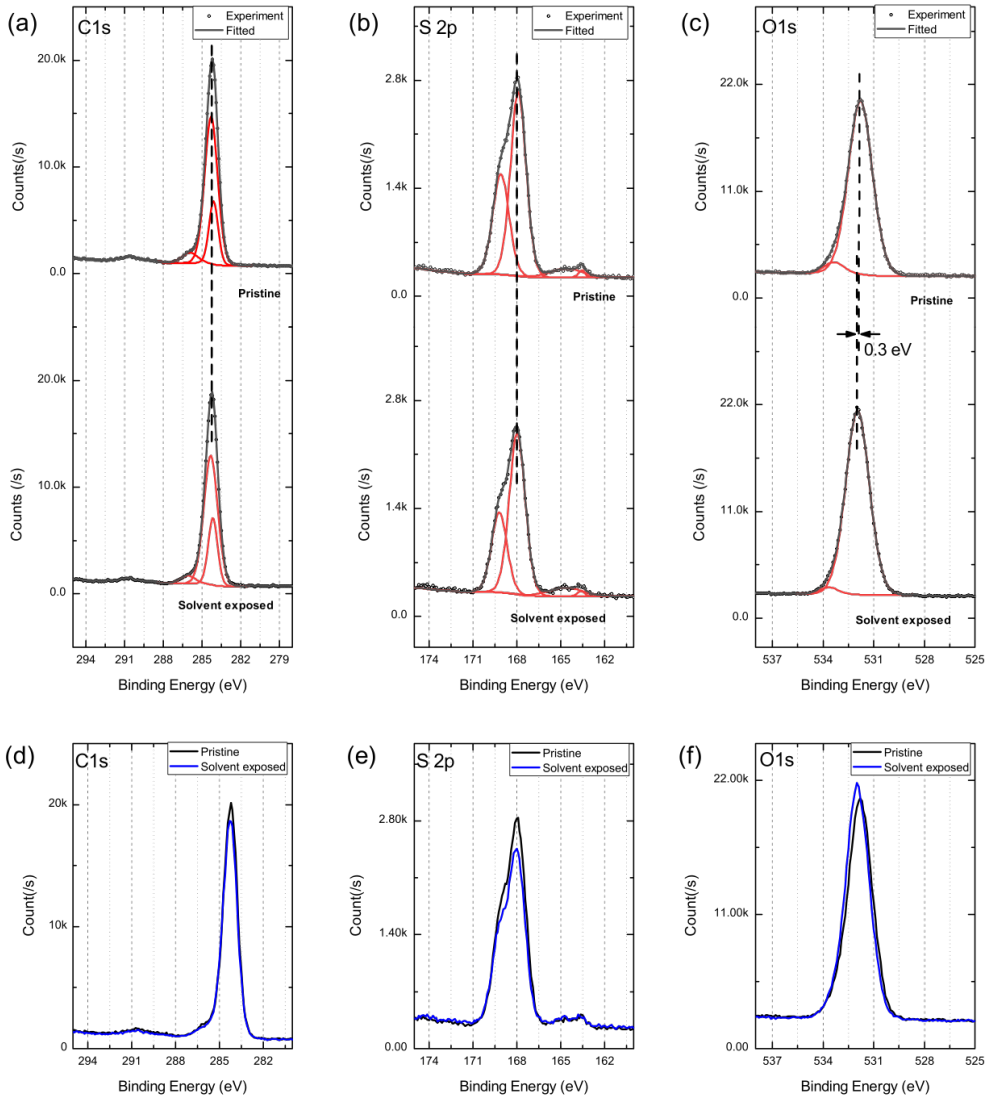

Figure 9.5: Deconvolution of (a) C 1s, (b) S 2p and (c) O1s spectra of pristine (upper panel) and solvent-exposed (lower panel) PEDOT:PSS films and the comparative XPS core level structure of (d) C1s, (e) S2p and (f) O1s of pristine and solvent-exposed PEDOT:PSS films.

Table 9.2: Elemental atomic concentrations (%) in the pristine and solvent-exposed PEDOT:PSS films.

	Atomic concentration (%)				
	C 1s	S 2p	O 1s	In 3d	Sn 3d
Pristine	61.11	7.02	31.36	0.32	0.19
Solvent exposed	60.20	6.19	33.22	0.25	0.14

their pristine counterparts). These observations suggest that the solvent exposure indeed leads to some modification of the PEDOT:PSS surface. To further appreciate these peak intensity changes, the relative atomic concentrations are estimated from the XPS spectra and presented in Table 9.2. The solvent-exposed films have a somewhat higher relative oxygen concentration (33.2% instead of 31.4%). As a result, the relative atomic concentrations of all of the other elements are correspondingly lower. Although the increase is not substantial, and the underlying mechanism is unclear, a higher oxygen concentration at the PEDOT:PSS surface in the case of solvent-exposed film could be expected to make hole injection more difficult [53, 54, 55]. This finding is consistent with the EL characteristics in Table 9.1, where device B and device C require a higher driving voltage than device A in driving the same current density. A reduction in charge injection efficiency can naturally lead to a decrease in OLED EL stability. Increased hole accumulation at the PEDOT:PSS/HTL interface, as a result of the higher injection barrier, may also contribute to the faster degradation in these devices [32].

9.3 Conclusion

In this study, we investigate the effects of exposing PEDOT:PSS HILs to toluene, a commonly used solvent in solution-coated HTLs, on OLED performance. Results show that the solvent

exposure leads to a significant decrease in device EL stability, revealing that the phenomenon plays a role in the lower stability of devices with solution-coated HTLs. The solvent exposure is found to reduce hole injection efficiency, possibly due to changes at the PEDOT:PSS/HTL interface, a phenomenon that likely plays a role in the lower EL stability in these devices. It also affects the HTL morphology. The findings bring to light one of the major root causes of the lower stability of solution-coated OLEDs.

Chapter 10

Conclusions and Future Work

10.1 Conclusions

This thesis focuses on studying the effects of exciton-stress in organic small molecule electroluminescent materials with the specific purpose of investigating two aspects: (i) the effect of exciton stress on material morphology and the subsequent effect of that on device performance; and (ii) the dependence of exciton-induced aging on device fabrication processes.

The main findings derived from the experiments and analysis presented in the thesis can be summarized in terms of specific research objectives as listed:

1. Exciton stress has been found to lead to an increase in surface roughness giving direct evidence of morphological changes and molecular aggregation as a result of excitation. Photoluminescence measurements show that the exposure to UV leads to a red shift in the PL spectra of the materials and a decrease in exciton lifetime consistent with molecular aggregation. Results also show that exciton-induced morphological changes in the films facilitate their crystallization upon heating.

2. Exciton stress in the ETL has been found to have a detrimental effect on device performance. Interactions between the ETL materials and exciton-induced host molecular aggregates are found to produce complex species, a phenomenon that underlies the red shift often observed in the electroluminescent spectra of PhOLEDs over time. Comparisons between the exciton

stress and thermal stress suggest that exciton-induced aggregation may be limited to short-range molecular ordering or pairing versus longer range ordering in the case of thermal stress.

3. Exciton stress in HTL also affects device performance; this is through the formation of quenchers that degrade efficiency and stability. This phenomenon affects PhOLEDs more significantly than their fluorescent counterparts because of the relatively longer exciton diffusion length of triplet excitons, which allows a larger fraction of triplets to reach the EML, and thus makes their quenching by quenchers in the HTL to more negatively impact EQE. Increasing the exciton stability of HTLs by introducing dopants in them or altering their morphology reduces this degradation mode and, therefore, helps increase device EL stability.

4. Changing the deposition rate of the HTL shows that the device stability is found to increase upon decreasing the HTL deposition rate. A lower deposition rate is found to enhance the exciton stability and decrease exciton lifetime, which could be attributed to the higher morphological order that reduces exciton-induced degradation in them.

5. Comparative investigations of solution-coated versus vacuum-deposited OLEDs shows that exciton stress brings about larger loses in PL quantum yield and in host-to-guest energy transfer in the case of solution-coated host:guest systems. The faster host to guest phase separation in the solution-coated films is attributed to their less homogenous morphologies that include guest-deficient aggregates of host molecules, which makes host-to-guest energy transfer less efficient in them in comparison to their vacuum-deposited counterparts.

6. Exposure of PEDOT:PSS, the hole injection material most widely used in solution-coated OLEDs, to solvents during the HTL coating process has been found to degrade the hole injection efficiency of the contact. Results show that solvent exposure leads to a significant decrease in device EL stability, revealing that the phenomenon plays a role in the lower

stability of devices with solution-coated HTLs. The solvent exposure is found to reduce hole injection efficiency, possibly due to changes at the PEDOT:PSS/HTL interface, a phenomenon that likely plays a role in the lower EL stability in these devices.

10.2 Future Work

CBP has been the most widely used host material in PhOLEDs. However, as this work reveals, it tends to aggregate under exciton stress. It also tends to form less homogeneous morphologies and increased aggregate formation when solution-coated, which accelerates its degradation by exciton-stress. Finding that exciton-induced degradation limits efficiency and stability of PhOLEDs, future work to control exciton-induced degradation in the organic films by increasing morphological stability would be beneficial.

One solution to improve the morphological stability of these carbazole based compounds is to replace the para-linkage by a meta-linkage of the carbazole substituents at the central biphenyl unit. It has been shown that CBP derivatives with a meta-linkage can lead to improved thermal and optical properties in thin films and to a much low tendency to crystallize [105]. Therefore, it would be interesting to examine exciton-induced degradation in this material and compare the films deposited by solution coating and vacuum-deposition.

It also has been found that the solvent used in coating one layer may affect the charge injection or transport properties of an underlying layer even if it does not affect its structural integrity or morphology. Residual solvent due to surface adsorption may be behind the altered electrical properties. In this context, investigating approaches for avoiding or reducing solvent adsorption such as baking in vacuum would be important. [53]. Therefore, it is interesting to study if this process can completely remove and therefore reduce the negative effect of the solvent on the HIL and solution-coated OLEDs.

Bibliography

[1] H. Ishii, K. Sugiyama, E. Ito, and K. Seki, "Energy Level Alignment and Interfacial Electronic Structures at Organic/Metal and Organic/Organic Interfaces," *Adv. Mater.*, vol. 11, pp. 605–625, jun 1999.

[2] M. A. Baldo, D. F. O'Brien, M. E. Thompson, and S. R. Forrest, "Excitonic singlet-triplet ratio in a semiconducting organic thin film," *Phys. Rev. B*, vol. 60, pp. 14422–14428, nov 1999.

[3] C. W. Tang and S. A. VanSlyke, "Organic electroluminescent diodes," *Appl. Phys. Lett.*, vol. 51, pp. 913–915, sep 1987.

[4] L. S. Hung, C. W. Tang, and M. G. Mason, "Enhanced electron injection in organic electroluminescence devices using an Al/LiF electrode," *Appl. Phys. Lett.*, vol. 70, pp. 152–154, jan 1997.

[5] S. Tokito, K. Noda, and Y. Taga, "Metal oxides as a hole-injecting layer for an organic electroluminescent device," *J. Phys. D. Appl. Phys.*, vol. 29, pp. 2750–2753, nov 1996.

[6] J. Scott, S. Carter, S. Karg, and M. Angelopoulos, "Polymeric anodes for organic light-emitting diodes," *Synth. Met.*, vol. 85, pp. 1197–1200, mar 1997.

[7] C. C. Wu, C. I. Wu, J. C. Sturm, and A. Kahn, "Surface modification of indium tin oxide by plasma treatment: An effective method to improve the efficiency, brightness, and reliability of organic light emitting devices," *Appl. Phys. Lett.*, vol. 70, pp. 1348–1350, mar 1997.

[8] J. S. Kim, M. Granström, R. H. Friend, N. Johansson, W. R. Salaneck, R. Daik, W. J. Feast, and F. Cacialli, "Indium–tin oxide treatments for single- and double-layer polymeric light-emitting diodes: The relation between the anode physical, chemical, and morphological properties and the device performance," *J. Appl. Phys.*, vol. 84, pp. 6859–6870, dec 1998.

[9] J.-S. Kim, F. Cacialli, and R. Friend, "Surface conditioning of indium-tin oxide anodes for organic light-emitting diodes," *Thin Solid Films*, vol. 445, pp. 358–366, dec 2003.

[10] C. Murawski, K. Leo, and M. C. Gather, "Efficiency Roll-Off in Organic Light-Emitting Diodes," *Adv. Mater.*, vol. 25, pp. 6801–6827, dec 2013.

[11] J.-S. Kim, P. K. H. Ho, N. C. Greenham, and R. H. Friend, "Electroluminescence emission pattern of organic light-emitting diodes: Implications for device efficiency calculations," *J. Appl. Phys.*, vol. 88, pp. 1073–1081, jul 2000.

[12] B. J. Chen, W. Y. Lai, Z. Q. Gao, C. S. Lee, S. T. Lee, and W. A. Gambling, "Electron drift mobility and electroluminescent efficiency of tris(8-hydroxyquinolinolato) aluminum," *Appl. Phys. Lett.*, vol. 75, pp. 4010–4012, dec 1999.

[13] C.-C. Lee, S.-W. Liu, and Y.-T. Chung, "Effect of deposition rate on device performance and lifetime of planar molecule-based organic light-emitting diodes," *J. Phys. D. Appl. Phys.*, vol. 43, p. 075102, feb 2010.

[14] S. F. Swallen, K. L. Kearns, M. K. Mapes, Y. S. Kim, R. J. McMahon, M. D. Ediger, T. Wu, L. Yu, and S. Satija, "Organic Glasses with Exceptional Thermodynamic and Kinetic Stability," *Science (80-.).*, vol. 315, pp. 353–356, jan 2007.

[15] S. S. Dalal, D. M. Walters, I. Lyubimov, J. J. de Pablo, and M. D. Ediger, "Tunable molecular orientation and elevated thermal stability of vapor-deposited organic semiconductors," *Proc. Natl. Acad. Sci.*, vol. 112, pp. 4227–4232, apr 2015.

[16] K. L. Kearns, P. Krzyskowski, and Z. Devereaux, "Using deposition rate to increase the thermal and kinetic stability of vapor-deposited hole transport layer glasses via a simple sublimation apparatus," *J. Chem. Phys.*, vol. 146, p. 203328, may 2017.

[17] "Universal Display Corporation."

[18] M. Koden, *OLED Displays and Lighting*. Wiley - IEEE, Wiley, 2016.

[19] H. Aziz and Z. D. Popovic, "Degradation Phenomena in Small-Molecule Organic Light-Emitting Devices," *Chem. Mater.*, vol. 16, pp. 4522–4532, nov 2004.

[20] P. E. Burrows and S. R. Forrest, "Electroluminescence from trap-limited current transport in vacuum deposited organic light emitting devices," *Appl. Phys. Lett.*, vol. 64, pp. 2285–2287, apr 1994.

[21] P. E. Burrows, V. Bulovic, S. R. Forrest, L. S. Sapochak, D. M. McCarty, and M. E. Thompson, "Reliability and degradation of organic light emitting devices," *Appl. Phys. Lett.*, vol. 65, pp. 2922–2924, dec 1994.

[22] H. Aziz, "Degradation mechanism of small molecule-based organic light-emitting devices," *Science (80-.).*, vol. 283, no. 5409, pp. 1900–1902, 1999.

[23] N. C. Giebink, B. W. D'Andrade, M. S. Weaver, J. J. Brown, and S. R. Forrest, "Direct evidence for degradation of polaron excited states in organic light emitting diodes," *J. Appl. Phys.*, vol. 105, p. 124514, jun 2009.

[24] Y. Luo, H. Aziz, G. Xu, and Z. D. Popovic, "Electron-induced quenching of excitons in luminescent materials," *Chem. Mater.*, vol. 19, no. 9, pp. 2288–2291, 2007.

[25] N. C. Giebink, B. W. D'Andrade, M. S. Weaver, P. B. Mackenzie, J. J. Brown, M. E. Thompson, and S. R. Forrest, "Intrinsic luminance loss in phosphorescent small-molecule organic light emitting devices due to bimolecular annihilation reactions," *J. Appl. Phys.*, vol. 103, p. 044509, feb 2008.

[26] M. Matsumura, A. Ito, and Y. Miyamae, "Accumulation of positive charges in organic light-emitting diodes with a double-layer structure," *Appl. Phys. Lett.*, vol. 75, pp. 1042–1044, aug 1999.

[27] D. Y. Kondakov, J. R. Sandifer, C. W. Tang, and R. H. Young, "Nonradiative recombination centers and electrical aging of organic light-emitting diodes: Direct connection between accumulation of trapped charge and luminance loss," *J. Appl. Phys.*, vol. 93, pp. 1108–1119, jan 2003.

[28] D. Y. Kondakov, "Direct observation of deep electron traps in aged organic light emitting diodes," *J. Appl. Phys.*, vol. 97, no. 2, pp. 1–6, 2005.

[29] L. J. Rothberg and A. J. Lovinger, "Status of and prospects for organic electroluminescence," *J. Mater. Res.*, vol. 11, pp. 3174–3187, dec 1996.

[30] D. Y. Kondakov, W. C. Lenhart, and W. F. Nichols, "Operational degradation of organic light-emitting diodes: Mechanism and identification of chemical products," *J. Appl. Phys.*, vol. 101, p. 024512, jan 2007.

[31] S.-C. Dong, L. Xu, and C. W. Tang, "Chemical degradation mechanism of TAPC as hole transport layer in blue phosphorescent OLED," *Org. Electron.*, vol. 42, pp. 379–386, mar 2017.

[32] Q. Wang and H. Aziz, "Degradation of Organic/Organic Interfaces in Organic Light-Emitting Devices due to Polaron–Exciton Interactions," *ACS Appl. Mater. Interfaces*, vol. 5, pp. 8733–8739, sep 2013.

[33] Q. Wang, B. Sun, and H. Aziz, "Exciton-Polaron-Induced Aggregation of Wide-Bandgap Materials and its Implication on the Electroluminescence Stability of Phosphorescent Organic Light-Emitting Devices," *Adv. Funct. Mater.*, vol. 24, pp. 2975–2985, may 2014.

[34] Q. Wang and H. Aziz, "Exciton-Polaron-Induced Aggregation of Organic Electroluminescent Materials: A Major Degradation Mechanism in Wide-Bandgap Phosphorescent and Fluorescent Organic Light-Emitting Devices," *Adv. Opt. Mater.*, vol. 3, pp. 967–975, jul 2015.

[35] Q. Wang and H. Aziz, "The different influence of singlet and triplet excitons in the degradation of phosphorescent organic light-emitting devices due to exciton–polaron-induced aggregation of host materials," *Org. Electron.*, vol. 26, pp. 464–470, nov 2015.

[36] Y. Zhang and H. Aziz, "Influence of the Guest on Aggregation of the Host by Exciton–Polaron Interactions and Its Effects on the Stability of Phosphorescent Organic Light-Emitting Devices," *ACS Appl. Mater. Interfaces*, vol. 8, pp. 14088–14095, jun 2016.

[37] S. R. Forrest, "The path to ubiquitous and low-cost organic electronic appliances on plastic," *Nature*, vol. 428, pp. 911–918, apr 2004.

[38] Y.-F. Liu, J. Feng, Y.-G. Bi, D. Yin, and H.-B. Sun, "Recent Developments in Flexible Organic Light-Emitting Devices," *Adv. Mater. Technol.*, vol. 4, p. 1800371, jan 2019.

[39] M. Cai, T. Xiao, E. Hellerich, Y. Chen, R. Shinar, and J. Shinar, "High-Efficiency Solution-Processed Small Molecule Electrophosphorescent Organic Light-Emitting Diodes," *Adv. Mater.*, vol. 23, pp. 3590–3596, aug 2011.

[40] B. Zhang, G. Tan, C.-S. Lam, B. Yao, C.-L. Ho, L. Liu, Z. Xie, W.-Y. Wong, J. Ding, and L. Wang, "High-Efficiency Single Emissive Layer White Organic Light-Emitting Diodes Based on Solution-Processed Dendritic Host and New Orange-Emitting Iridium Complex," *Adv. Mater.*, vol. 24, pp. 1873–1877, apr 2012.

[41] T.-H. Han, M.-R. Choi, C.-W. Jeon, Y.-H. Kim, S.-K. Kwon, and T.-W. Lee, "Ultrahigh-efficiency solution-processed simplified small-molecule organic light-emitting diodes using universal host materials," *Sci. Adv.*, vol. 2, p. e1601428, oct 2016.

[42] L. Duan, L. Hou, T.-W. Lee, J. Qiao, D. Zhang, G. Dong, L. Wang, and Y. Qiu, "Solution processable small molecules for organic light-emitting diodes," *J. Mater. Chem.*, vol. 20, no. 31, p. 6392, 2010.

[43] T.-W. Lee, T. Noh, H.-W. Shin, O. Kwon, J.-J. Park, B.-K. Choi, M.-S. Kim, D. W. Shin, and Y.-R. Kim, "Characteristics of Solution-Processed Small-Molecule Organic Films and Light-Emitting Diodes Compared with their Vacuum-Deposited Counterparts," *Adv. Funct. Mater.*, vol. 19, pp. 1625–1630, may 2009.

[44] Y. J. Cho, Y. Zhang, H. Yu, and H. Aziz, "The Root Causes of the Limited Stability of Solution-Coated Small-Molecule Organic Light-Emitting Devices: Faster Host Aggregation by Exciton-Polaron Interactions," *Adv. Funct. Mater.*, vol. 26, pp. 8662–8669, dec 2016.

[45] K. S. Yook and J. Y. Lee, "Solution processed deep blue phosphorescent organic light-emitting diodes with over 20% external quantum efficiency," *Org. Electron. physics, Mater. Appl.*, vol. 12, no. 10, pp. 1711–1715, 2011.

[46] X. Xing, L. Zhong, L. Zhang, Z. Chen, B. Qu, E. Chen, L. Xiao, and Q. Gong, "Essential Differences of Organic Films at the Molecular Level via Vacuum Deposition and Solution Processes for Organic Light-Emitting Diodes," *J. Phys. Chem. C*, vol. 117, pp. 25405–25408, dec 2013.

[47] S. Feng, L. Duan, L. Hou, J. Qiao, D. Zhang, G. Dong, L. Wang, and Y. Qiu, "A Comparison Study of the Organic Small Molecular Thin Films Prepared by Solution Process and Vacuum Deposition: Roughness, Hydrophilicity, Absorption, Photoluminescence, Density, Mobility, and Electroluminescence," *J. Phys. Chem. C*, vol. 115, pp. 14278–14284, jul 2011.

[48] K. S. Yook and J. Y. Lee, "Small Molecule Host Materials for Solution Processed Phosphorescent Organic Light-Emitting Diodes," *Adv. Mater.*, vol. 26, pp. 4218–4233, jul 2014.

[49] H. Kim, Y. Byun, R. R. Das, B.-K. Choi, and P.-S. Ahn, "Small molecule based and solution processed highly efficient red electrophosphorescent organic light emitting devices," *Appl. Phys. Lett.*, vol. 91, p. 093512, aug 2007.

[50] M. Shibata, Y. Sakai, and D. Yokoyama, "Advantages and disadvantages of vacuum-deposited and spin-coated amorphous organic semiconductor films for organic light-emitting diodes," *J. Mater. Chem. C*, vol. 3, no. 42, pp. 11178–11191, 2015.

[51] Y. J. Cho and H. Aziz, "Root Causes of the Limited Electroluminescence Stability of Organic Light-Emitting Devices Made by Solution-Coating," *ACS Appl. Mater. Interfaces*, vol. 10, pp. 18113–18122, may 2018.

[52] L. Liu, X. Liu, B. Zhang, J. Ding, Z. Xie, and L. Wang, "A binary solvent mixture-induced aggregation of a carbazole dendrimer host toward enhancing the performance of solution-processed blue electrophosphorescent devices," *J. Mater. Chem. C*, vol. 3, no. 19, pp. 5050–5055, 2015.

[53] Q. Wang, Y. Zhou, H. Zheng, J. Shi, C. Li, C. Q. Su, L. Wang, C. Luo, D. Hu, J. Pei, J. Wang, J. Peng, and Y. Cao, "Modifying organic/metal interface via solvent treatment to improve electron injection in organic light emitting diodes," *Org. Electron.*, vol. 12, pp. 1858–1863, nov 2011.

[54] Q. Wang, Y. Chen, Y. Zheng, N. Ai, S. Han, W. Xu, Z. Jiang, Y. Meng, D. Hu, J. Peng, J. Wang, and Y. Cao, "Solvent treatment as an efficient anode modification method to improve device performance of polymer light-emitting diodes," *Org. Electron.*, vol. 14, pp. 548–553, feb 2013.

[55] D.-J. Yun, J.-H. Kim, S. H. Kim, M. Seol, D. Yu, H. Kwon, Y. Ham, J. Chung, Y. Kim, and S. Heo, "Study on the disparate transition behaviors of the electrical/physical properties in PEDOT:PSS film depending on solvent species under a follow-up solution-treatment process," *Nanotechnology*, vol. 27, p. 165706, apr 2016.

[56] J. S. Kim, R. H. Friend, and F. Cacialli, "Improved operational stability of polyfluorene-based organic light-emitting diodes with plasma-treated indium-tin-oxide anodes," *Appl. Phys. Lett.*, vol. 74, no. 21, pp. 3084–3086, 1999.

[57] M. P. de Jong, L. J. van IJzendoorn, and M. J. A. de Voigt, "Stability of the interface between indium-tin-oxide and poly(3,4-ethylenedioxythiophene)/poly(styrenesulfonate) in polymer light-emitting diodes," *Appl. Phys. Lett.*, vol. 77, pp. 2255–2257, oct 2000.

[58] Y. Zhang and H. Aziz, "Degradation Mechanisms in Blue Phosphorescent Organic Light-Emitting Devices by Exciton–Polaron Interactions: Loss in Quantum Yield versus Loss in Charge Balance," *ACS Appl. Mater. Interfaces*, vol. 9, pp. 636–643, jan 2017.

[59] H. Yu, Y. Zhang, Y. J. Cho, and H. Aziz, "Exciton-Induced Degradation of Carbazole-Based Host Materials and Its Role in the Electroluminescence Spectral Changes in Phosphorescent Organic Light Emitting Devices with Electrical Aging," *ACS Appl. Mater. Interfaces*, vol. 9, pp. 14145–14152, apr 2017.

[60] Y. Zhang, J. Lee, and S. R. Forrest, "Tenfold increase in the lifetime of blue phosphorescent organic light-emitting diodes," *Nat. Commun.*, vol. 5, p. 5008, dec 2014.

[61] J.-A. Seo, S. K. Jeon, M. S. Gong, J. Y. Lee, C. H. Noh, and S. H. Kim, "Long lifetime blue phosphorescent organic light-emitting diodes with an exciton blocking layer," *J. Mater. Chem. C*, vol. 3, no. 18, pp. 4640–4645, 2015.

[62] J. S. Bangsund, K. W. Hershey, and R. J. Holmes, "Isolating Degradation Mechanisms in Mixed Emissive Layer Organic Light-Emitting Devices," *ACS Appl. Mater. Interfaces*, vol. 10, pp. 5693–5699, feb 2018.

[63] K. S. Yook and J. Y. Lee, "Organic materials for deep blue phosphorescent organic light-emitting diodes," *Adv. Mater.*, vol. 24, no. 24, pp. 3169–3190, 2012.

[64] L. Xiao, Z. Chen, B. Qu, J. Luo, S. Kong, Q. Gong, and J. Kido, "Recent progresses on materials for electrophosphorescent organic light-emitting devices," *Adv. Mater.*, vol. 23, no. 8, pp. 926–952, 2011.

[65] S. Gong, X. He, Y. Chen, Z. Jiang, C. Zhong, D. Ma, J. Qin, and C. Yang, "Simple CBP isomers with high triplet energies for highly efficient blue electrophosphorescence," *J. Mater. Chem.*, vol. 22, no. 7, pp. 2894–2899, 2012.

[66] E. A. Chandross, "Photolytic Dissociation of Dianthracene," *J. Chem. Phys.*, vol. 43, pp. 4175–4176, dec 1965.

[67] E. A. Chandross and J. Ferguson, "Absorption and Excimer Fluorescence Spectra of Sandwich Dimers of Substituted Anthracenes," *J. Chem. Phys.*, vol. 45, pp. 3554–3564, nov 1966.

[68] Q. Wang, Y. Luo, and H. Aziz, "Evidence of intermolecular species formation with electrical aging in anthracene-based blue organic light-emitting devices," *J. Appl. Phys.*, vol. 107, p. 084506, apr 2010.

[69] W. Li, J. Zhao, X. Kong, X. Du, X. Li, C. Zheng, and S. Tao, "Improving the performance of solution-processed small molecule OLEDs via micro-aggregation formed by an alcohol additive incorporation," *Org. Electron.*, vol. 64, pp. 252–258, jan 2019.

[70] R. Jakubiak, C. J. Collison, W. C. Wan, L. J. Rothberg, and B. R. Hsieh, "Aggregation Quenching of Luminescence in Electroluminescent Conjugated Polymers," *J. Phys. Chem. A*, vol. 103, pp. 2394–2398, apr 1999.

[71] Y. Kawamura, J. Brooks, J. J. Brown, H. Sasabe, and C. Adachi, "Intermolecular Interaction and a Concentration-Quenching Mechanism of Phosphorescent Ir(III) Complexes in a Solid Film," *Phys. Rev. Lett.*, vol. 96, p. 017404, jan 2006.

[72] Y. J. Cho, S. Taylor, and H. Aziz, "Increased Electromer Formation and Charge Trapping in Solution-Processed versus Vacuum-Deposited Small Molecule Host Materials of Organic Light-Emitting Devices," *ACS Appl. Mater. Interfaces*, vol. 9, pp. 40564–40572, nov 2017.

[73] M. H. Tsai, Y. H. Hong, C. H. Chang, H. C. Su, C. C. Wu, A. Matoliukstyte, J. Simokaitiene, S. Grigalevicius, J. V. Grazulevicius, and C. P. Hsu, "3-(9-carbazolyI)carbazoles and 3,6-Di(9-carbazolyl)carbazoles as effective host materials for efficient blue organic electrophosphorescence," *Adv. Mater.*, vol. 19, pp. 862–866, mar 2007.

[74] J. B. Birks, "Excimers," *Reports Prog. Phys.*, vol. 38, pp. 903–974, aug 1975.

[75] J. Kalinowski, G. Giro, M. Cocchi, V. Fattori, and P. Di Marco, "Unusual disparity in electroluminescence and photoluminescence spectra of vacuum-evaporated films of 1,1-bis ((di-4-tolylamino) phenyl) cyclohexane," *Appl. Phys. Lett.*, vol. 76, pp. 2352–2354, apr 2000.

[76] T. Granlund, L. A. A. Pettersson, M. R. Anderson, and O. Inganäs, "Interference phenomenon determines the color in an organic light emitting diode," *J. Appl. Phys.*, vol. 81, pp. 8097–8104, jun 1997.

[77] Y.-S. Park, S. Lee, K.-H. Kim, S.-Y. Kim, J.-H. Lee, and J.-J. Kim, "Exciplex-Forming Co-host for Organic Light-Emitting Diodes with Ultimate Efficiency," *Adv. Funct. Mater.*, vol. 23, pp. 4914–4920, oct 2013.

[78] S. Yang and M. Jiang, "White light generation combining emissions from exciplex, excimer and electromer in TAPC-based organic light-emitting diodes," *Chem. Phys. Lett.*, vol. 484, pp. 54–58, dec 2009.

[79] T. Glaser, S. Beck, B. Lunkenheimer, D. Donhauser, A. Köhn, M. Kröger, and A. Pucci, "Infrared study of the MoO3 doping efficiency in 4,4'-bis(N-carbazolyl)-1,1'-biphenyl (CBP)," *Org. Electron.*, vol. 14, pp. 575–583, feb 2013.

[80] H.-W. Lu, H.-L. Weng, P.-C. Kao, S.-Y. Chu, and Y.-D. Juang, "Fabrication of Color-Tunable Blue-Violet Organic Light Emitting Diodes for White Light Source," *ECS J. Solid State Sci. Technol.*, vol. 5, pp. R104–R109, apr 2016.

[81] M. Wei, G. Gui, Y.-H. Chung, L. Xiao, B. Qu, and Z. Chen, "Micromechanism of electroplex formation," *Phys. status solidi*, vol. 252, pp. 1711–1716, aug 2015.

[82] J. Zhang, Z. Chen, Y. Liu, M. Huang, Q. Wei, and Q. Gong, "Improvement on the photorefractive performance of a monolithic molecular material by introducing electron traps," *Appl. Phys. Lett.*, vol. 85, pp. 1323–1325, aug 2004.

[83] R. Phatak, T. Y. Tsui, and H. Aziz, "Dependence of dark spot growth on cathode/organic interfacial adhesion in organic light emitting devices," *J. Appl. Phys.*, vol. 111, p. 054512, mar 2012.

[84] Y.-F. Liew, H. Aziz, N.-X. Hu, H. S.-O. Chan, G. Xu, and Z. Popovic, "Investigation of the sites of dark spots in organic light-emitting devices," *Appl. Phys. Lett.*, vol. 77, pp. 2650–2652, oct 2000.

[85] J. Lee, C. Jeong, T. Batagoda, C. Coburn, M. E. Thompson, and S. R. Forrest, "Hot excited state management for long-lived blue phosphorescent organic light-emitting diodes," *Nat. Commun.*, vol. 8, p. 15566, aug 2017.

[86] Y. J. Kang and J. Y. Lee, "High triplet energy electron transport type exciton blocking materials for stable blue phosphorescent organic light-emitting diodes," *Org. Electron.*, vol. 32, pp. 109–114, may 2016.

[87] Y. Zhang, M. M. A. Abdelmalek, Q. Wang, and H. Aziz, "Degradation mechanism in simplified phosphorescent organic light-emitting devices utilizing one material for hole transport and emitter host," *Appl. Phys. Lett.*, vol. 103, p. 063307, aug 2013.

[88] Y. Zhang, M. Sims, S. Li, and H. Aziz, "Triplet-induced degradation: An important consideration in the design of solution-processed hole injection materials for organic light-emitting devices," *Org. Electron.*, vol. 48, pp. 217–222, sep 2017.

[89] O. V. Mikhnenko, P. W. M. Blom, and T.-Q. Nguyen, "Exciton diffusion in organic semiconductors," *Energy Environ. Sci.*, vol. 8, no. 7, pp. 1867–1888, 2015.

[90] C. W. Tang, S. A. VanSlyke, and C. H. Chen, "Electroluminescence of doped organic thin films," *J. Appl. Phys.*, vol. 65, pp. 3610–3616, may 1989.

[91] Y. Qiu, L. W. Antony, J. J. de Pablo, and M. D. Ediger, "Photostability Can Be Significantly Modulated by Molecular Packing in Glasses," *J. Am. Chem. Soc.*, vol. 138, pp. 11282–11289, sep 2016.

[92] W. R. Mateker, T. Heumueller, R. Cheacharoen, I. T. Sachs-Quintana, M. D. McGehee, J. Warnan, P. M. Beaujuge, X. Liu, and G. C. Bazan, "Molecular Packing and Arrangement Govern the Photo-Oxidative Stability of Organic Photovoltaic Materials," *Chem. Mater.*, vol. 27, pp. 6345–6353, sep 2015.

[93] Y. W. Soon, S. Shoaee, R. S. Ashraf, H. Bronstein, B. C. Schroeder, W. Zhang, Z. Fei, M. Heeney, I. McCulloch, and J. R. Durrant, "Material crystallinity as a determinant of triplet dynamics and oxygen quenching in donor polymers for organic photovoltaic devices," *Adv. Funct. Mater.*, vol. 24, no. 10, pp. 1474–1482, 2014.

[94] S. M. Menke and R. J. Holmes, "Exciton diffusion in organic photovoltaic cells," *Energy Environ. Sci.*, vol. 7, no. 2, pp. 499–512, 2014.

[95] Y. H. Lee, W. J. Kim, T. Y. Kim, J. H. Yang, K. S. Cho, J. W. Hong, J. Y. Shin, and T. W. Kim, "Effect of Deposition Rate of Organic Layer on Electrical and Optical Characteristics of OLEDs," *Mol. Cryst. Liq. Cryst.*, vol. 462, pp. 143–148, dec 2006.

[96] W. Song and J. Y. Lee, "Degradation Mechanism and Lifetime Improvement Strategy for Blue Phosphorescent Organic Light-Emitting Diodes," *Adv. Opt. Mater.*, vol. 5, p. 1600901, may 2017.

[97] S. Scholz, D. Kondakov, B. Lüssem, and K. Leo, "Degradation Mechanisms and Reactions in Organic Light-Emitting Devices," *Chem. Rev.*, vol. 115, pp. 8449–8503, aug 2015.

[98] W. Song, J. Y. Lee, T. Kim, Y. Lee, and H. Jeong, "Comprehensive understanding of degradation mechanism of high efficiency blue organic light-emitting diodes at the interface by hole and electron transport layer," *Org. Electron.*, vol. 57, pp. 158–164, jun 2018.

[99] H. Yu and H. Aziz, "Direct Observation of Exciton-Induced Molecular Aggregation in Organic Small-Molecule Electroluminescent Materials," *J. Phys. Chem. C*, vol. 123, pp. 16424–16429, jul 2019.

[100] S. Liu, C. Peng, A. Cruz, Y. Chen, and F. So, "Degradation study of organic light-emitting diodes with solution-processed small molecule phosphorescent emitting layers," *J. Mater. Chem. C*, vol. 4, no. 37, pp. 8696–8703, 2016.

[101] Q. Niu, W. Huang, J. Tong, H. Lv, Y. Deng, Y. Ma, Z. Zhao, R. Xia, W. Zeng, Y. Min, and W. Huang, "Understanding the mechanism of PEDOT: PSS modification via solvent on the morphology of perovskite films for efficient solar cells," *Synth. Met.*, vol. 243, no. May, pp. 17–24, 2018.

[102] H. Alhummiany, S. Rafique, and K. Sulaiman, "XPS Analysis of the Improved Operational Stability of Organic Solar Cells Using a V 2 O 5 and PEDOT:PSS Composite Layer: Effect of Varied Atmospheric Conditions," *J. Phys. Chem. C*, vol. 121, pp. 7649–7658, apr 2017.

[103] S. Jönsson, J. Birgerson, X. Crispin, G. Greczynski, W. Osikowicz, A. Denier van der Gon, W. Salaneck, and M. Fahlman, "The effects of solvents on the morphology and sheet resistance in poly(3,4-ethylenedioxythiophene)–polystyrenesulfonic acid (PEDOT–PSS) films," *Synth. Met.*, vol. 139, pp. 1–10, aug 2003.

[104] G. Greczynski, T. Kugler, and W. Salaneck, "Characterization of the PEDOT-PSS system by means of X-ray and ultraviolet photoelectron spectroscopy," *Thin Solid Films*, vol. 354, pp. 129–135, oct 1999.

[105] P. Schrögel, N. Langer, C. Schildknecht, G. Wagenblast, C. Lennartz, and P. Strohriegl, "Meta-linked CBP-derivatives as host materials for a blue iridium carbene complex," *Org. Electron. physics, Mater. Appl.*, vol. 12, no. 12, pp. 2047–2055, 2011.